International Telecommunication Union

ITU-R

Radiocommunication Sector of ITU

Report ITU-R P.2406-0
(09/2017)

Studies for short-path propagation data and models for terrestrial radiocommunication systems in the frequency range 6 GHz to 100 GHz

P Series

Radiowave propagation

Foreword

The role of the Radiocommunication Sector is to ensure the rational, equitable, efficient and economical use of the radio-frequency spectrum by all radiocommunication services, including satellite services, and carry out studies without limit of frequency range on the basis of which Recommendations are adopted.

The regulatory and policy functions of the Radiocommunication Sector are performed by World and Regional Radiocommunication Conferences and Radiocommunication Assemblies supported by Study Groups.

Policy on Intellectual Property Right (IPR)

ITU-R policy on IPR is described in the Common Patent Policy for ITU-T/ITU-R/ISO/IEC referenced in Annex 1 of Resolution ITU-R 1. Forms to be used for the submission of patent statements and licensing declarations by patent holders are available from http://www.itu.int/ITU-R/go/patents/en where the Guidelines for Implementation of the Common Patent Policy for ITU-T/ITU-R/ISO/IEC and the ITU-R patent information database can also be found.

Series of ITU-R Reports

(Also available online at http://www.itu.int/publ/R-REP/en)

Series	Title
BO	Satellite delivery
BR	Recording for production, archival and play-out; film for television
BS	Broadcasting service (sound)
BT	Broadcasting service (television)
F	Fixed service
M	Mobile, radiodetermination, amateur and related satellite services
P	**Radiowave propagation**
RA	Radio astronomy
RS	Remote sensing systems
S	Fixed-satellite service
SA	Space applications and meteorology
SF	Frequency sharing and coordination between fixed-satellite and fixed service systems
SM	Spectrum management

***Note**: This ITU-R Report was approved in English by the Study Group under the procedure detailed in Resolution ITU-R 1.*

Electronic Publication
Geneva, 2017

REPORT ITU-R P.2406-0

Studies for short-path propagation data and models for terrestrial radiocommunication systems in the frequency range 6 GHz to 100 GHz

(2017)

1 Introduction

In recent years, many research projects, research institutes and organizations have undertaken activities in characterizing terrestrial propagation environments in higher frequency bands (above 6 GHz) as one of the emerging areas of research. This is especially important since there is not yet a complete set of verified and agreed-upon propagation data, channel models and prediction methods for higher frequencies in ITU-R to evaluate emerging terrestrial radiocommunication systems and applications and to conduct sharing studies between the same or different systems.

This Report provides visibility on progresses and trends reported to ITU-R related to short-path propagation models and related characteristics in the frequency range 6 GHz to 100 GHz.

2 Scope

This Report provides experimental and theoretical results related to:

– propagation models and characteristics relevant to terrestrial radiocommunication services;

– indoor and outdoor environments;

– line-of-sight and non-line-of-sight propagation conditions;

– the frequency range 6 GHz to 100 GHz.

This Report includes the following information:

– results of propagation experiments, analyses and simulations related to the above environments and scenarios;

– preliminary proposals of channel models and prediction methods, based on results of experiments, analyses, simulations;

– additional background information that complements the Recommendations ITU-R P.1411 and ITU-R P.1238, e.g. explanations on how the propagation data and models were obtained and derived.

3 Related documents and list of studies

3.1 Related documents

Recommendation ITU-R P.1411

Recommendation ITU-R P.1238

3.2 List of studies

The studies described in this ITU-R Report for outdoor environments are shown in Table 1. The studies for indoor environments are shown in Table 2.

TABLE 1

List of studies for outdoor environments

Section	Study title	Frequency bands/ranges (GHz)	Related version of Rec. ITU-R P.1411	Related section(s) in Rec. ITU-R P.1411
Urban and sub-urban environments				
5.1.1	Site-general models	0.8 ~ 73	9	4.1.1, 4.2.1
5.1.2	Site-specific model, propagation within street canyons and modelling for chamfered shape buildings at intersections	2.2, 4.7, 26.4, 37.1	9	4.1.3.2
5.1.3	Site-specific model, propagation within street canyons	28, 38	9	4.1.3.2
5.1.4	Site-specific model, propagation over-rooftop in suburban environments	28, 38	9	4.2.2.2
5.1.5	**Delay spread, propagation in urban environments, below-rooftop and over-rooftop**	25.5-28.5, 51-57, 67-73	9	5.1.1, 5.1.2.2
5.1.6	**Delay spread, propagation in urban environments, below-rooftop**	28, 38	9	5.1.2.2
5.1.7	**Delay spread, propagation in urban environments, below-rooftop**	29.3-31.5, 58.7-63.1	9	5.1.2.2
5.1.8	Prediction models of delay and angular spreads as a function of antenna beamwidth	28, 38	9	5.3
5.1.9	Cross-polarization discrimination	51-57, 67-73	9	6
Residential environments				
5.2.1	Path loss model for propagation between terminals located below roof-top height in residential environments	2.4, 4.7, 26.4	9	4.3.3
5.2.2	Delay spread, propagation in residential environments, below-rooftop	25.5-28.5, 67-73	9	5.1.2.2

TABLE 2

List of studies for indoor environments

Section	Study title	Applicable frequency bands/ranges (GHz)	Related version of Rec. ITU-R P.1238	Related section(s) in Rec. ITU-R P.1238
6.1	Power loss coefficients and shadow fading statistics	0.8, 2.2, 4.7, 26, 37	9	3.1
6.2	Power loss coefficients and shadow fading statistics	28, 38	9	3.1
6.3	Power loss coefficients, shadow fading statistics, rms delay spread parameters	51-57, 67-73	9	3.1, 4.3
6.4	Power loss coefficients	70	9	3.1
6.5	Power loss coefficients	300	9	3.1
6.6	Rms delay spread parameters	28, 38	9	4.3
6.7	Rms delay spread parameters	30, 60	9	4.3
6.8	Antenna directivity dependence of static rms delay spread in NLoS	60	9	5.1.2
6.9	Effects of antenna beamwidth to multipath delay and angular spread	28, 38	9	5.1.2
6.10	Effect of movement of objects in the room	70	9	8

4 General considerations for mobile systems

In order to be of practical use, propagation data and models must take into account the following likely technological developments and deployment scenarios associated with future terrestrial mobile systems operating in the range 6 GHz to 100 GHz:

– Mobile systems operating in the range 6 GHz to 100 GHz will likely be deployed predominantly in areas where the density of mobile traffic is very high, such as indoor, outdoor and outdoor-to-indoor urban environments.

– There is growing evidence that several frequency bands above 6 GHz can be used to provide non-line-of-sight mobile services over hundreds of metres or more, as well as under mobility.

– Overcoming the propagation limitations associated with spectrum in the range 6 GHz to 100 GHz will likely require the use of highly directional, steerable antennas at the transmitter, receiver, or both.

– To be able to provide anticipated future data rates, mobile systems operating in the range 6 GHz to 100 GHz should support contiguous bandwidths of hundreds of megahertz or more.

5 Studies for outdoor environments

5.1 Urban and suburban environments

5.1.1 Study 1: Site-general models (Frequency range: variable in 0.8 ~ 73 GHz)

5.1.1.1 Executive summary

This section provides additional information related to the development of site-general models for urban and suburban environments included in Recommendation ITU-R P.1411.

5.1.1.2 Background and proposal

The site-general model is provided by the following equation:

$$PL(d,f) = 10\alpha \log_{10}(d) + \beta + 10\gamma \log_{10}(f) + N(0,\sigma) \quad \text{(dB)} \tag{1}$$

where:

d : 3D direct distance between the transmitting and receiving stations (m)

f : operating frequency (GHz)

α : coefficient associated with the increase of the path loss with distance

β : coefficient associated with the offset value of the path loss

γ : coefficient associated with the increase of the path loss with frequency

$N(0,\sigma)$: Gaussian distribution with standard deviation σ.

5.1.1.3 Measurement setup and procedure

Table 3 provides the list of data sets used to develop the site-general models.

TABLE 3

Data sets for the development of site-general models for urban and suburban environments

Propagation category	Environment	Link type	Frequency (GHz)	Distance (m)	Contributors
Below roof top	Urban high-rise	LoS	0.8	10-530	NTT
			2.2	10-530	NTT
			4.7	10-500	NTT
			6	5-650	RRA
			10	40-660	RRA
			18	35-565	RRA
			26.4	10-500	NTT
			28	10-380	ETRI
			37.1	10-500	NTT
			38	10-320	ETRI
			60	5-50	Intel
		NLoS	0.8	45-690	NTT
			2.2	45-690	NTT
			4.7	40-690	NTT

TABLE 3 (*end*)

Propagation category	Environment	Link type	Frequency (GHz)	Distance (m)	Contributors
			6	50-705	RRA
			10	65-715	RRA
			18	50-570	RRA
			26.4	40-690	NTT
			28	25-235	ETRI
			37.1	40-610	NTT
			38	30-230	ETRI
Below roof top	Urban low-rise / Suburban	LoS	10	10-210	Intel
			27 (25.5-28.5)	20-140	Durham University
			28	10-250	ETRI, Samsung
			38	10-250	ETRI, Samsung
			54 (51-57)	20-140	Durham University
			60	10-210	Intel
			70 (67-73)	10-140	Durham University
		NLoS	10	10-165	Intel
			27 (25.5-28.5)	10-140	Durham University
			28	30-250	ETRI, Samsung
			38	30-240	ETRI, Samsung
			60	10-150	Intel
			70 (67-73)	10-170	Durham University
Above roof top	Urban high-rise	LoS	2.2	155-1140	NTT
			4.7	155-1140	NTT
			26.4	155-1140	NTT
			66.5	170-340	NTT
		NLoS	2.2	260-1630	NTT
			4.7	260-1630	NTT
			26.4	260-1630	NTT
			66.5	260-340	NTT
Above roof top	Urban low-rise / Suburban	LoS	27 (25.5-28.5)	55-145	Durham University
			70 (67-73)	55-145	Durham University

The following methodology was applied to gather and harmonize the different sets of data:

– Sub-sample all measurement data with local median every 1 meter.

– Develop a single propagation model encompassing all available frequencies per environment (urban high-rise, urban low-rise/suburban) and condition (below-rooftop, above-rooftop).
– For each environment and condition, use a common distance range available across all available data sets and frequencies for path loss fitting. However the minimum and maximum distance range was used for distance range applicability of the models (e.g. the min-max ranges for urban high-rise NLoS below-rooftop were 30-715 m, while the common distance range based on which path loss fitting was performed, was 65-230 m).
– A 10 dB minimum SNR level above noise-floor was applied on every data set.
– All path loss measurements were given with respect to the 3D direct distance between the Tx and Rx antennas.

5.1.1.4 Validation results

Path loss obtained for different environments and situations, based on all data sets and the methodology above, are depicted in the following Figures:

– Figure 1: LoS situations in below-rooftop urban and suburban environments.
– Figure 2: NLoS situations in below-rooftop urban environments.
– Figure 3: NLoS situations in below-rooftop suburban environments.
– Figure 4: LoS situations in over-rooftop urban and suburban environments.
– Figure 5: NLoS situations in over-rooftop urban environments.

FIGURE 1

Path loss for LoS in below-rooftop urban and suburban environments

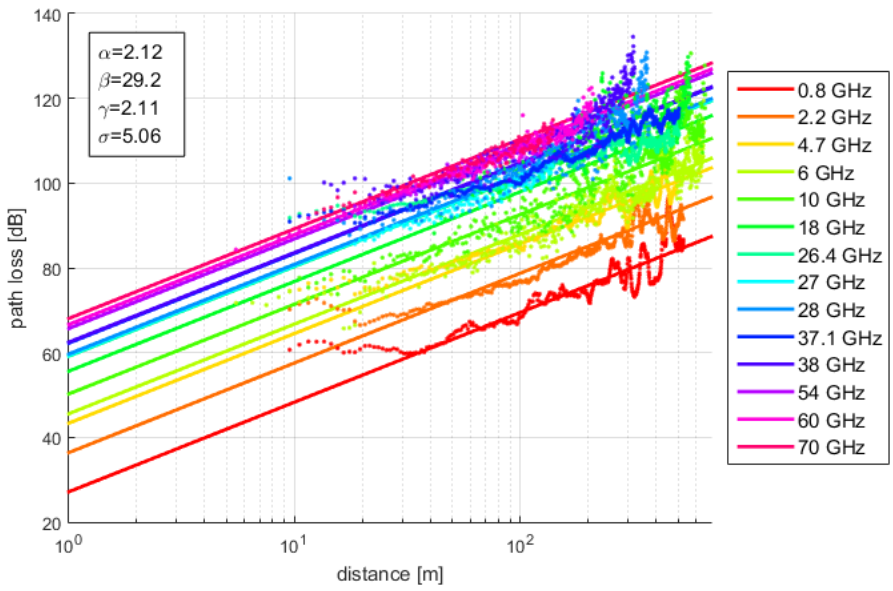

FIGURE 2

Path loss for NLoS in below-rooftop urban environments

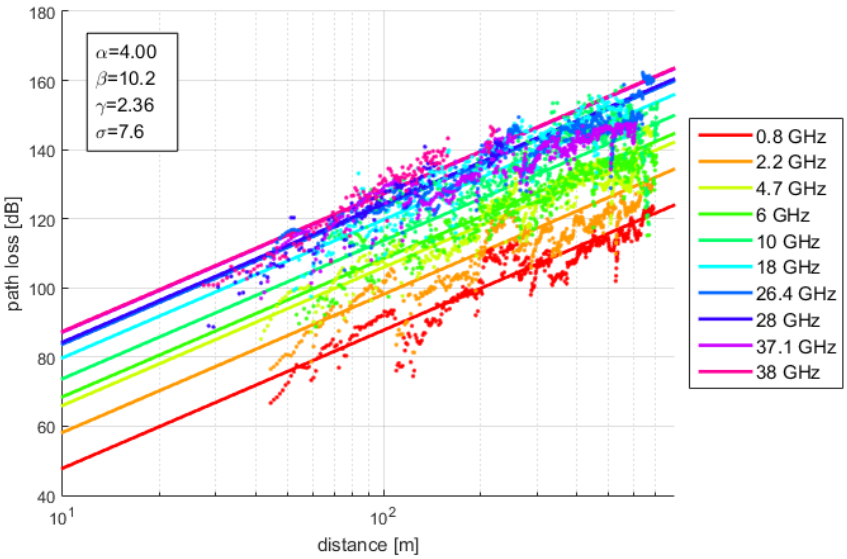

FIGURE 3

Path loss for NLoS in below-rooftop suburban environments

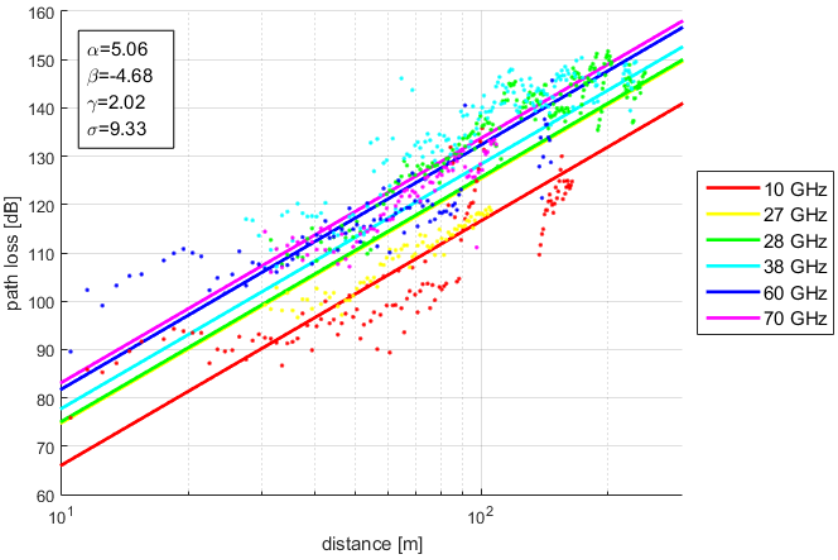

FIGURE 4

Path loss for LoS in above-rooftop urban and suburban environments

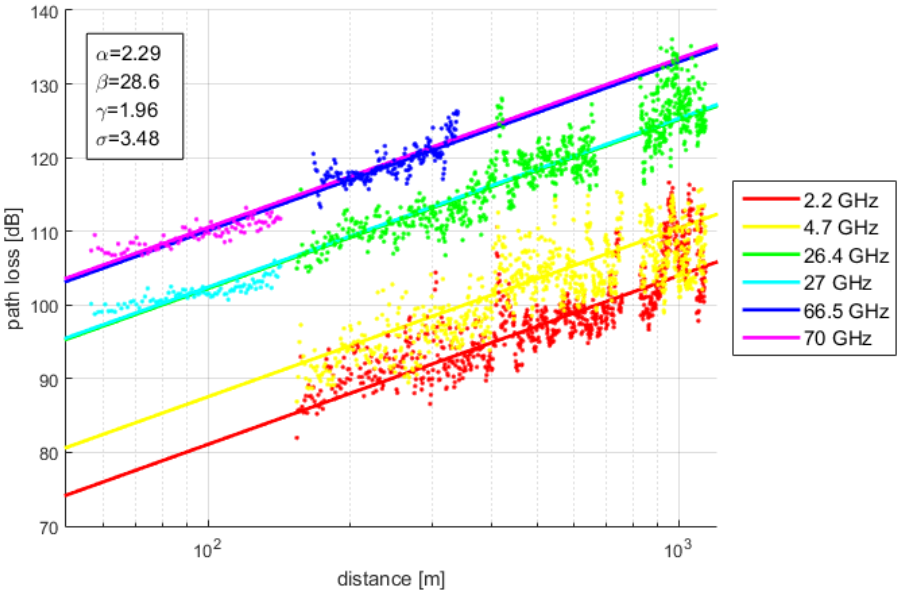

FIGURE 5

Path loss for NLoS in above-rooftop urban environments

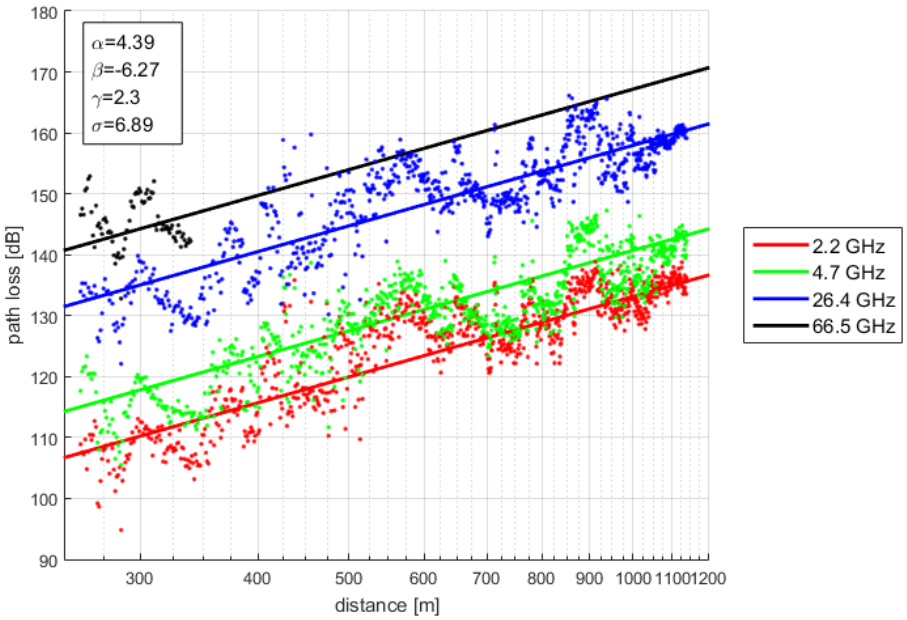

5.1.1.5 Conclusion

The results from the different data sets showed consistent behaviour across all frequency ranges for both LoS and NLoS situations in the different environments studied. The resulting coefficients (α, β, γ, σ) associated with the model have been included in Recommendation ITU-R P.1411.

5.1.2 Study 2: Site-specific model, propagation within street canyons and modelling for chamfered shape buildings at intersections (Frequency bands: 2.2, 4.7, 26.4, 37.1 GHz)

5.1.2.1 Executive summary

This section provides additional information on the site-specific model for propagation within street canyons, included in Recommendation ITU-R P.1411. This study focuses on the extension of the upper frequency limit of the model to 37.1 GHz and modelling for chamfered shape buildings at intersections.

5.1.2.2 Background and proposal

5.1.2.2.1 Site-specific model for propagation below-rooftop within street canyons

The site-specific model is provided by the following expression:

$$L_{NLoS\,2} = L_{LoS} + L_c + L_{att} \tag{2}$$

$$L_c = \begin{cases} \dfrac{L_{corner}}{\log_{10}(1+d_{corner})}\ \log_{10}(x_2 - w_1/2) & w_1/2+1 < x_2 \le w_1/2+1+d_{corner} \\ L_{corner} & x_2 > w_1/2+1+d_{corner} \end{cases} \tag{3}$$

$$L_{att} = \begin{cases} 10\beta\log_{10}\left(\dfrac{x_1+x_2}{x_1+w_1/2+d_{corner}}\right) & x_2 > w_1/2+1+d_{corner} \\ 0 & x_2 \le w_1/2+1+d_{corner} \end{cases} \tag{4}$$

where:

L_{NLoS2} : total path loss (dB)
L_{LoS} : path loss before the corner region (dB)
L_c : path loss expression at the corner region (dB)
L_{att} : path loss expression after the corner region (dB)
d_{corner} : distance of the corner region (m)
L_{corner} : path loss at the corner region (dB)
w_1 : street width at the position of the Station 1 (m)
w_2 : street width at the position of the Station 2 (m)
x_1 : distance from Station 1 to the corner region (m)
x_2 : distance from the corner region to Station 2 (m).

L_{LoS} is the path loss in the LoS street for x_1 (> 20 m). In equation (3), L_{corner} is given as 20 dB in an urban environment and 30 dB in a residential environment. And d_{corner} is 30 m in both environments.

5.1.2.2.2 Path loss model for chamfered shape building at intersection

In equation (4), β = 6 in urban and residential environments for wedge-shaped buildings at four corners of the intersection as illustrated in case (a) of Fig. 6. If a particular building is chamfered at the intersection in urban environments as illustrated in case (b) of Fig. 6, β is calculated by equation (5). Because the specular reflection paths from chamfered-shape buildings significantly affect path loss in NLoS region, the path loss for case (b) is different from that for case (a).

$$\beta = 4.2 + (1.4\log_{10} f - 7.8)(0.8\log_{10} x_1 - 1.0) \tag{5}$$

where f is frequency in MHz.

FIGURE 6

Case (a) Wedge shaped buildings layout Case (b) Chamfered shape buildings layout

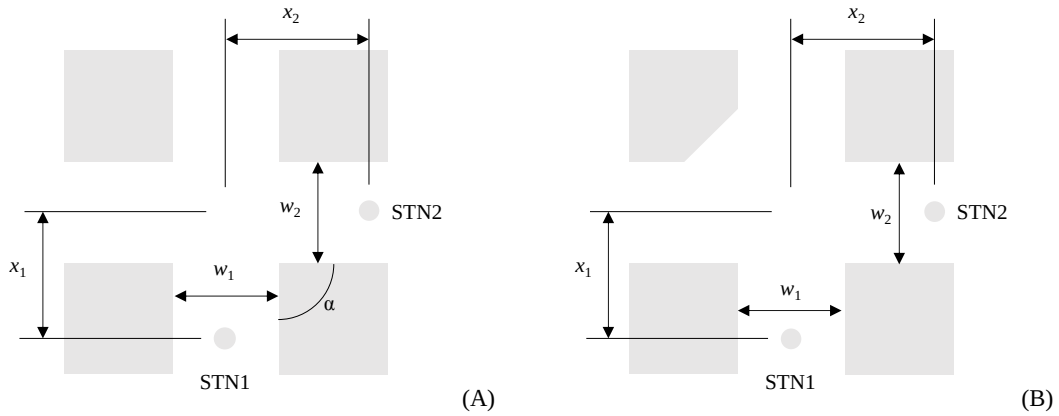

5.1.2.3 Measurement setup and procedure

The propagation characteristics were measured around Tokyo Station, Tokyo, Japan. Most buildings in this area fall into the high-rise (over 30 m) category, and the gaps between buildings are small compared with the building width. This environment is called a "street canyon".

The path loss measurements in four NLoS routes, NLoS1 to 4, including LoS, were taken as shown in Fig. 7. The measurements were taken in four frequency bands: 2.2, 4.7, 26.4 and 37.1 GHz. Tx antennas were set at two different positions (Tx1 and Tx2), at 10-m height. They were used to transmit continuous waves (CW). An Rx antenna was fixed on the roof of a measurement car whose height was 2.5 m. The antenna radiation pattern was omni-directional. Table 4 summarizes these parameters. The distance to the intersection was about 242 m for NLoS 1, 57 m for NLoS 2, 169 m for NLoS 3, and 192 m for NLoS4. The moving distance after the corner was 913 m for NLoS1, 440 m for NLoS2, 925 m for NLoS3, and 372 m for NLoS4. Figure 8 shows photographs of the measurement environment.

FIGURE 7

Measurement routes at (a) Tx1 (b) Tx2

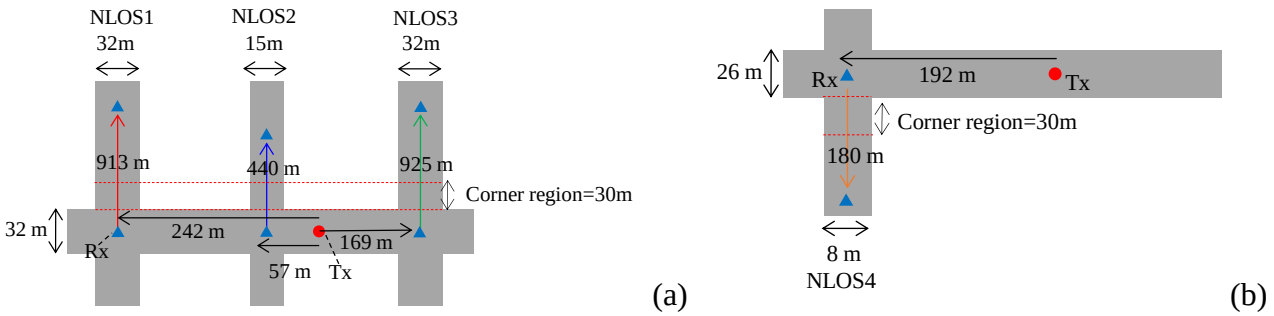

TABLE 4

Measurement Parameters

Measured frequency (GHz)	2.2, 4.7, 26.4 and 37.1 (CW)
Antenna radiation pattern	Omni-directional in horizontal plane for both Tx and Rx
Antenna gain	Around 2 dBi for each antenna
Tx antenna height	10 m from the ground
Rx antenna height	2.5 m from the ground

FIGURE 8

View from (a) Tx1 (b) Tx2

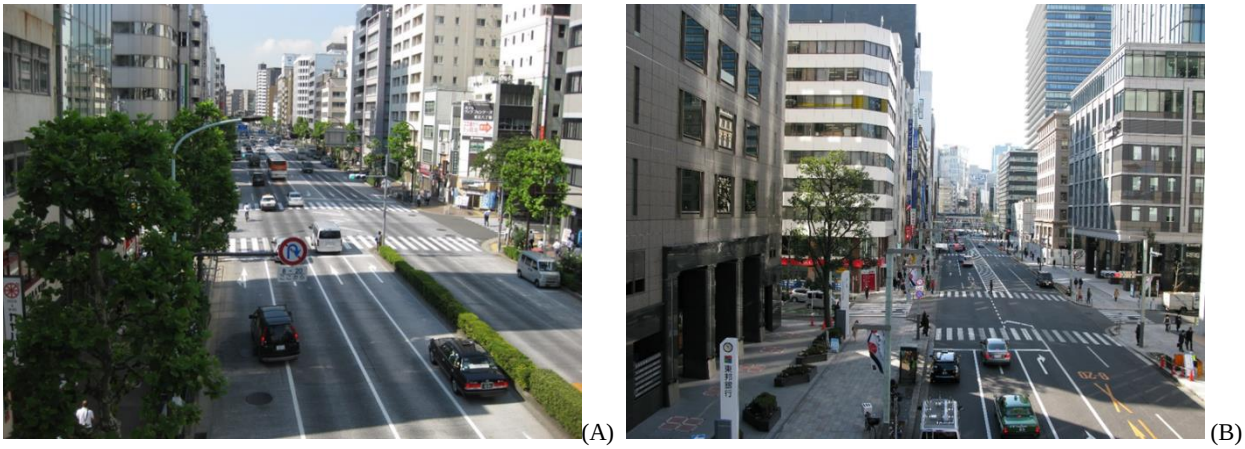

(A) (B)

In a second measurement campaign, the path loss measurements were taken as shown in Fig. 9. The measurements were taken in four frequency bands: 2.2, 4.7, 26.4 and 37.1 GHz. Tx antennas were set at 10 m height. They were used to transmit continuous waves (CW). An Rx antenna was fixed on the roof of a measurement car whose height was 2.5 m. The antenna radiation pattern was omni-directional. Table 5 summarizes these parameters. The distance to the intersection was about 169 m. The moving distance after the corner was 431 m.

FIGURE 9

Measurement route

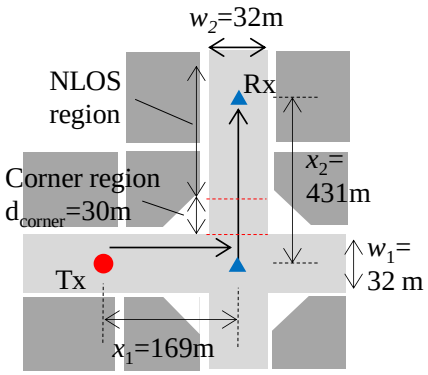

TABLE 5

Measurement parameters

Measured frequency (GHz)	2.2, 4.7, 26.4 and 37.1 (CW)
Antenna radiation pattern	Omni-directional in horizontal plane for both Tx and Rx
Tx antenna height	10 m from the ground
Rx antenna height	2.5 m from the ground

5.1.2.4 Validation results

5.1.2.4.1 Wedge shaped building at intersection

This subsection shows comparison results in the case of a wedge shaped building at the intersection. This shape is utilized by a Manhattan grid layout. The measurements for NLoS4 at Tx2 and predictions are summarized in Fig. 10. From this Figure, the prediction with Recommendation ITU-R P.1411 seems relatively accurate. Quantitative evaluation is given where root mean square (RMSE) values of each frequency band are calculated. Figure 10 shows RMSE to be about 3.7 dB at 2.2 GHz, 3.2 dB at 4.7 GHz, 3.0 dB at 26.4 GHz, and 3.3 dB at 37.1 GHz with Recommendation ITU-R P.1411. This shows that the Recommendation ITU-R P.1411 model can cover the frequency range up to 37.1 GHz for a wedge shaped building layout.

FIGURE 10

Comparison of measurement results and predicted results with ITU-R model for NLoS4

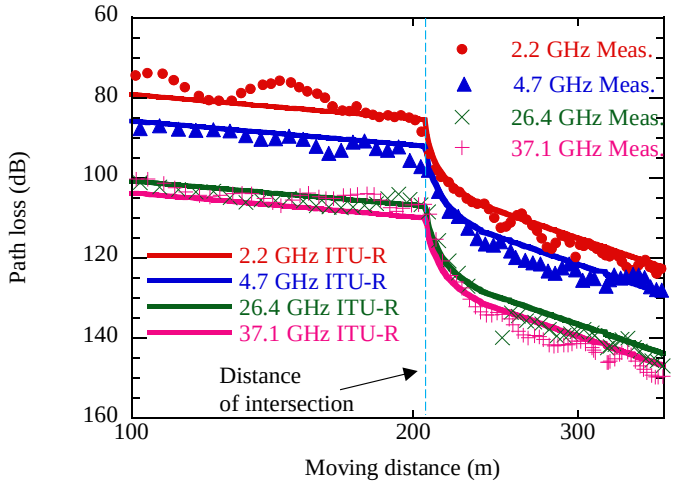

5.1.2.4.2 Chamfered shape building at intersection

Figure 11 compares measurement results with prediction results. Table 6 shows the median prediction error values for prediction results obtained with the proposed and current models at the distance range from 185 to 600 m and at the distance range from 185 to 300 m. The Table shows that the prediction error values obtained with the former are almost the same as those obtained with the latter at places near the intersection. On the other hand, Table 6 shows that the prediction error values obtained with the former are smaller than those obtained with the latter at places far from the intersection. In the chamfered shape building case, the proposed model is valid at distances relatively far from the intersection because the specular reflection paths from chamfered shape buildings significantly affect path loss in NLoS regions and the coefficient parameter β becomes smaller than for the wedge shaped building case. As a result, it was possible to confirm that the proposed model covers all distances from the intersection.

FIGURE 11

Comparison of prediction results obtained with proposed and current models

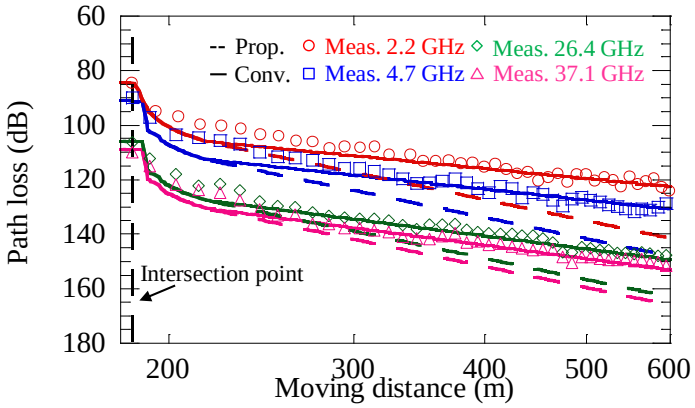

TABLE 6

Prediction error values

Frequency (GHz)	Prediction error (dB) Places far from an intersection (from 185 to 600 m)		Prediction error (dB) Places near an intersection (from 185 to 300 m)	
	Proposed model	**Current model**	**Proposed model**	**Current model**
2.2	−1.4	−11.9	−4.2	−7.1
4.7	−0.9	−10.6	−4.4	−7.4
26.4	−1.3	−9.3	−2.1	−4.4
37.1	−1.0	−8.6	−2.3	−4.2

5.1.2.5 Conclusion

This study presented the verification results obtained for a site-specific path loss model in street canyon environments. An extension model of Recommendation ITU-R P.1411 that is applicable for chamfered shape buildings was proposed. To verify the model's validity, ray tracing calculation was used to obtain results which were compared with measurement results. It was clarified that specular reflection paths from chamfered shaped buildings strongly contribute to path loss, since in this case the prediction error values ranged from about 4.1 to 7.0 dB for bands between 2.2 and 37.1 GHz. In addition, it was confirmed that the prediction error obtained with the proposed and current models is almost the same at distances relatively near the intersection, thus confirming the proposed model's validity at distances relatively far from the intersection in NLoS streets. These results indicate that the proposed model covers all distances from the intersection.

5.1.3 Study 3: Site-specific model, propagation within street canyons (Frequency bands: 28, 3 GHz)

5.1.3.1 Executive summary

This section provides additional information on the site-specific model for propagation within street canyons, included in Recommendation ITU-R P.1411. This study focuses on the extension of the upper frequency limit of the model to 38 GHz.

5.1.3.2 Background and proposal

The site-specific model is provided by the following expression:

$$L_{NLoS\,2} = L_{LoS} + L_c + L_{att} \tag{6}$$

$$L_c = \begin{cases} \dfrac{L_{corner}}{\log_{10}(1+d_{corner})}\ \log_{10}(x_2 - w_1/2) & w_1/2+1 < x_2 \le w_1/2+1+d_{corner} \\ L_{corner} & x_2 > w_1/2+1+d_{corner} \end{cases} \tag{7}$$

$$L_{att} = \begin{cases} 10\beta\log_{10}\left(\dfrac{x_1+x_2}{x_1+w_1/2+d_{corner}}\right) & x_2 > w_1/2+1+d_{corner} \\ 0 & x_2 \le w_1/2+1+d_{corner} \end{cases} \tag{8}$$

where:

L_{NLoS2} : total path loss (dB)

L_{LoS} : path loss before the corner region (dB)

L_c : path loss expression at the corner region (dB)

L_{att} : path loss expression after the corner region (dB)

d_{corner} : distance of the corner region (m)

L_{corner} : path loss at the corner region (dB)

w_1 : street width at the position of the Station 1 (m)

w_2 : street width at the position of the Station 2 (m)

x_1 : distance from Station 1 to the corner region (m)

x_2 : distance from the corner region to Station 2 (m).

L_{LoS} is the path loss in the LoS street for x_1 (> 20 m). In equation (7), L_{corner} is given as 20 dB in an urban environment and 30 dB in a residential environment. And d_{corner} is 30 m in both environments.

Note that the applicable frequency range was from 2 to 16 GHz in Recommendation ITU-R P.1411-8 and the range was extended up to 38 GHz in Recommendation ITU-R P.1411-9 based on the study described here.

5.1.3.3 Measurement setup and procedure

Figure 12 shows the 28/38 GHz channel sounder, where detailed specification relevant to path loss measurements is listed in Table 7.

FIGURE 12

Measurement equipment

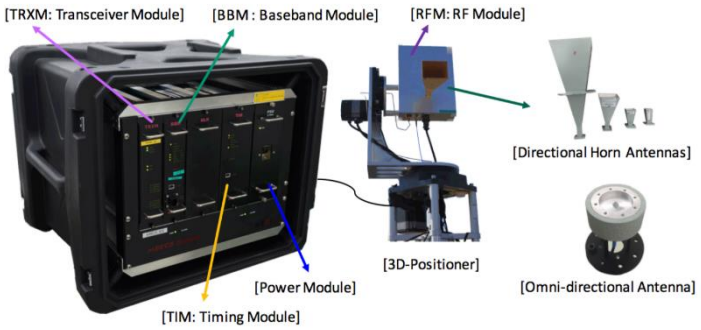

TABLE 7

Measurement equipment specification

System parameters	Specifications
Centre frequency	28 and 38 GHz
Max TX RF power (w/o antenna gain)	29 dBm (28 GHz) 21 dBm (38 GHz)
AGC range	60 dB
Measureable path loss range	170 dB

Measurement campaigns were conducted in urban street environments with the following configurations:

– 4 m TX height and 1.5 m RX height;

– 30-50 m building height and 30 m street width;

– Two different TX locations.

Figure 13(a) shows the measurement environment, which can be considered as a street canyon environment. This street is in a downtown metro station in Daejeon near the City Hall. The average street width is 30 m and the building height is between 30 m and 50 m.

Figure 13(b) shows the measurement layout on which the location of TX and the measurement route of RX are marked. During the measurements, TX was held stationary and RX was moved along the designated measurement route. As can be seen, the RX measurement route is perpendicular to the TX street, the corner is the NLoS obstruction source. To see the effect of the distance between the corner and TX, measurements were conducted in two different TX locations: 65 m (denoted by TX1) and 105 m (denoted by TX2). Considering two frequencies (28 and 38 GHz) and two TX locations, four sets of measurements were collected.

FIGURE 13

(a) Measurement street environment (b) Measurement layout

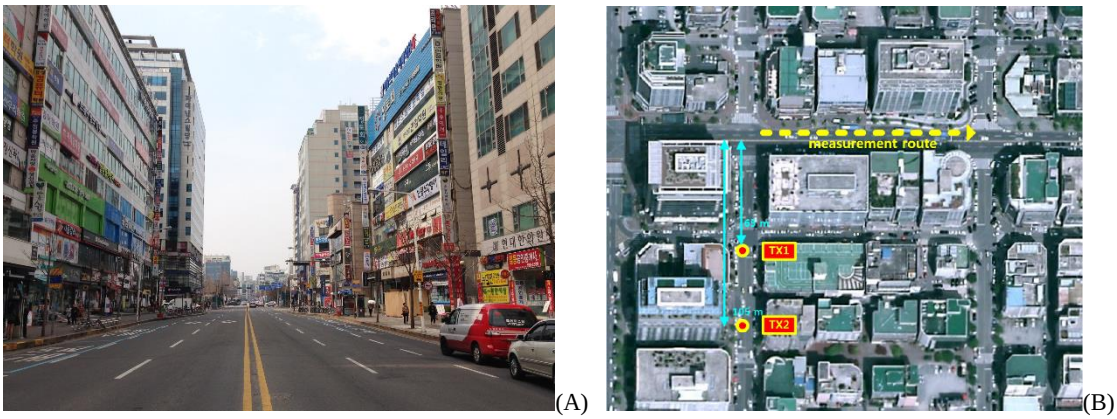

(A) (B)

5.1.3.4 Validation results

This section retraces the archived documents relevant to the Recommendation ITU-R P.1411 NLoS path loss model. The first proposal was made in 2001, in which a then-new propagation model for the SHF band was proposed based on 3.35, 8.45 and 15.75 GHz measurements. By comparing these frequency band measurements to the then-existing UHF propagation model, it claimed that the

propagation behaviour in the SHF band is different, and proposed an initial model. With continuing discussions in the Working Party 3K meetings, the current form of the model was adopted in 2007.

If measurement conditions of previous measurements and results are briefly reviewed, their x_1 distance (distance between TX and the corner) is 65 and 430 m (ours is 65 and 105 m). With their x_1 distance setting, they obtained L_{corner} and β, as listed in Table 8. Note that since they have only two TX-location measurements, the "ranges" in Table 8 were derived from only these two measurements.

TABLE 8

Rec. ITU-R P.1411 NLoS path loss model parameters for urban environments obtained from previous measurements

Frequency (GHz)	L_{corner} (dB)	β
3.35	16-17	4.7-12
8.45	22-28	5.2
15.75	22-23	4.2-12
Rec. ITU-R P.1411 nominal (typical) value	20	6

Although the literature and archived documents were searched, it was not possible to find a nominal (typical) value determination process, which was set to $L_{corner} = 20$ dB and $\beta = 6$ for urban environments. According to a previous contribution in 2005, the "typical value" of β was chosen as 8, since the range of β was from 4.7 to 12. In another contribution (2006), the typical value of β was changed to 6 since the range was adjusted from 4.2 to 12. A similar argument is applied to L_{corner}.

According to the two contributions mentioned above, the typical value of L_{corner} was chosen as 20 dB in urban environments, considering that measurements were given by 16-28 dB. The reason for this choice was drawn from arguments regarding the importance of cell-edge interference in practical cellular network designs, which emphasized the importance of the lower bound. It can be observed that the parameter range from the measurements as listed in Table 9 are also in, or close to, the parameter range of the original document listed in Table 8. Considering the small RMSE differences, it is proposed that the same typical value can be used for 28 and 38 GHz. Figure 14 shows the 28 and 38 GHz measurement data along with the predictions generated by the existing Recommendation ITU-R P.1411 street canyon NLoS propagation model.

TABLE 9

Parameter range from measurement data

Frequency (GHz)	L_{corner} (dB)	β
28	10-19	4-11
38	14-20	6-10

FIGURE 14

Measurement data and prediction to the existing Recommendation ITU-R P.1411 model

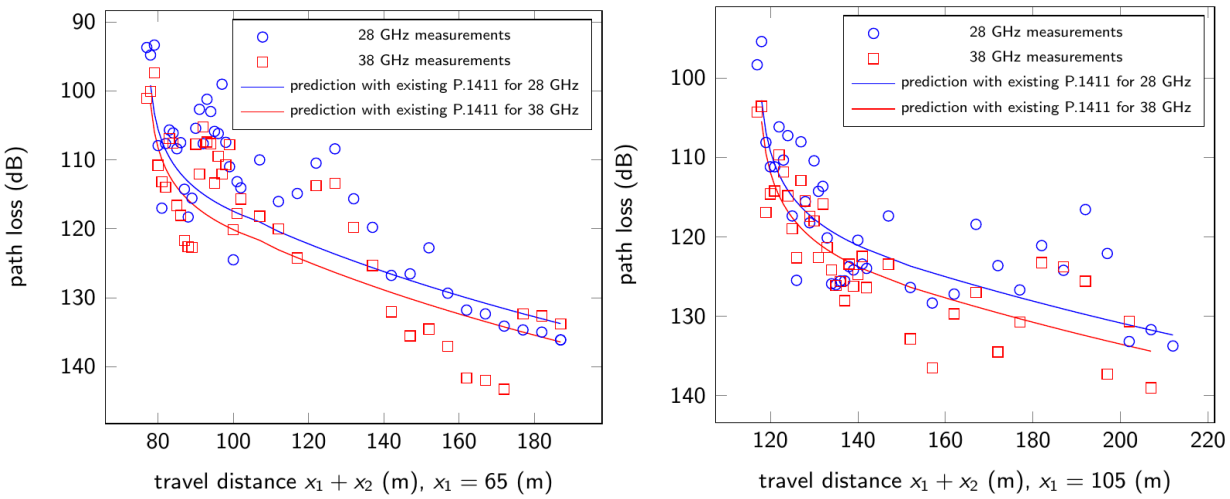

5.1.3.5 Conclusion

Based on the results and analyses above, it can be concluded that the applicable frequency range of the site-specific model for NLoS propagation in street canyon environments can be extended to 38 GHz.

5.1.4 Study 4: Site-specific model, propagation over-rooftop in suburban environments (Frequency bands: 28, 38 GHz)

5.1.4.1 Executive summary

This section provides additional information on the site-specific model for propagation over-rooftop in suburban environments, included in Recommendation ITU-R P.1411. This study focuses on the extension of the upper frequency limit of the model to 38 GHz.

5.1.4.2 Background and proposal

The site-specific model is provided by the following expression:

$$L_{NLoS1} = \begin{cases} 20 \cdot \log_{10}\left(\frac{4\pi d}{\lambda}\right) & \text{for } d < d_0 \quad \text{(Direct wave dominant region)} \\ L_{0n} & \text{for } d_0 \le d < d_{RD} \quad \text{(Reflected wave dominant region)} \\ 32.1 \cdot \log_{10}\left(\frac{d}{d_{RD}}\right) + L_{d_{RD}} & \text{for } d \ge d_{RD} \quad \text{(Diffracted wave dominant region)} \end{cases} \tag{9}$$

where:

d : 3D direct distance between the transmitting and receiving stations (m)

λ : wavelength (m)

d_0 : distance separating the direct and reflected wave dominant regions (m)

L_{0n} : pathloss expression for the reflected wave dominant region (dB)

d_{RD} : distance separating the reflected and diffracted wave dominant regions (m)

$L_{d_{RD}}$: pathloss expression for the diffracted wave dominant region (dB).

Equations that further detail this model can be found in Recommendation ITU-R P.1411.

5.1.4.3 Measurement setup and procedure

The measurement campaign was conducted in Gwanpyeong, Daejeon Korea. Transmitter (Tx) was installed on the top of a 30 m high building. The average height of buildings surrounding Tx was 11 m and the average width of the streets was 10 m. Receiver (Rx) was set on the streets and its height was 1.7 m. The beam width of Tx was 30 degrees and an omni-directional receive antenna was used. In Fig. 15(a), Tx and Rx which were used in the measurement campaign are shown. To obtain various path loss with respect to distance, Rx was consistently moved in small increments. Thus, Rx routes were made. The location of Tx and Rx routes are provided in Fig. 15(b). The frequency band of 28 GHz and 38 GHz were measured at the same streets, thus the number of Rx routes for 28 GHz and 38 GHz are the same. However, the number of total path loss samples are different (28 GHz: 810, 38 GHz, 666). It is assumed that a limitation of measurement performance makes the difference.

FIGURE 15

(a) View from Tx and Rx (b) Locations of Tx and Rx

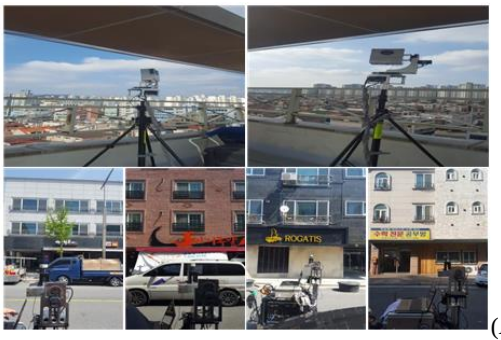

(A)

(B)

5.1.4.4 Validation results

In Fig. 16, a comparison of the measurements and Recommendation ITU-R P.1411 over rooftops path loss model are provided. The parameters of Recommendation ITU-R P.1411 over rooftops path loss model are shown in Table 10. As a matter of fact, every angle of street orientation (φ) of the samples is different. However, to compare the measurements and the path loss model, 45 degree is chosen to represent the rest of φ. The boundary between the reflected and diffracted wave dominant regions (d_{RD}) of Recommendation ITU-R P.1411 over rooftops path loss model becomes 121.86 and 125.07 at 28 GHz and 38 GHz respectively. To verify the application of Recommendation ITU-R P.1411 over rooftops the path loss model at 28 GHz and 38 GHz, RMS errors, which are tabulated in Table 11, are calculated. RMS errors of the reflected wave dominant region and the diffracted wave dominant region are 7.77 dB and 7.71 dB, respectively, thus the total RMS error becomes 7.73 dB. Considering the RMS error of 7.73 dB, it is clear that the Recommendation ITU-R P.1411 over rooftops path loss model matches the measurements at 28 GHz and 38 GHz.

FIGURE 16

Comparison of the measurements and Rec. ITU-R P.1411 over rooftops at (a) 28 GHz and (b) 38 GHz

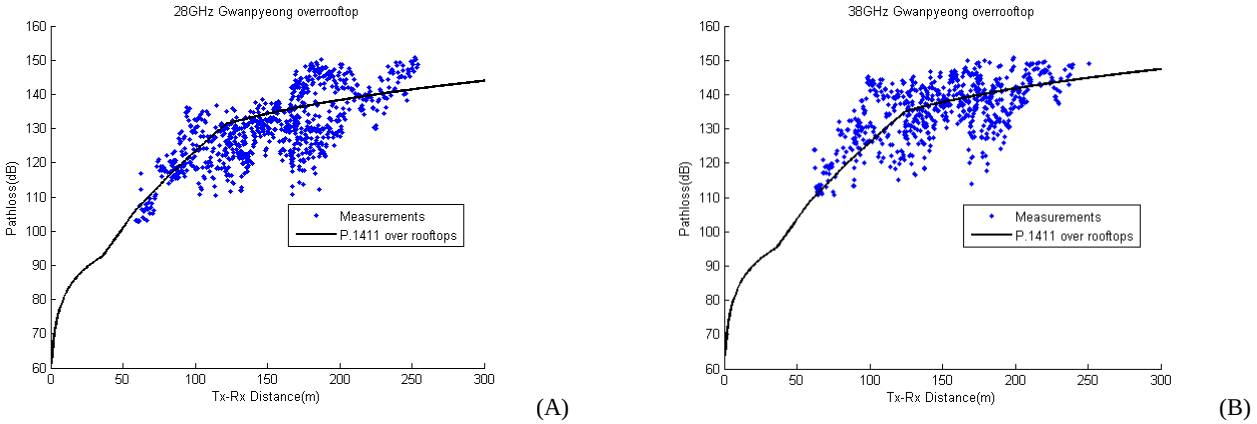

TABLE 10

Over rooftops parameter list

h_1	BS antenna height (m)	30
h_2	MS antenna height(m)	1.7
h_r	Average building height(m)	11
w	Average distance between buildings (m)	10
φ	Angle of street orientation(degree)	45
d_{RD}	BS-MS separation at the boundary between the reflected and diffracted wave dominant regions (m)	121.86 (28 GHz) 125.07(38 GHz)

TABLE 11

RMS error of the measurements and P.1411 over rooftops path loss model

	28 GHz (dB)	**38 GHz (dB)**
Reflected wave dominant region	6.41	8.96
Reflected wave dominant region (28 GHz + 38 GHz)	7.77	
Diffracted wave dominant region	8.43	6.67
Diffracted wave dominant region (28 GHz + 38 GHz)	7.71	
All regions	7.97	7.41
All regions(28 GHz + 38 GHz)	7.73	

5.1.4.5 Conclusion

The results show that the reflected wave dominant region and diffracted wave dominant region are well matched with the measurements. In addition, a total RMS error of 7.73 dB is small enough that a higher frequency, up to 38 GHz, is applicable. As a result, it can be concluded that the Recommendation ITU-R P.1411 over rooftops path loss model can be applied up to 38 GHz.

5.1.5 Study 5: Delay spread, propagation in urban environments, below-rooftop and over-rooftop (Frequency bands: 25.5-28.5 GHz, 51-57 GHz, 67-73 GHz)

5.1.5.1 Executive summary

This section provides additional information for the rms delay spread values included in Recommendation ITU-R P.1411. This study focuses on the frequency ranges 25.5-28.5 GHz, 51-57 GHz and 67-73 GHz based on measurements made in urban high-rise and low-rise environments.

5.1.5.2 Background and proposal

Table 12 and Table 13 show the proposed rms delay spread values for over-rooftop and below-rooftop, respectively.

TABLE 12

Rms delay spread values for 25.5-28.5 GHz, 51-57 GHz and 67-73 GHz, over-rooftop case

Measurement conditions										**rms delay spread (ns)**	
Area	**Scenario**	***f*** **(GHz)**	h_1 **(m)**	h_2 **(m)**	**Range (m)**	**TX beam-width (degree)**	**RX beam-width (degree)**	**Time delay resolution (ns)**	**Polarization**	**50%**	**95%**
Urban high-rise	LoS	25.5-28.5	20	1.6	54-142	33	omni	0.5	VV	2.2(1)	6.9(1)
									HV	9.8(1)	28.1(1)
		51-57	18.2	1.6	50-180	56.3	18.4	0.5	VV/HH	1.6(1)	40.2(1)
									VH/HV	2.7(1)	37.9(1)
									VV/HH	7.5(2)	92.1(2)
									VH/HV	4.8(2)	81.9(2)
		67-73	18.2	1.6	50-180	40	14.4	0.5	VV/HH	1.7(1)	31.3(1)
									VH/HV	2(1)	19.2(1)
									VV/HH	6(2)	78.7(2)
		67-73	20	1.6	54-142	40	omni	0.5	VV	2	9.8
	NLoS	25.5-28.5	20	1.6	61-77	33	omni	0.5	VV	74.5	159.1

(1) Receiver antenna rotated around 360 degrees. The values represent when the bore-sight of receiver antenna is aligned to the direction of transmitter.

(2) Receiver antenna rotated in a step of 5º around 360 degrees. The value represents a directional delay spread when the bore-sight of receiver antenna is not aligned to the direction of transmitter.

TABLE 13

Rms delay spread values for 25.5-28.5 GHz, 51-57 GHz and 67-73 GHz, below-rooftop case

Measurement conditions										rms delay spread (ns)	
Area	**Scenario**	***f*** **(GHz)**	h_1 **(m)**	h_2 **(m)**	**Range (m)**	**TX beam-width (degree)**	**RX beam-width (degree)**	**Time delay resolution (ns)**	**Polarization**	**50%**	**95%**
Urban low-rise	LoS	25.5-28.5	3	1.6	18-140	33	Omni	0.5	VV	3.5	43.6
									HV	8.7	57
		51-57	3	1.6	11-180	56.3	18.4	0.5	VV/HH	0.74(1)	3(1)
									VH/HV	1.7(1)	7.5(1)
									VV/HH	11.2(2)	72.9(2)
									VH/HV	8.5(2)	40.9(2)
		67-73	3	1.6	11-180	40	14.4	0.5	VV/HH	0.6(1)	3.5(1)
									VH/HV	1.6(1)	5.9(1)
									VV/HH	8.9(2)	80(2)
									VH/HV	5(2)	39.8(2)
			3	1.6	18-140	40	Omni	0.5	VV	2.6	36
	NLoS	25.5-28.5	3	1.6	40-84	33	Omni	0.5	VV	13.4	30.3
		67-73	3	1.6	40-84	40	Omni	0.5	VV	10	23.7

(1) Receiver antenna was rotated around 360 degrees in measurements. The value represents a directional delay spread when the bore-sight of receiver antenna is aligned to the direction of transmitter.

(2) Receiver antenna was rotated in a step of 5º around 360 degrees in measurements. The value represents a directional delay spread when the bore-sight of receiver antenna is not aligned to the direction of transmitter.

5.1.5.3 Measurement setup and procedure

To study the radio channel in these wave bands, a custom designed radio channel sounder capable of measuring with two transmit and two receive antennas has been designed [1] and used for measurements in an outdoor environment with a transmit antenna height at ~3 m for below roof top measurements and 18.2 m for above roof top measurements. The receiver antenna height was set at 1.6 m for all the measurements.

In a first set of measurements, horn antennas were used at the receiver with a beam width (18.4º in the E plane and 19.7º in the H plane at 50 GHz and 14.4º in the E plane and 15.4º in the H plane at 67.5 GHz). At the transmitter two horn antennas with beam widths (56.3º in the E plane and 51.4º in the H plane at 50 GHz and 40º in the E plane and 38º in the H plane at 67.5 GHz). To perform dual polarisation measurements, a twist was used at one of the transmit channels and another at one of the receive channels. To enable LoS measurements (including both cases where the bore-sight of the receive antenna is aligned and not aligned to the direction of the transmitter) the receiver was mounted on a turntable which was rotated in 5 degree steps. The measurements were performed with a 6 GHz bandwidth with a 305 Hz waveform repetition frequency and data were acquired over 1 second for each angle of rotation. Measurements were performed in two frequency bands: 51-57 GHz and 67-73 GHz along a number of routes in a low rise urban environment which included street canyons, open squares, pedestrian paths and road side scenarios. The data were analysed with a 2 GHz

bandwidth, to give a 0.5 ns time delay resolution and the power delay profiles from all angles of rotation were used to estimate the rms delay spread in the two frequency bands for 20 dB threshold.

In a second set, measurements were performed with dual polarised antennas at the transmitter and an omni-directional antenna at the receiver with vertical polarisation. At the transmitter two horn antennas with beam widths (40º in the E-plane and 38º in the H-plane) were used in the 67-73 GHz band with a twist at one of the transmit channels. In addition, a new set of dual polarised transmitters and two receivers were designed and implemented to perform measurements in the 25.5-28.5 GHz band. The transmit antenna has a 3 dB beam width of ~36º in the H-plane and 33º in the E-plane and the receive antenna was omni-directional. The measured environments include above rooftop and below roof top in both residential and low rise urban environments. The measurements were performed in both line of sight and non-line of sight where the transmitter was placed around the corner of a street. The data were systematically collected by moving the receiver trolley over consecutive 1 m intervals and the power delay profiles were then obtained by dividing the 1 m data into five sections. The data were analysed with 2 GHz bandwidth to give a 0.5 ns time delay resolution and the power delay profiles were used to estimate the rms delay spread in the two frequency bands for 20 dB threshold using the method defined in Recommendation ITU-R P.1407.

Figure 17 shows some of the measured environments.

FIGURE 17

View of the measured environment (a) above rooftop, (b) below rooftop

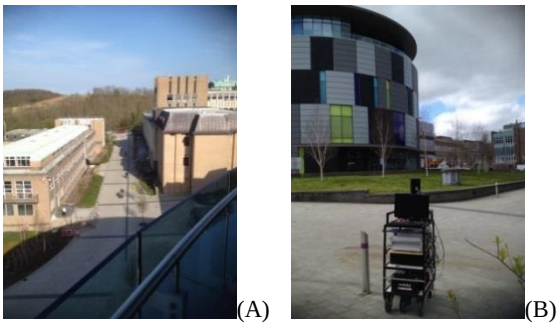

(A) (B)

5.1.5.4 Validation results

For the first set of experiments described in the previous section, Table 14 gives the parameters of the rms delay spread for the 51-57 GHz and 67-73 GHz bands for the co-polar and cross polar antennas for the LoS case (where the bore-sight of receiver antenna is not aligned to the direction of transmitter) for a 20 dB threshold from the maximum of the power delay profile in the street canyon and open square environment.

TABLE 14

Rms delay spread (ns) for LoS
(Tx and Rx antenna directions not aligned; street canyon and open square)
(a) 52 GHz (b) 68 GHz

(a)

CDF %	VV	VH	HV	HH
50%	6.07	9.88	16.56	3.66
95%	20.98	86.44	139.48	67.62

(b)

CDF %	VV	VH	HV	HH
50%	3.39	10.16	12.43	5.53
95%	9.13	132.96	166.87	20.18

The data from all the below the roof top measured scenarios were then combined together and the cumulative distribution function (CDF) generated for each polarisation for the two frequency bands. The co-polarised (VV and HH) and cross-polarised (VH and HV) data for each of the two frequency bands were then combined as shown in Fig. 18. Similarly the combined data for the over roof top were used to generate CDF's for the LoS and NLoS as in Fig. 19.

FIGURE 18

CDF of rms delay spread for LoS and "NLoS" (i.e. LoS but with Tx-Rx antenna directions not aligned) for below the roof top scenario (a) 51-57 GHz, (b) 67-73 GHz

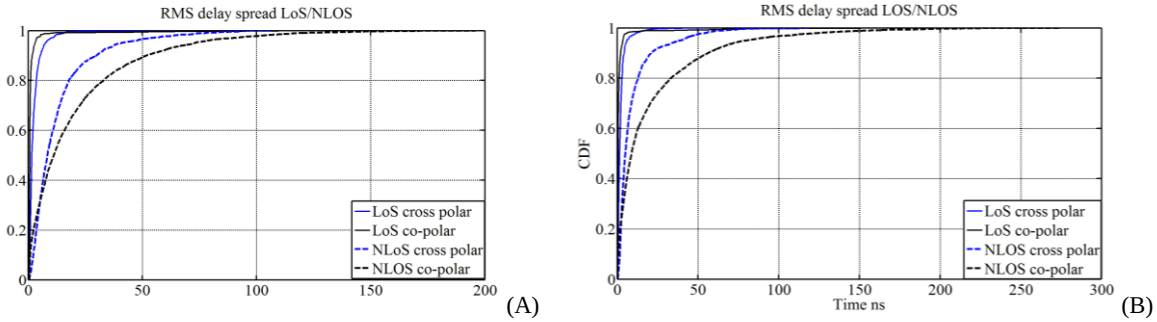

FIGURE 19

CDF of rms delay spread for LoS and "NLoS" (i.e. LoS but with Tx-Rx antenna directions not aligned) for over the roof top scenario (a) 51-57 GHz, (b) 67-73 GHz.

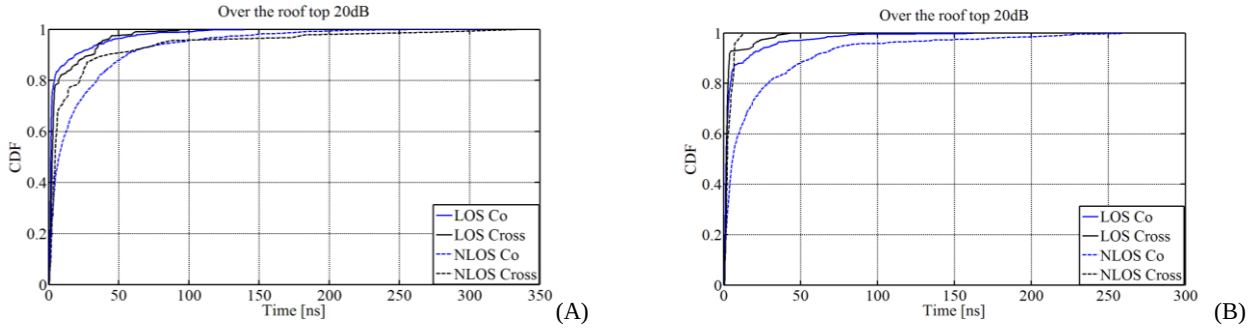

For the second set of experiments described in the previous section, Fig. 20 displays the CDF of the rms delay spread obtained from all the measured locations below rooftop environments for the two bands (with VV at 67-73 GHz and VV co-polarised and HV cross-polarised in the 25.5-28.5 GHz band). Similarly, Fig. 21 displays the delay spread for the above roof top scenario for LoS and only the VV in the 25.5-28.5 GHz for the NLoS scenario due to the limited number of data points that met the 20 dB threshold.

FIGURE 20

Rms delay spread for 20 dB threshold in the 25.5-28.5 GHz and 67-73 GHz bands for the (a) LoS, (b) NLoS scenarios for below roof top

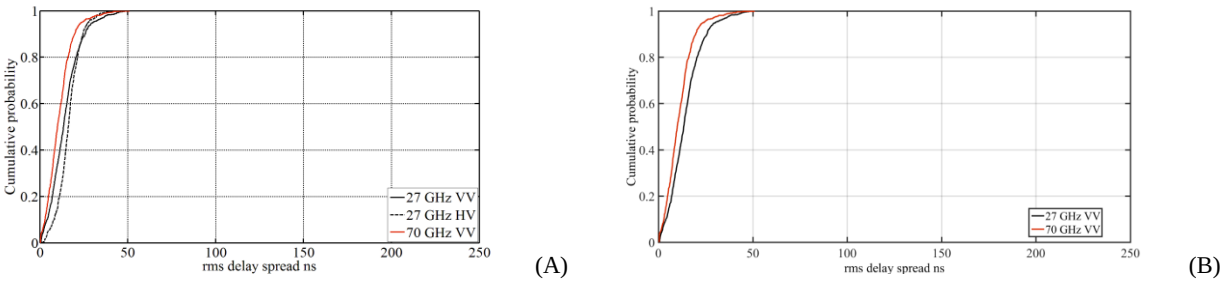

FIGURE 21

Rms delay spread for 20 dB threshold in the 25.5-28.5 GHz and 67-73 GHz bands for the (a) LoS, (b) NLoS scenarios for above roof top

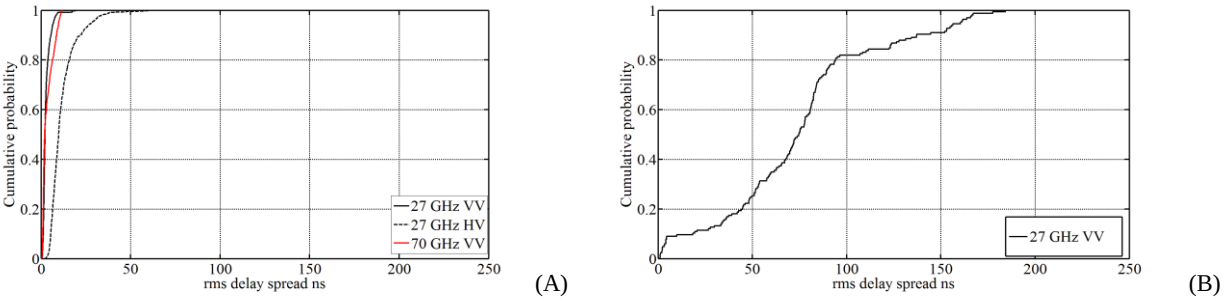

The 50% and 95% values were estimated from the CDF's and these are summarised in Table 13.

5.1.5.5 Conclusion

These results and analyses were used as basis to propose the new rms delay spread values.

5.1.5.6 References

[1] Salous, Sana, Feeney, Stuart, Raimundo, Xavier & Cheema, Adnan (2016). Wideband MIMO channel sounder for radio measurements in the 60 GHz band. *IEEE Transactions on Wireless Communications* **15**(4): 2825-2832.

5.1.6 Study 6: Delay spread, propagation in urban environments, below-rooftop (Frequency bands: 28, 38 GHz)

5.1.6.1 Executive summary

This section provides additional information for the rms delay spread values included in Recommendation ITU-R P.1411. This study focuses on the frequency bands 28 GHz and 38 GHz based on measurements made in urban low-rise and very high-rise environments.

5.1.6.2 Background and proposal

Table 15 shows the proposed rms delay spread values.

TABLE 15

Rms delay spread values for 28 GHz and 38 GHz, below-rooftop case

Measurement conditions										rms delay spread (ns)	
Area	**Scenario**	***f*** **(GHz)**	h_1 **(m)**	h_2 **(m)**	**Range (m)**	**TX beam-width (degree)**	**RX beam-width (degree)**	**Time delay resolution (ns)**	**Polarization**	**50%**	**95%**
Urban low-rise	LoS	28	4	1.5	100-400	30	10	2	VV	1.9(1)	5.9(1)
		38	4	1.5	50-400	30	10	2	VV	1.2(1)	4.8(1)
		28	4	1.5	90-350	30	10	2	VV	48.5(2)	112.4(2)
		38	4	1.5	90-250	30	10	2	VV	25.9(2)	75.0(2)
Urban very high-rise	LoS	28	4	1.5	50-350	30	10	2	VV	1.7(1)	7.8(1)
		38	4	1.5	20-350	30	10	2	VV	1.6(1)	7.4(1)
	NLoS	28	4	1.5	90-350	30	10	2	VV	67.2(2)	177.9(2)
		38	4	1.5	90-350	30	10	2	VV	57.9(2)	151.6(2)

(1) Receiver antenna was rotated around 360 degrees in measurements. The value represents a directional delay spread when the bore-sight of receiver antenna is aligned to the direction of transmitter.

(2) Receiver antenna was rotated around 360 degrees in measurements. The value represents a directional delay spread regardless of antenna alignment.

5.1.6.3 Measurement setup and procedure

The delay spread measurement campaign has been performed using the millimetre wave channel sounder, which was developed by Electronics and Telecommunications Research Institute (ETRI), Korea [1]. Figure 22 is a wideband channel sounder for measuring the spatial and temporal channel characteristics of 500 MHz bandwidth in the 28/38 GHz band. The RF modules including antenna can rotates from 0° to 360° horizontally and tilts from −90° to 90° vertically. Table 16 shows detailed specifications of the channel sounder.

FIGURE 22

28/38 GHz wideband channel sounding system

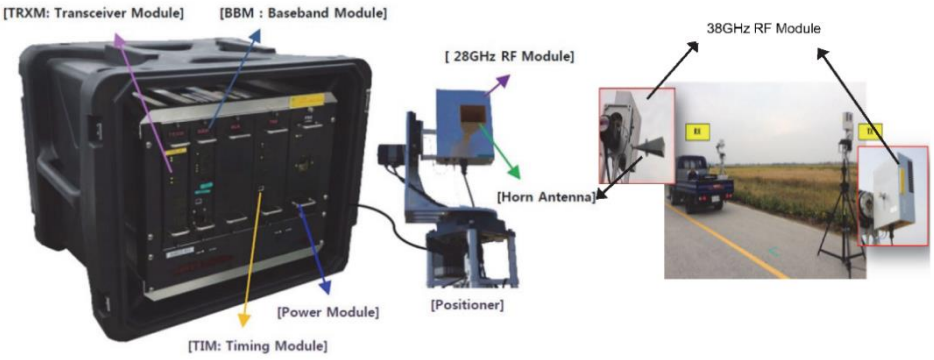

TABLE 16

Specifications of the channel sounder

Description	Specifications
Carrier Frequency	28/38 GHz
Channel Bandwidth	500 MHz
PN Code length	4 095 chips
Sliding factor	12,500
Receiver chip rate	499.96 MHz
Maximum TX Power	29/21 dBm
Automatic Gain Control range	< 60 dB

The measurement campaign was done in Seoul and Daejeon of Korea. Seoul is an urban very high-rise environment, which has a downtown area with 50-200 m height buildings and 54 m wide streets. Daejeon is an urban low-rise environment, which has a small town area with 3~5 story buildings (11~14 m height) and 18 m wide streets.

Directional horn antennas were used for 28/38 GHz. They have a gain of 15.4 dBi (30° HPBW, Half Power Beam Width) at TX and 24.4 dBi (10° HPBW) at RX for 28 GHz, and 16.4 dBi (30° HPBW) antenna at TX and 24.6 dBi (10° HPBW) antenna at RX for 38 GHz. The azimuthal rotation step size was 10° for 28 GHz and 9° for 38 GHz from 0° to 360°. The elevation range was –10° to 10° for both bands. The TX antenna was installed at a height of 4 m (assumed lamp-post level) and the RX antenna at 1.5 m for both bands

The measurements were taken at 17 positions (7 LoS/11 NLoS) at the Seoul site and 21 positions (6 LoS/15 NLoS) at the Daejeon site for 28 GHz, and 35 positions (17 LoS/18 NLoS) at the Seoul site and 26 (9 LoS/17 NLoS) positions at the Daejeon site for 38 GHz. In the NLoS case, each position has 36 × 3 = 108 samples for 28 GHz and 40 × 3 = 120 samples for 38 GHz. However, in the LoS case, it refers to the case when the antennas are aligned; each position has 3 × 3 = 9 samples for both bands. So the positions for LoS and NLoS are different from each other at 28/38 GHz.

5.1.6.4 Validation results

Figure 23 shows CDFs of all measurement results at each site and at each band. The typical rms delay spread values of 50% and 95% of cumulative probability are shown in Table 15. The threshold value of 20 dB is used for the rms delay spread calculation.

FIGURE 23

Cumulative probability of RMS delay spread in urban environments: (a) CDF of LoS (b) CDF of NLoS

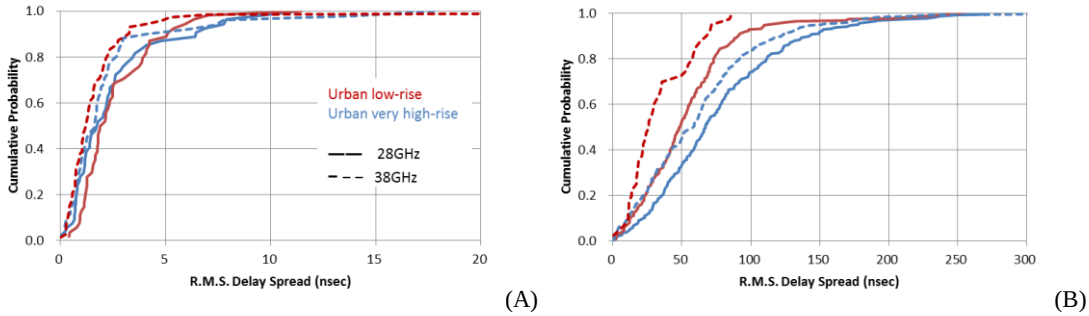

(A) (B)

5.1.6.5 Conclusion

These results and analyses were used as a basis to propose the new rms delay spread values.

5.1.6.6 References

[1] Jong Ho Kim, Y Yoon, Y. Chong and M Kim. "28 GHz Wideband Characteristics at Urban Area." Vehicular Technology Conference (IEEE 82nd VTC-Fall) 2015.

5.1.7 Study 7: Delay spread, propagation in urban environments, below-rooftop (Frequency bands: 29.3-31.5 GHz, 58.7-63.1 GHz)

5.1.7.1 Executive summary

This section provides additional information for the rms delay spread values included in Recommendation ITU-R P.1411. This study focuses on the frequency ranges 29.3-31.5 GHz and 58.7-63.1 GHz based on measurements made in urban low-rise environments.

5.1.7.2 Background and proposal

Table 17 shows the proposed rms delay spread values.

TABLE 17

Rms delay spread values for 29.3-31.5 GHz and 58.7-63.1 GHz, below-rooftop case

Measurement conditions										rms delay spread (ns)	
Area	**Scenario**	***f*** **(GHz)**	h_1 **(m)**	h_2 **(m)**	**Range (m)**	**TX beam-width (degree)**	**RX beam-width (degree)**	**Time delay resolution (ns)**	**Polarization**	**50%**	**95%**
Urban low-rise	LoS	29.3-31.5	3	1.3	6-60	35	35	0.45	VV/HH	1.5(1)	5(1)
									VH/HV	6(1)	14.3(1)
		58.7-63.1	2.4	1.5	20-200	15.4	15.4	0.22	VV	0.6(1)	1.2(1)
			3	1.6	6-60	15.4	2.2	0.9	VV	6.6(2)	40.7(2)

(1) Receiver antenna was rotated around 360 degrees in measurements. The value represents a directional delay spread when the bore-sight of receiver antenna is aligned to the direction of transmitter.

(2) Receiver antenna was rotated in a step of 5º around 360 degrees in measurements. The value represents a directional delay spread when the bore-sight of receiver antenna is not aligned to the direction of transmitter.

5.1.7.3 Measurement setup and procedure

To study the radio channel in the 60 GHz band, a custom designed radio channel sounder capable of measuring with two transmit and two receive antennas has been designed and used for measurements in an outdoor environment with a transmit antenna height of ~3 m and a receiver antenna height of 1.6 m. A lens antenna was used at the receiver with a narrow beam width (2.2 in the E plane and 2.6 in the H plane). The lens antenna was mounted on a turntable which was rotated in 5 degree steps. The transmission bandwidth used in the measurements was 4.4 GHz and the waveform repetition frequency was 1.2 kHz enabling Doppler measurements. The data were analysed with 1.1 GHz to evaluate rms delay spread for different angles of arrival. The transmitter antenna has a theoretical gain equal to 20.7 dB and 15.4º azimuthal angular width and the transmit power was 7 dBm. The data

were acquired with a 14 bit ADC in one second at each location while the receiver was stationary. Measurements were performed over a distance from 5 m up to ~ 60 m. The measurement environment is shown in Fig. 24 where the transmitter and receiver were in line of sight of each other but the receive antenna rotated to capture the variations as a function of angle of arrival.

The same environment was measured at 30 GHz with dual polarised antennas where the transmit antenna was mounted at about 3 m and the receiver antenna at 1.3 m above ground. The data were analysed for a 20 dB threshold, for both co-polarised and cross polarised antennas.

FIGURE 24

Measurement environment

(a) Receiver trolley with lens antenna

(b) Transmitter antenna

(c) Measurement path

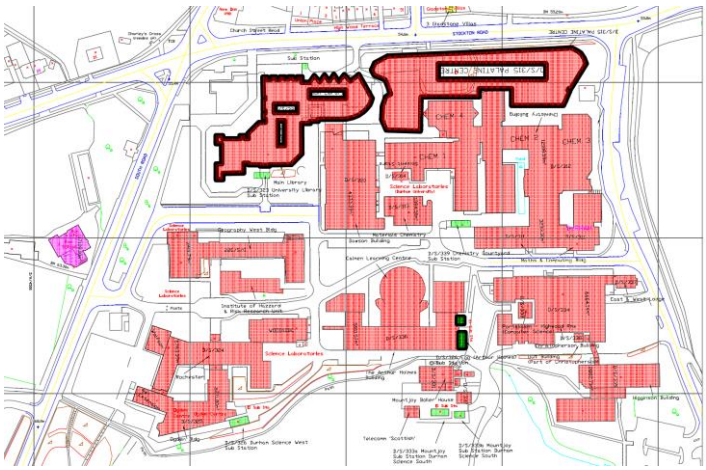

(d) Plan of measurements: green: transmitter, purple: receiver

5.1.7.4 Validation results

Figure 25 displays an example of the measured power delay profile for one location at 60 GHz over the 73 angular positions. The dynamic range for most of the measured profiles exceeded 20 dB hence the rms delay spread channel parameters were estimated for a threshold level of 20 dB down from the peak. Figure 26 displays the CDF for the rms delay results which are summarised in Table 18 for the 95% and for the 50% value as obtained from the CDF curve.

FIGURE 25

Power delay profile at a single location as a function of angle of rotation

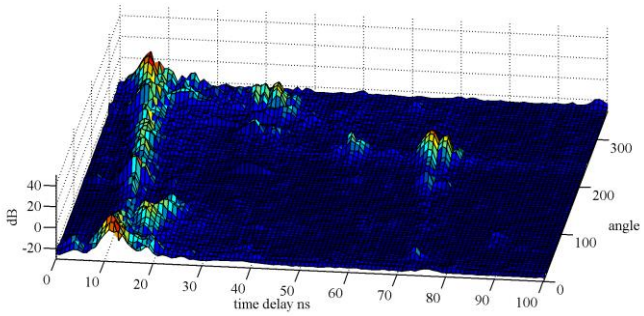

FIGURE 26

CDF of rms delay spread at 60 GHz for the combined data from the all the angles

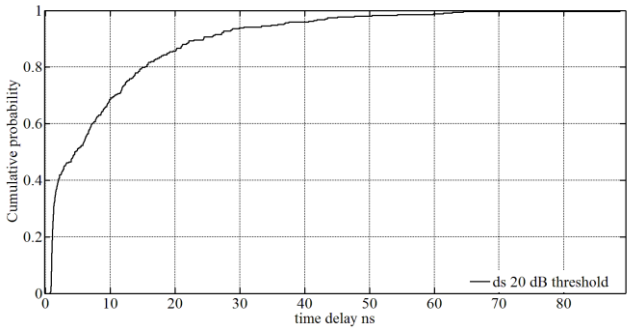

TABLE 18

Summary of rms delay spread scaled from Fig. 26 for 20 dB threshold value

	From all angles
	20 dB threshold
95% CDF value	36.8 ns
50% CDF value	4.7 ns

The resulting CDF for 30 GHz is displayed in Fig. 27. Table 19 summarises the 50% and 95% for all the data regardless of polarisation.

FIGURE 27

rms delay spread for 20 dB threshold for co-polarised and cross polarised transmission

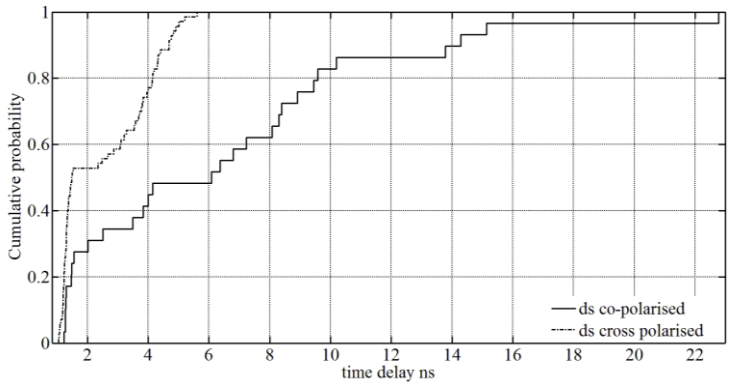

TABLE 19

Summary of rms delay results for 50% and 95% values

	Co-polarised	Cross-polarised	All data
95%	15.2 ns	5 ns	10.2
50%	6 ns	1.5 ns	2.7

5.1.7.5 Conclusion

These results and analyses were used as basis to propose the new rms delay spread values.

5.1.8 Study 8: Prediction models of delay and angular spreads as a function of antenna beamwidth (Frequency bands: 28 GHz, 38 GHz)

5.1.8.1 Executive summary

This section provides additional information for the prediction models of rms delay spread and angular spreads as a function of antenna beamwidth, included in Recommendation ITU-R P.1411. This study focuses on the frequency ranges 28 GHz and 38 GHz based on measurements made in urban low-rise and very high-rise environments.

5.1.8.2 Background and proposal

The rms delay spread (*DS*) depends on half-power beamwidth of antenna θ (degree):

$$DS(\theta) = \alpha \times \log_{10} \theta \tag{10}$$

where α is a coefficient of rms delay spread and the range of θ is defined as $10^{o} \leq \theta \leq 120^{o}$. Table 20 lists the typical values of the coefficients and standard deviation σ based on each measurement condition. The coefficients of delay spread represent cases when the boresights of antennas were aligned to have maximum receiving power in LoS and NLoS situations, respectively.

TABLE 20

Typical coefficients for rms delay spread

Measurement conditions								Coefficients of rms delay spread	
f **(GHz)**	**Environment**	**Scenario**	h_1 **(m)**	h_2 **(m)**	**Range (m)**	**TX beamwidth (degree)**	**RX beamwidth (degree)**	**α**	**σ (ns)**
28	Urban low-rise	LoS	4	1.5	20-400	30	10	2.32	5.83
		NLoS			20-300			35.1	43
	Urban very high-rise	LoS			40-300			3.67	7.07
		NLoS			80-340			43.19	38.62
38	Urban low-rise	LoS	4	1.5	20-400	30	10	2.14	7.3
		NLoS			20-200			30.01	35.51
	Urban very high-rise	LoS			20-340			1.61	3.15
		NLoS			80-210			26.93	27.95

The rms angular spread *AS* depends on the half power beamwidth of an antenna θ (degree):

$$AS(\theta) = \alpha \times \theta^{\beta} \text{ degree} \quad (11)$$

where α and β are coefficients of rms angular spread and the range of θ is defined as $10^{o} \leq \theta \leq 120^{o}$. Table 21 lists the typical values of the coefficients and standard deviation σ based on each measurement condition. The coefficients of angular spread represent cases when the boresights of antennas are aligned to have maximum receiving power in LoS and NLoS situations, respectively.

TABLE 21

Typical coefficients for rms angular spread

Measurement conditions								Coefficients of rms angular spread		
f **(GHz)**	**Environment**	**Scenario**	h_1 **(m)**	h_2 **(m)**	**Range (m)**	**TX beam-width (degree)**	**RX beam-width (degree)**	α	β	σ **(degree)**
28	Urban low-rise	LoS	4	1.5	20-400	30	10	1.84	0.39	2.1
		NLoS			20-300			0.42	0.84	3.42
	Urban very high-rise	LoS			40-300			1.98	0.34	1.45
		NLoS			80-340			0.38	0.89	2.47

TABLE 21 (*end*)

Measurement conditions								Coefficients of rms angular spread		
f **(GHz)**	**Environment**	**Scenario**	h_1 **(m)**	h_2 **(m)**	**Range (m)**	**TX beam-width (degree)**	**RX beam-width (degree)**	α	β	σ **(degree)**
38	Urban low-rise	LoS	4	1.5	20-400	30	10	1.76	0.36	1.5
		NLoS			20-200			0.33	0.91	3.39
	Urban very high-rise	LoS			20-340			1.7	0.38	1.95
		NLoS			80-210			0.23	1.03	3.3

5.1.8.3 Measurement setup and procedure

The measurement campaigns have been performed using the millimetre-wave Band Exploration and Channel Sounder (mBECS) system, which was developed by ETRI, Korea. The mBECS system is a wideband channel sounder for measuring the spatial and temporal characteristics of a 500 MHz bandwidth channel at the centre frequency of 28 GHz [1] and 38 GHz. It is noted that the channel sounder can measure the multipath distribution characteristics using a 500 MHz wideband probing signal with a temporal resolution of 2 ns and an angular domain of 1 degree. Table 22 lists a detailed specification of the channel sounder.

TABLE 22

Specifications of ETRI's channel sounder

System parameters		Specifications
Centre frequency		28 / 38 GHz
Channel Bandwidth		500 MHz
PN code length of probing signal		4095 chips
Maximum TX power (w/o antenna)	28 GHz	29 dBm
	38 GHz	21 dBm
Multipath resolution		2 ns
HPBW of pyramidal horn antenna and gain	28 GHz	10^o(24.4 dBi), 30^o (15.4 dBi)
	38 GHz	10^o(24.6 dBi), 30^o (16.4 dBi)

The measurement campaign has been carried out in a typical urban low-rise and an urban very high-rise environment, respectively as follows:

- Site 1 (Urban low-rise, Daejeon): Urban area with low-rise buildings (3-5 storey, 11-14 m height) which are located at both side of a 2- lane road (18 m wide).
- Site 2 (Urban very high-rise, Seoul): Urban area with skyscrapers and very high buildings (50-120 m height) which are located at both side of a 12-lane road (50 m wide).

Figure 28 shows the layouts of measurement places on which locations of a transmitter (TX) and a receiver (RX) are marked. During measurement, the location of each TX was fixed, and the RXs were positioned at line-of-sight (LoS) and non-line-of-sight (NLoS) situations. In the TX side, a 30^o half-

power-beam-width (HPBW) horn antenna was installed at the height of 4 m above the ground. On the other hand, a 10º HPBW antenna was installed in the RX side at the height of 1.5 m, and the bore-sight of antenna was rotated with a step size of 10º in azimuth from 0º to 350º.

FIGURE 28

Second measurement campaign locations: (a) Site 1 (urban low-rise) (b) Site 2 (urban very high-rise)

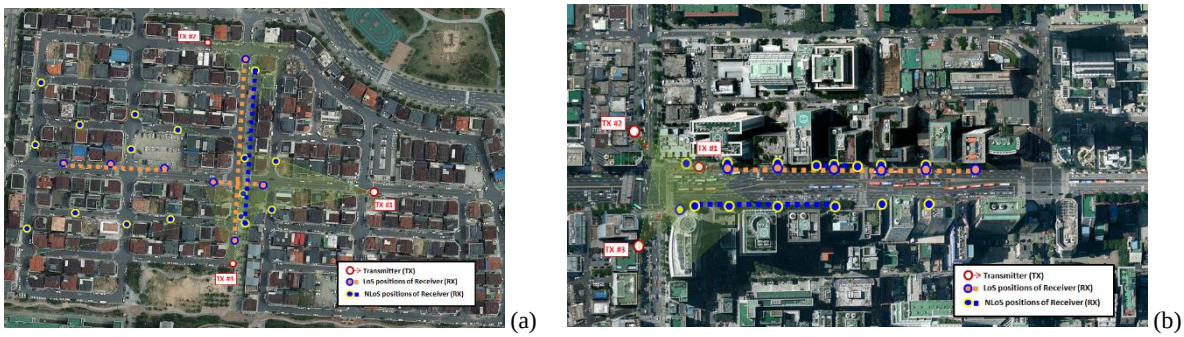

(a) (b)

In order to calculate the directional rms delay spread (DS) with respect to the beamwidth of the receive antenna, the RX antenna in the measurements is rotated by a certain number of steps (N = 36) in azimuth directions. Therefore, each channel impulse response (CIR) is collected at a different bore-sight direction, respectively. From measured CIRs, it is possible to derive a directional rms delay spread (DS) with the following steps [2]-[4].

- The power azimuth-delay spectrum (PADS) is calculated by using the Bartlett beamforming technique [5] for decoupling the influence of the antenna radiation pattern from measured CIRs.
- Define a power angular window (PAW) depending on the antenna's beamwidth to search.
- Search an angular range having the highest power using the PAW in the 3-dimentional PADS i.e. power, delay and angle of arrival domain.
- The power delay profile (PDP) is obtained by summation in the angular domain within the observed angular range in the PADS.
- Calculate a DS from multipath components which are only within a given threshold level in the PDP.

The threshold was set to 20 dB to determine received multipath components since the power delay profiles have enough peak-to-spurious dynamic range to ensure the integrity of the results.

The range of PAW was given from 10º to 120º. The directional rms delay spread values of each LoS and NLoS case were derived separately. It is noted that a delay spread is calculated within the observed angular range in which the highest received power is obtained. That is, it can be understood that the beam alignment between TX and RX is well established.

For the calculation of the directional rms angular spread (AS) with respect to the beamwidth of ther receive antenna, the AS can be easily derived from the power azimuth spectrum (PAS). The PAS is calculated from the PADS by summation in the delay domain [2]-[4]. To calculate the directional rms AS, the threshold level was set to 20 dB.

5.1.8.4 Validation results

Figure 29 shows the DS curves obtained from measurement data at 28 and 38 GHz for the LoS and NLoS case. To obtain the best fitted curves, mean values of rms DS for each beamwidth are utilized.

FIGURE 29

Measurement results of rms delay spread for 28 and 38 GHz: (a) LoS case (b) NLoS case

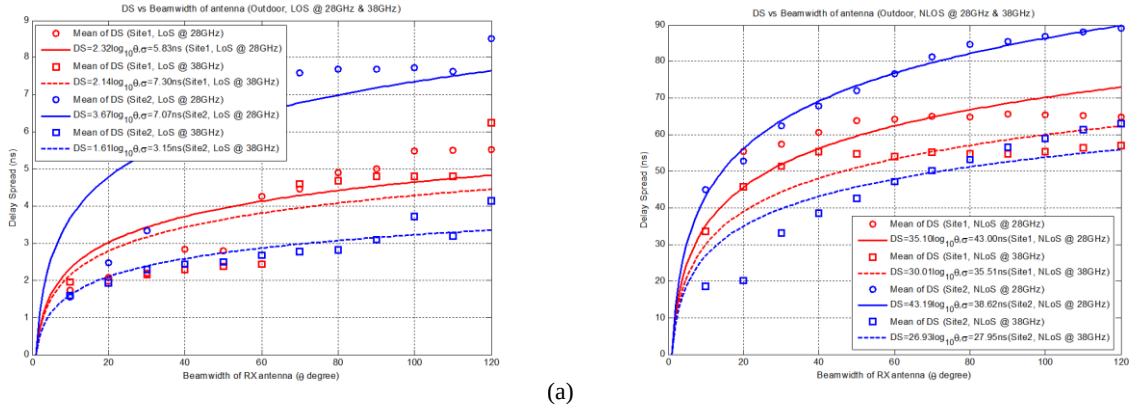

(a) (b)

Based on the measurement results, the following observations can be made:

– The DS has a strong dependency on the antenna beamwidth. The wider beamwidth has the larger DS.

– The DSs in NLoS case is larger than the values of LoS case.

– These particular properties are very similar to the measurement results in a previous contribution.

– In both LoS and NLoS cases, the curves of 28 GHz are higher than 38 GHz

The rms AS with respect to θ with the standard deviation σ is given by equation (10).

Figure 30 shows the AS curves obtained from measurement data at 28 and 38 GHz for LoS and NLoS cases. To obtain the best fitted curves, mean values of rms AS for each beamwidth are utilized.

FIGURE 30

Measurement results of rms angular spread for 28 and 38 GHz: (a) LoS case (b) NLoS case

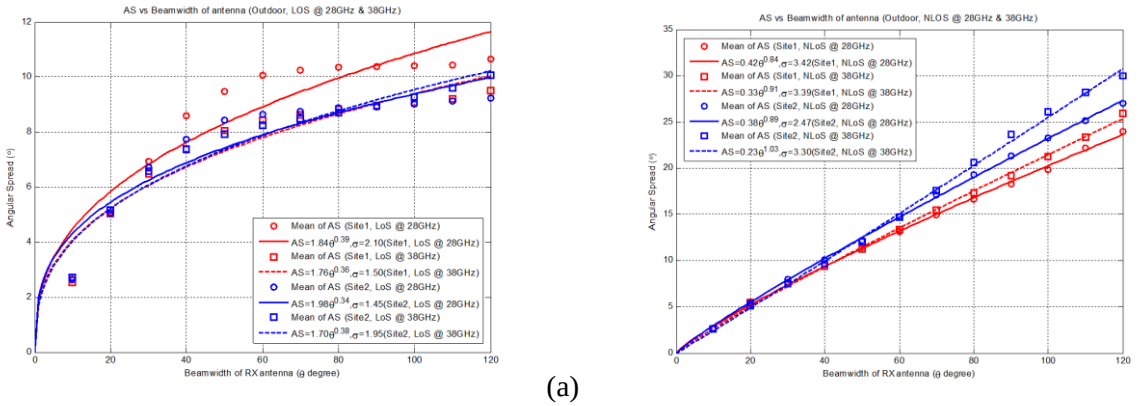

(a) (b)

From measurement results, the following can be observed.

– The AS shows a strong dependency on the antenna beamwidth as similar to the DS. The wider beamwidth of the antenna is the larger angular spread.

– Frequency dependency of AS is not clearly seen in both LoS and NLoS cases.

– At NLoS case, the angular spread monotonously increases from a narrow beam to a wider beam.

– These particular properties are very similar to the measurement results in a previous contribution.

The rms AS with respect to θ with the standard deviation σ is given by equation (11).

5.1.8.5 Conclusion

This study presented prediction methods and coefficients for delay spread and angular spread associated with antenna beamwidth based on additional measurement results in the 28 and 38 GHz bands. The results and analyses show that both delay spread and angular spread have a strong dependency on the antenna beamwidths.

5.1.8.6 References

[1] H.-K. Kwon et al., "Implementation and Performance Evaluation of mmWave Channel Sounding System", in Proc. IEEE AP-S 2015, July 2015.

[2] M.-D. Kim et al., "Directional Multipath Propagation Characteristics based on 28 GHz Outdoor Channel Measurements," in Proc. The European Conference on Antennas and Propagation (EuCAP), April, 2016.

[3] M.-D. Kim et al., "Directional Delay Spread Characteristics based on Indoor Channel Measurements at 28 GHz," PIMRC 2015, pp. 505–509, Aug. 2015.

[4] M.-D. Kim et al., "Investigating the Effect of Antenna Beamwidth on Millimeter-wave Channel Charaterization," accepted in 2016 The URSI Asia-Pacific Radio Science Conference (AP-RASC), August, 2016.

[5] M. Bartlett, "Smoothing Periodograms from Time-Series with Continuous Spectra", Nature, vol. 161, 1948.

5.1.9 Study 9: Cross-polarization discrimination (Frequency bands: 51-57, 67-73 GHz)

5.1.9.1 Executive summary

This section provides additional information related to the cross-polarization discrimination values included in Recommendation ITU-R P.1411 for the 51-57 GHz and 67-67 GHz bands.

5.1.9.2 Background and proposal

In the millimetre band the measured cross-polarization characteristics for the bands 51-57 GHz and 67-73 GHz in a low rise urban environment has a median value of 16 dB for the LoS component with 3 dB variance and 9 dB for NLoS paths with a 6 dB variance.

5.1.9.3 Measurement setup and procedure

To study the radio channel in the millimetre wave band, a custom designed radio channel sounder capable of measuring with two transmit and two receive antennas has been designed [1] and used for measurements in an outdoor environment in a low rise urban environment with the transmit antenna height being either below the roof top at 3 m or above the roof tops at 18.2 m and a receiver antenna height of 1.6 m. Horn antennas were used at the receiver with a beam width (18.4^o in the E plane and 19.7^o in the H plane at 50 GHz with 19 dB gain and 14.4^o in the E plane and 15.4^o in the H plane with 21 dB gain at 67.5 GHz). At the transmitter two horn antennas were used and these have beam widths (56.3^o in the E plane and 51.4^o in the H plane with 11 dB gain at 50 GHz and 40^o in the E plane and 38^o in the H plane with 13.5 dB gain at 67.5 GHz). To perform dual polarisation measurements, a twist was used at one of the transmit channels and another at one of the receive channels. To enable LoS, NLoS and the synthesis of non-directional propagation, the receiver was mounted on a turntable which was rotated in 5 degree steps. The measurements were performed with a 6 GHz bandwidth at 305 Hz waveform repetition frequency and data were acquired over 1 second for each angle of rotation. Measurements were performed in two frequency bands: 51-57 GHz and 67-73 GHz along a number of routes as in Table 23 with the corresponding routes highlighted in Fig. 31(a) and (b).

TABLE 23

Measurements Scenarios

Outdoor Scenarios	Location/Route	Transmitter level
Urban low rise	Street canyon, open square, hilly terrain (R1d), (R1b) (R1c) and (R1a)	Over Rooftop Tx 18.2 m Rx 1.6 m
	Street canyon and open square (R2)	Below Rooftop Tx 3 m Rx 1.6 m
	Roadside terminals (R4)	
	Hilly terrain (R7)	
	Pathway with vegetation either side (R3a)	
	Car park (R8) and (R3c)	

FIGURE 31

Routes of measurement scenarios (a) routes 1-3 and 8, (b) routes 4 and 7

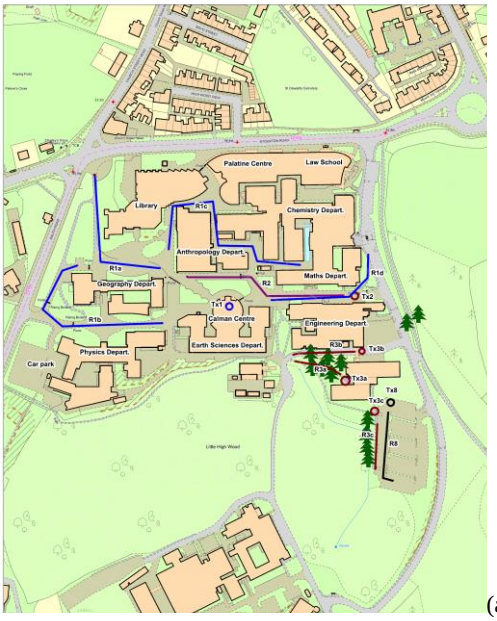

(a)

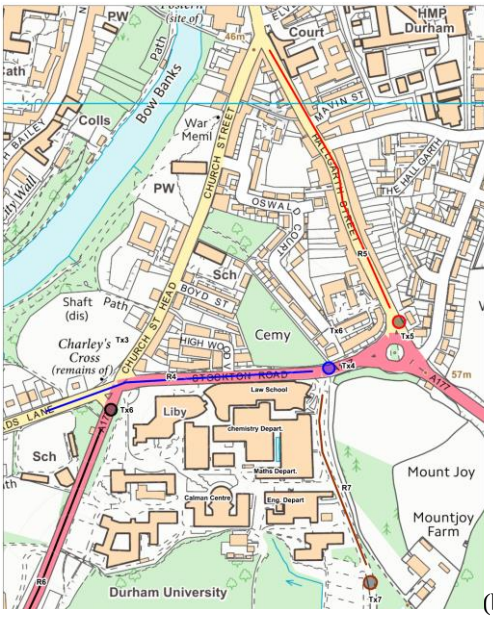

(b)

Dual polarised power delay profiles in the measured environments for the 51-57 GHz and 67-73 GHz bands were generated. The power delay profiles were then used to estimate the received power by taking the area under the profile for each angle.

Following full calibration of the data, the received power was then used to estimate the path loss for the following antenna beam widths:

1 Strongest beam: The maximum received power representing the main beam of the receive antenna. When unobstructed by vegetation or buildings it represents the LoS.

2 40^{o} main beam power: The received power for a 40^{o} beam width around the maximum received power.

3 NLoS: The sum of the received power from the remaining angles outside the 40^{o} main beam.

4 360^{o} (omni-directional): The sum from all the azimuthal angles.

Since the antenna azimuthal beam width is larger than the rotational angular step, the path loss was adjusted for the additional antenna gain due to the overlap of the beam.

These were then used to estimate path loss coefficients for the different measurement scenarios. The scenario in Fig. 32 corresponds to route 2, which combines non-line of sight around the corner of the building and locations where the receiver antenna when pointed toward the transmitter was in the line of sight. For the LoS component path loss estimation, the NLoS data were filtered out.

FIGURE 32

Measurement environment for route 2 (street canyon and open square) indicated by the blue line

5.1.9.4 Validation results

Tables 24 to 28 give a summary of the results of path loss parameters for the dual polarised transmissions for the 51-56 GHz and 67-73 GHz frequency bands using equation (12) which corresponds to equation (12) in Recommendation ITU-R P.1411-8 with the additional term σ which represents the standard deviation of the fit, where *n* represents the path loss coefficient, L_o is the path loss at a reference distance, $d_o = 1$

$$PL(d) = L_o + 10nlog10\left(\frac{d}{d_o}\right) + L_{gas} + L_{rain} + \sigma\ dB \tag{12}$$

TABLE 24

Model parameters (street canyon and open square) (A) 51-57 GHz, (B) 67-73 GHz

(A)

Antenna polarisation	Strongest beam	Synthesised 40° beam width	Synthesised omni	Synthesised 320° back beam
	n, L_o, σ	n, L_o, σ	n, L_o, σ	n, L_o, σ
VH	2.38, 66.12, 2.40	2.33, 66.48, 2.15	2.21, 66.91, 1.86	2.31, 66.51, 2.12
VV	2.83, 40.90, 3.72	2.91, 38.88, 3.92	2.81, 39.79, 3.59	2.45, 54.01, 2.78
HH	2.23, 49.82, 3.56	2.24, 48.86, 3.69	2.15, 49.86, 3.22	1.66, 67.87, 2.09
HV	2.14, 71.56, 3.05	2.17, 70.28, 2.92	2.18, 68.90, 2.49	2.26, 74.05, 1.91

(B)

Antenna polarisation	Strongest beam	Synthesised 40º beam width	Synthesised omni	Synthesised 320º back beam
	n, L_o, σ	n, L_o, σ	n, L_o, σ	n, L_o, σ
VH	1.74, 85.99, 3.66	1.90, 83.16, 3.91	1.89, 81.58, 3.08	2.12, 79.87, 2.92
VV	2.16, 56.77, 3.76	2.20, 56.25, 3.81	2.11, 57.09, 3.42	1.72, 72.44, 2.31
HH	1.98, 59.97, 3.86	1.97, 60.39, 3.98	1.85, 61.91, 3.40	1.24, 83.50, 2.18
HV	1.42, 89.87, 3.72	1.61, 86.37, 3.94	1.73, 82.64, 3.06	2.00, 84.15, 2.10

TABLE 25

Model parameters (roadside terminals) (A) 51-57 GHz, (B) 67-73 GHz

(A)

Antenna polarisation	Strongest beam	Synthesised 40º beam width	Synthesised omni	Synthesised 320º back beam
	n, L_o, σ	n, L_o, σ	n, L_o, σ	n, L_o, σ
VH	1.66, 73.74, 2.15	1.64, 73.08, 2.09	1.83, 68.02, 1.92	1.89, 69.31, 2.29
VV	1.44 , 59.34, 1.82	1.55, 56.91, 1.40	1.56, 56.07, 1.31	1.67, 63.62, 1.01
HH	1.58, 57.65, 1.59	1.66, 55.46, 1.51	1.67, 54.99, 1.46	1.70, 65.82, 1.63
HV	1.46, 80.50, 2.12	1.46, 79.69, 2.35	1.74, 73.06, 1.84	2.19, 70.36, 1.68

(B)

Antenna polarisation	Strongest beam	Synthesised 40º beam width	Synthesised omni	Synthesised 320º back beam
	n, L_o, σ	n, L_o, σ	n, L_o, σ	n, L_o, σ
VH	2.53, 66.09, 4.03	2.73, 61.81, 3.62	2.81, 58.93, 3.22	3.19, 54.34, 3.53
VV	2.33, 50.47, 2.04	2.34, 49.79, 2.03	2.34, 49.20, 1.99	2.35, 58.13, 1.82
HH	1.65, 63.86, 2.38	1.78, 60.83, 1.98	1.81, 60.05, 1.93	2.27, 64.55, 1.76
HV	3.31, 50.73, 3.79	3.17, 52.78, 3.41	3.17, 51.38, 2.97	3.08, 59.57, 1.67

TABLE 26

Model parameters (hilly terrain with roadside vegetation), (A) 51-57 GHz, (B) 67-73 GHz

(A)

Antenna polarisation	Strongest beam	Synthesised 40º beam width	Synthesised omni	Synthesised 320º back beam
	n, L_o, σ	n, L_o, σ	n, L_o, σ	n, L_o, σ
VH	1.54, 79.94, 2.74	1.69, 77.60, 2.50	1.76, 75.16, 2.37	4.16, 40.89, 12.49
VV	2.70, 45.83, 4.60	2.87, 43.44, 5.08	2.85, 43.03, 4.92	2.93, 50.83, 4.85
HH	2.69, 45.01, 5.35	2.88, 42.07, 5.72	2.87, 42.05, 5.61	2.75, 57.10, 4.64
HV	1.58, 82.30, 4.03	1.83, 78.18, 3.45	1.87, 76.72, 3.26	2.42, 76.29, 5.94

(B)

Antenna polarisation	Strongest beam	Synthesised 40° beam width	Synthesised omni	Synthesised 320° back beam
	n, L_o, σ	n, L_o, σ	n, L_o, σ	n, L_o, σ
VH	1.86, 84.16, 3.31	2.03. 81.84, 3.71	2.01, 79.94, 2.31	2.65, 70.57, 5.01
VV	2.86, 45.71, 4.70	2.84, 46.77, 4.45	2.82, 46.43, 4.28	2.77, 56.62, 3.53
HH	2.78, 48.92, 4.54	2.86, 48.41, 4.74	2.81, 48.87, 4.54	2.29, 71.06, 3.27
HV	2.11, 79.13, 4.16	2.17, 78.27, 3.86	2.37, 73.21, 3.43	2.87, 70.92, 2.83

TABLE 27

Model parameters (pathway with vegetation either side) (A) 51-57 GHz, (B) 67-73 GHz

(A)

Antenna polarisation	Strongest beam	Synthesised 40° beam width	Synthesised omni	Synthesised 320° back beam
	n, L_o, σ	n, L_o, σ	n, L_o, σ	n, L_o, σ
VH	2.65, 64.53, 1.75	2.52, 65.63, 1.42	2.08, 70.48, 1.34	2.22, 69.15, 1.31
VV	3.95, 27.82, 4.71	3.76, 30.17, 4.27	3.49, 33.27, 3.85	2.66, 53.56, 2.73
HH	3.76, 30.15, 4.14	3.70, 30.74, 4.10	3.33, 35.38, 3.44	1.47, 73.45, 1.43
HV	2.03, 78.46, 1.55	1.89, 79.67, 1.34	1.76, 79.21, 1.13	1.64, 84.86, 1.42

(B)

Antenna polarisation	Strongest beam	Synthesised 40° beam width	Synthesised omni	Synthesised 320° back beam
	n, L_o, σ	n, L_o, σ	n, L_o, σ	n, L_o, σ
VH	1.95, 86.01, 2.52	1.93, 85.66, 2.00	1.69, 86.90, 1.62	2.42, 76.77, 0.97
VV	4.49, 23.62, 4.25	4.37, 25.94, 4.18	3.98, 31.07, 3.85	2.79, 57.38, 2.93
HH	4.01, 32.72, 4.53	3.88, 34.90, 4.31	3.54, 39.55, 3.80	1.43, 83.47, 1.25
HV	2.18, 81.78, 2.39	2.14, 81.62, 1.74	2.10, 79.68, 1.48	2.08, 83.67, 1.52

TABLE 28

Model parameters (car park) (A) 51-57 GHz, (B) 67-73 GHz

(A)

Antenna polarisation	Strongest beam	Synthesised 40° beam width	Synthesised omni	Synthesised 320° back beam
	n, L_o, σ	n, L_o, σ	n, L_o, σ	n, L_o, σ
VH	2.59, 61.31, 1.89	2.47, 62.39, 1.52	2.36, 62.51, 1.28	2.07, 69.83, 0.99
VV	1.93, 55.17, 2.21	1.93, 54.29, 2.08	1.87, 54.50, 1.90	1.66, 66.13 1.54
HH	1.75, 57.56, 1.27	1.79, 55.94, 1.24	1.76, 56.08, 1.12	1.61, 69.87, 1.36
HV	2.76, 63.52, 1.63	2.71, 63.26, 1.46	2.55, 63.78, 1.28	2.26, 73.09, 1.52

(B)

Antenna polarisation	Strongest beam	Synthesised 40° beam width	Synthesised omni	Synthesised 320° back beam
	n, L_o, σ	n, L_o, σ	n, L_o, σ	n, L_o, σ
VH	2.85, 66.99, 2.79	2.71, 68.68, 2.50	2.56, 69.17, 1.94	2.51, 73.02, 1.67
VV	2.45, 53.20, 1.92	2.34, 54.70, 2.04	2.33, 54.22, 1.95	2.31, 63.59, 1.60
HH	2.51, 53.96, 1.62	2.43, 54.90, 1.75	2.41, 54.95, 1.73	2.07, 72.55, 1.73
HV	3.32, 59.60, 2.37	3.18, 61.35, 2.29	2.95, 62.99, 1.95	2.42, 76.13, 2.05

Taking the parameters for the vertical to vertical polarisation the Tables indicate that the coefficients, the synthesised beam around the strongest component, and the synthesised omni-directional beam give values which are fairly close with about 18-19 dB increase in path loss for the synthesised NLoS beam. For all values, the co-polarised antennas give lower path loss than the cross-polarised antennas. To quantify this, the cross-polarisation was also estimated from the measurements and a CDF for cross-polar discrimination was generated. The CDF for one of the measured routes is shown in Fig. 33.

FIGURE 33

Cross polar discrimination for route shown in Fig. 32 in the frequency range 67-73 GHz

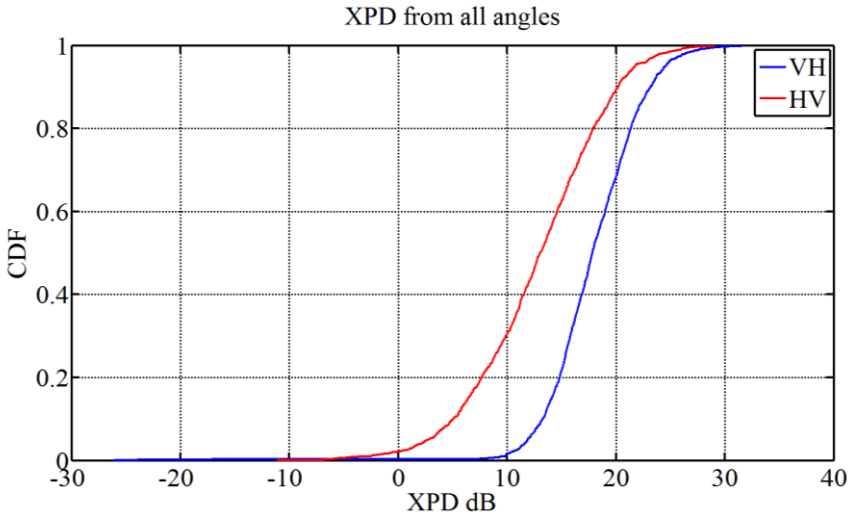

Table 29 summarises the cross polar discrimination XPD for the 50%, 90% and 95%. The Table shows the feasibility of using cross polarised antennas in the mm wave band

TABLE 29

XPD for route shown in Figure 32 in the frequency range 67-73 GHz

XPD	50%	90%	95%
HV	13.02	20.16	21.72
VH	17.82	23.18	24.56

5.1.9.5 Conclusion

These results and analyses were used as basis to propose the new cross-polarization discrimination values.

5.1.9.6 References

[1] Salous, Sana, Feeney, Stuart, Raimundo, Xavier & Cheema, Adnan (2016). Wideband MIMO channel sounder for radio measurements in the 60 GHz band. *IEEE Transactions on Wireless Communications* **15**(4): 2825-2832.

5.2 Residential environment

5.2.1 Study 1: Path loss model for propagation between terminals located below roof-top height in residential environments (Frequency bands: 2.4, 4.7, 26.4 GHz)

5.2.1.1 Executive summary

This study proposes a path loss calculation method for propagation between terminals located below roof-top height in residential environments, which uses three propagation paths between terminals: a path along a road, a path between buildings, and an over-roof propagation path.

5.2.1.2 Background and proposal

This study proposes a path loss model for propagation between terminals below roof-top height in residential environments. The path loss model is constructed by using three types of propagation paths.

Figure 34 describes a propagation model that predicts whole path loss L between two terminals of low height in residential environments as represented by equation (13) by using path loss along a road L_r, path loss between houses L_b, and over-roof propagation path loss L_v. L_r, L_b, and L_v are respectively calculated by equations (14) to (16), (17), and (18) to (23).

This model is recommended for frequencies in the 2-26 GHz range. The maximum distance between terminals d is up to 1 000 m. The applicable road angle range is 0-90 degrees. The applicable range of the terminal antenna height is set to be from 1.2 m to h_{Bmin}, where h_{Bmin} is the height of the lowest building in the area (normally 6 m for a detached house in a residential area).

FIGURE 34

Propagation model for paths between terminals located below roof-top height

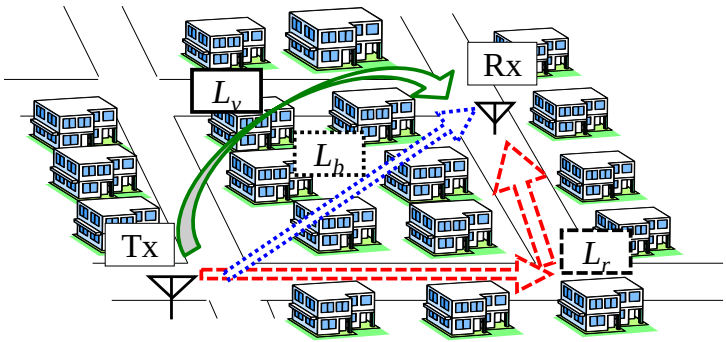

$$L = -10\log(1/10^{(L_r/10)} + 1/10^{(L_b/10)} + 1/10^{(L_v/10)}) \quad (13)$$

$$L_r = \begin{cases} L_{rbc} & (before\ corner) \\ L_{rac} & (after\ corner) \end{cases} \tag{14}$$

$$L_{rbc} = 20\log(4\pi d/\lambda) \tag{15}$$

$$L_{rac} = L_{rbc} + \sum_i (7.18\log(\theta_i) + 0.97\log(f) + 6.1) \cdot \left\{1 - \exp\left(-3.72 \cdot 10^{-5}\theta_i x_{1i} x_{2i}\right)\right\} \tag{16}$$

$$L_b = 20\log(4\pi d/\lambda) + 30.6\log(d/R) + 6.88\log(f) + 5.76 \tag{17}$$

$$L_v = 20\log(4\pi d/\lambda) + L_1 + L_2 + L_c \tag{18}$$

$$L_1 = 6.9 + 20\log\left(\sqrt{(v_1 - 0.1)^2 + 1} + v_1 - 0.1\right) \tag{19}$$

$$L_2 = 6.9 + 20\log\left(\sqrt{(v_2 - 0.1)^2 + 1} + v_2 - 0.1\right) \tag{20}$$

$$v_1 = \left(h_{bTx} - h_{Tx}\right)\sqrt{\frac{2}{\lambda}\left(\frac{1}{a} + \frac{1}{b}\right)} \tag{21}$$

$$v_2 = \left(h_{bRx} - h_{Rx}\right)\sqrt{\frac{2}{\lambda}\left(\frac{1}{b} + \frac{1}{c}\right)} \tag{22}$$

$$L_c = 10\log\left[\frac{(a+b)(b+c)}{b(a+b+c)}\right] \tag{23}$$

The relevant parameters for this model are:

d: distance between two terminals (m)
λ: wavelength (m)
f: frequency (GHz)
θ_i: road angle of i-th corner (degrees)
x_{1i}: road distance from transmitter to i-th corner (m)
x_{2i}: road distance from i-th corner to receiver (m)
R: mean visible distance (m)
h_{bTx}: height of nearest building from transmitter in receiver direction (m)
h_{bRx}: height of nearest building from receiver in transmitter direction (m)
h_{Tx}: transmitter antenna height (m)
h_{Rx}: receiver antenna height (m)
a: distance between transmitter and nearest building from transmitter (m)
b: distance between nearest buildings from transmitter and receiver (m)
c: distance between receiver and nearest building from receiver (m).

5.2.1.3 Measurement setup and procedure

The measurement parameters are summarized in Table 30.

TABLE 30

Measurement parameters

Frequency (GHz)	2.1975, 4.703, 26.365
Tx antenna height (m)	2.5
Rx antenna height (m)	2.5
Antenna type	Omni-directional (Tx and Rx)

Measurement frequencies were 2.1975, 4.703, and 26.365 GHz. To measure path loss characteristics below house-roof height, the heights of the Tx and Rx antennas were set at 2.5 m. Omni-directional antennas were used at Tx and Rx.

Tx was set at the roadside, and Rx was set on the measurement vehicle. Figure 35 shows the measurement environment and routes. The average building height is 6.7 m, and the mean visible distance R is 67 m, which were calculated using the building database. The measurement area has many detached houses and is a typical residential environment. The measurement route has four corners (the black dashed lines in Fig. 35) and can be separated to five parts, A to E.

The corners from A to B and from D to E are right-angle corners, and so, the road angles are 90 degrees at these corners. The corners from B to C and from C to D are gently curved, and the LoS between Tx and Rx is shielded. Both road angles of these gently curved corners are 10 degrees. Part C is LoS, and the other parts are NLoS. The measurement data were obtained by running the measurement vehicle along the route from part A to E.

FIGURE 35

Measurement environment and routes

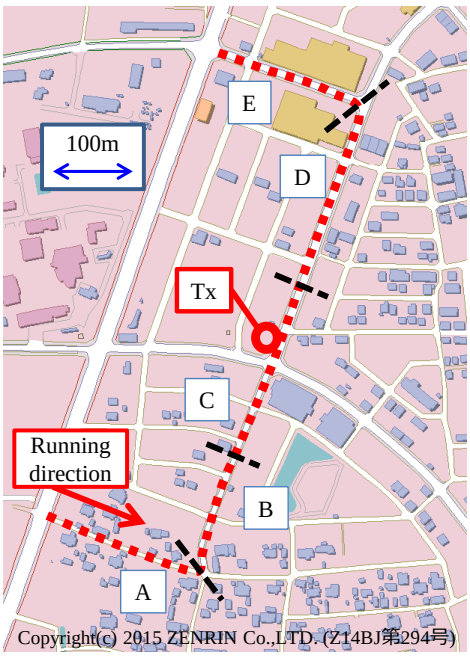

5.2.1.4 Validation results

Figure 36 compares the predicted total path losses calculated with the proposed model and the measured results. The parts of the measurement route are also represented in the Figure. This Figure shows that the predictions and measurements have good agreement over the whole route.

Further analyses show that the path along the road is dominant on almost the whole route of parts B, C and D. On the other hand, in parts A and E, the path between buildings become dominant, and the over-rooftop path as well as the path along the road becomes strong. Also, the effects of the path between buildings and the over-rooftop path decrease with increasing frequency, and the path along road become dominant on the whole measurement route.

Figure 37 shows the prediction error calculated from the measured path losses and predictions. The error values lie between −20 dB and 20 dB for the areas where a single path type is dominant. The root mean square values of the prediction error are 5.5 dB, 5.0 dB, and 5.5 dB at 2.2 GHz, 4.7 GHz, and 26 GHz, respectively. These results show that the model can predict the actual path loss accurately in the environment.

FIGURE 36

Predicted and measured total path loss

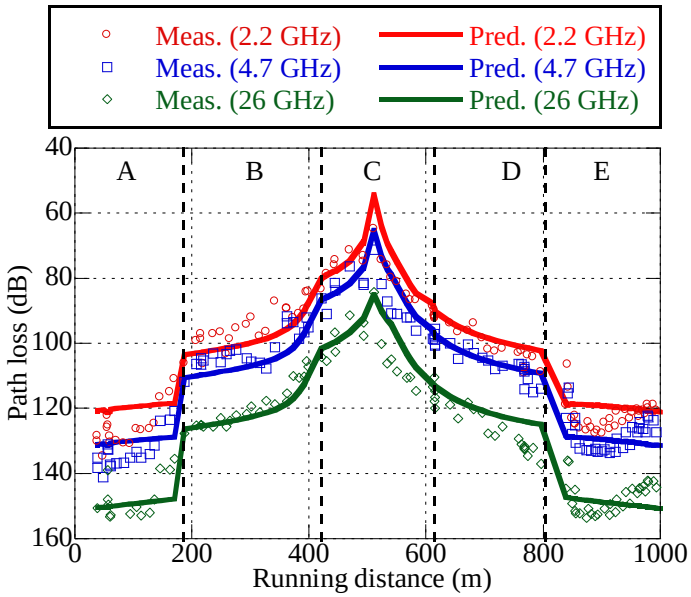

FIGURE 37

Prediction error versus running distance

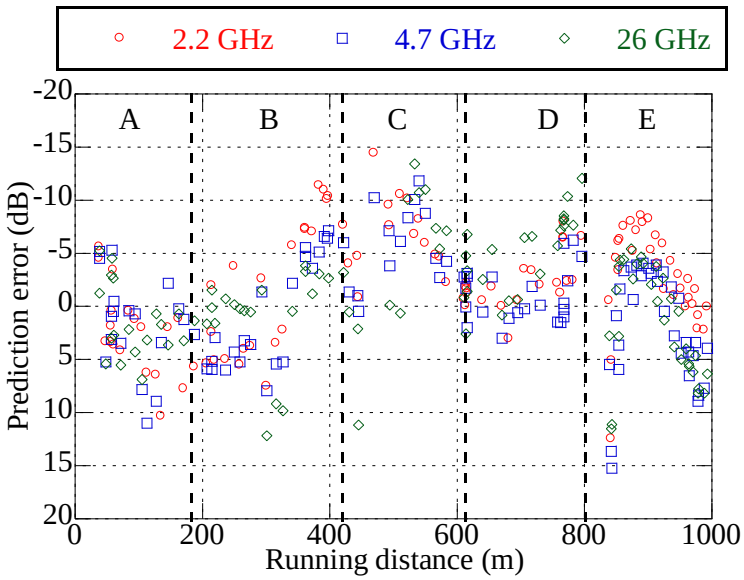

5.2.1.5 Conclusion

The results showed that the model can accurately predict path loss characteristics in residential areas.

5.2.2 Study 2: Delay spread, propagation in residential environments, below-rooftop (Frequency bands: 25.5-28.5, 67-73 GHz)

5.2.2.1 Executive summary

This section provides additional information for the rms delay spread values included in Recommendation ITU-R P.1411. This study focuses on the frequency ranges 25.5-28.5 GHz and 67-73 GHz based on measurements made in residential environments.

5.2.2.2 Background and proposal

Table 31 shows the proposed rms delay spread values.

TABLE 31

Rms delay spread values for 25.5-28.5 GHz and 67-73 GHz

Measurement conditions										rms delay spread (ns)	
Area	**Scenario**	***f*** **(GHz)**	h_1 **(m)**	h_2 **(m)**	**Range (m)**	**TX beam-width (degree)**	**RX beam-width (degree)**	**Time delay resolution (ns)**	**Polarization**	**50%**	**95%**
Residential	NLoS	25.5-28.5	3	1.6	37-167	33	Omni	0.5	VV	5.3	13.6
									HV	9.1	15.5
		67-73	3	1.6	37-167	40	Omni	0.5	VV	7.4	15.4

5.2.2.3 Measurement setup and procedure

Measurements were performed with dual polarised antennas at the transmitter and an omni-directional antenna at the receiver with vertical polarisation. At the transmitter two horn antennas with beam widths (40º in the E-plane and 38º in the H-plane) were used in the 67-73 GHz band with a twist at one of the transmit channels. In addition, a new set of dual polarised transmitters and two receivers were designed and implemented to perform measurements in the 25.5-28.5 GHz band. The transmit antenna has a 3 dB beam width of ~36º in the H-plane and 33º in the E-plane and the receive antenna was omni-directional. The measured environments include above rooftop and below roof top in both residential and low rise urban environments. The measurements were performed in both line of sight and non-line of sight where the transmitter was placed around the corner of a street. The data were systematically collected by moving the receiver trolley over consecutive 1 m intervals and the power delay profiles were then obtained by dividing the 1 m data into five sections. The data were analysed with 2 GHz bandwidth to give a 0.5 ns time delay resolution and the power delay profiles were used to estimate the rms delay spread in the two frequency bands for 20 dB threshold using the method defined in Recommendation ITU-R P.1407. Figure 38 shows the measured residential environment.

FIGURE 38

View of the measured environment (residential street)

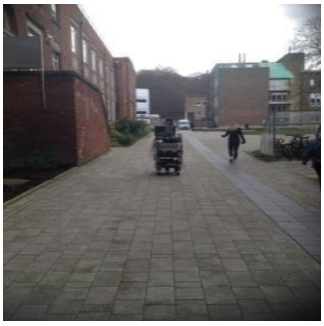

5.2.2.4 Validation results

Figure 39 gives the corresponding CDFs of the rms delay spread obtained from all the measured locations in the NLoS residential environment.

FIGURE 39

rms delay spread for 20 dB threshold in the two bands for the NLoS residential scenario

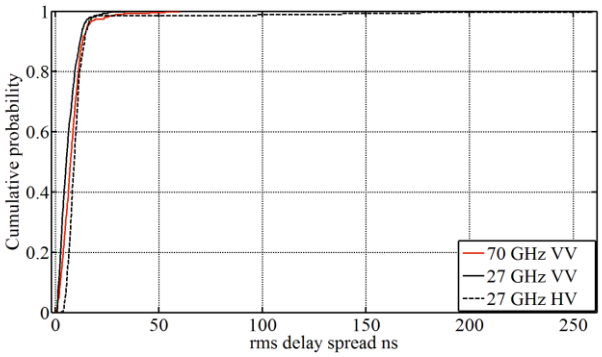

The 50% and 95% values were estimated from the CDFs and these are summarised in Table 31.

5.2.2.5 Conclusion

These results and analyses were used as a basis to propose the new rms delay spread values.

6 Studies for indoor environments

6.1 Study 1: Power loss coefficients and shadow fading statistics (Frequency bands: 0.8, 2.2, 4.7, 26, 37 GHz)

6.1.1 Executive summary

This section provides additional information for the power loss coefficients and shadow fading statistics included in Recommendation ITU-R P.1238. This study focuses on the frequency bands 0.8, 2.2, 4.7, 26, 37 GHz based on measurements made in an indoor open office environment.

6.1.2 Background and proposal

Table 32 and Table 33 show the proposed power loss coefficients and shadow fading statistics, respectively.

TABLE 32

Power loss coefficients, *N*, for indoor transmission loss calculation

Frequency (GHz)	Residential	Office	Commercial	Factory	Corridor	Data Centre
0.8	–	22.5(1)	–	–	–	–
2.2	–	20.7(1)	–	–	–	–
4.7	–	19.8(1)	–	–	–	–
26	–	19.5(1)	–	–	–	–
37	–	15.6(1)	–	–	–	–

(1) Open office (50 m × 16 m × 2.7 m (H)): LoS case. Averaged results with Tx heights of 2.6 and 1.2 m. Rx height was 1.5 m height. Both Tx and Rx are omni-directional antennas.

TABLE 33

Shadow fading statistics, standard deviation (dB), for indoor transmission loss calculation

Frequency (GHz)	Residential	Office	Commercial
0.8	–	3.4	–
2.2	–	2.3	–
4.7	–	2.7	–
26	–	2.8	–
37	–	2.4	–

6.1.3 Measurement setup and procedure

Figure 40 shows the measurement environment and measurement parameters summarized in Table 34. The measurement environment was a large office environment (50 m width × 16 m depth × 2.7 m above-floor height). Transmitter (Tx) antennas were placed in two locations (Tx1/3 and Tx2). Tx 1/3 were set near the centre of the room and Tx2 was placed near the edge of the room as shown in Fig. 40. For Tx1 and Tx2, the height of the Tx antennas was 2.6 m above the floor (0.1 m from the ceiling), and the antenna height of Tx3 was 1.2 m above the floor. Receive (Rx) antennas with a height of 1.5 m above the floor (1.2 m from the ceiling) were set on a push car. When the Tx antenna height was 2.6 m (Tx1 and Tx2), the measurements were taken in LoS between Tx and Rx antennas. For an antenna height of 1.2 m (Tx3), obstacles on the desk and partitions in the room caused quasi LoS because of blockages between Tx and Rx. The received power was measured by moving the push car as shown along the red line in Fig. 40. Five measurement frequencies were used, including high frequency bands above 6 GHz (0.8, 2.2, 4.7, 26.4, 37.1 GHz). A continuous wave was used at all five frequencies. Both the Tx and Rx antennas' radiation patterns were omni-directional in the horizontal plane with a 60-degree half-power beam width in the vertical plane. The path loss was obtained by subtracting gains and losses of the measurement setup after calibration. In order to exclude the effects of fast fading, median values were obtained at 1-meter intervals.

FIGURE 40

Measurement environment

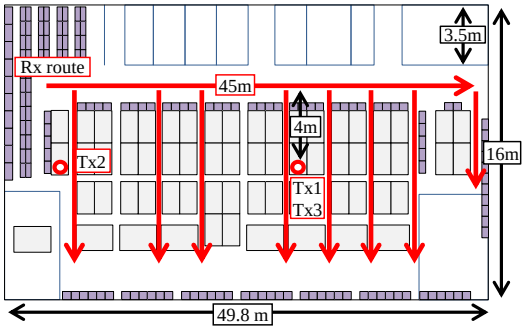

TABLE 34

Measurement parameters

Frequency (GHz)	0.8, 2.2, 4.7, 26.4, 37.1	
Tx antenna height (m)	Tx1	2.6
	Tx2	2.6
	Tx3	1.2
Rx antenna height (m)	1.5	
Tx / Rx antenna half power beam width	H-plane: Omni-directional V-plane: 60 degrees	

6.1.4 Validation results

In order to obtain the power loss coefficients, the path loss characteristics were analysed with the Tx-Rx direct distance. Figure 41 shows the measurement results at each Tx position using frequencies from 0.8 GHz to 37.1 GHz. The measurement results for Tx1, Tx2, and Tx3 are respectively shown in (a), (b), and (c). In this Figure, the solid lines represent regression results obtained by using the site-general path loss model in Recommendation ITU-R P.1238-8. The equation used for regression is as follows.

$$L = L(d_o) + N \log_{10} \frac{d}{d_o} + L_f(n) \quad \text{dB} \tag{24}$$

where N is a distance power loss coefficient, f is frequency in MHz, d is separation distance between the base station and portable terminal (where $d > 1$ m), d_o is a reference distance, L_f is a floor penetration loss factor, n is the number of floors between base station and portable terminal, and $L(d_o)$ is path loss at d_o (dB). Here, 1 m is used as the reference distance d_o and $(20 \log_{10} f - 28)$ as the free space path loss $L(d_o)$. As the Figure shows, the regression results a have good agreement with the measurement results.

FIGURE 41

Measurement results and regression results: (a) Tx1, (b) Tx2, (c) Tx3

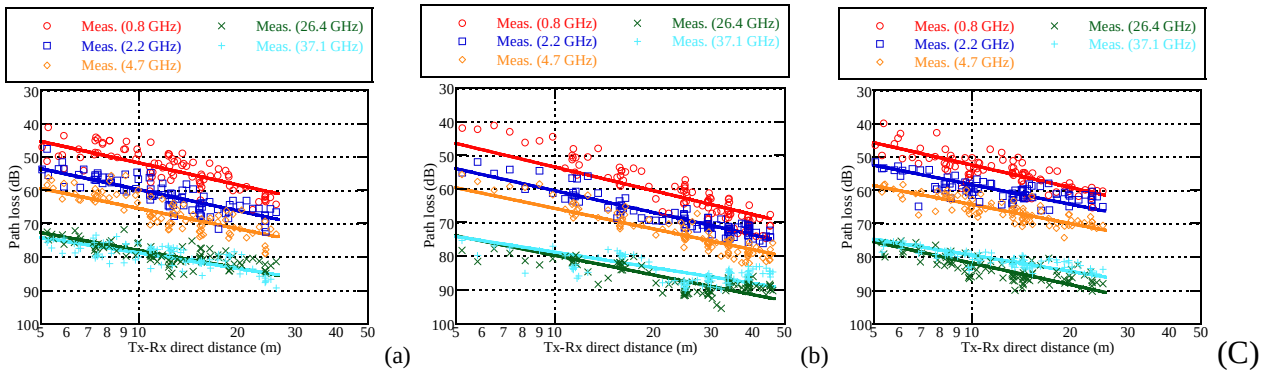

To further analyse prediction error characteristics of the regression results, the CDF of the prediction error was derived. Figure 42 shows the CDF curve at each Tx position. As the Figure shows, median values of the prediction error at each frequency and each Tx position are almost 0 dB, which means the regression results can accurately predict the path loss.

FIGURE 42

CDF of prediction error: (a) Tx1, (b) Tx2, (c) Tx3

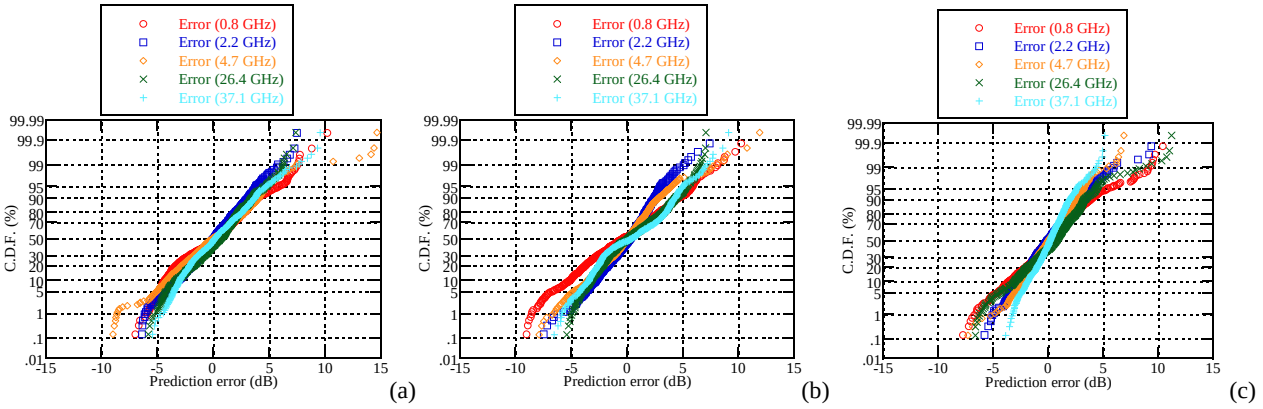

The derived coefficients are summarized in Table 35. In this Table, the mean value of the coefficients at the three Tx positions is also shown. In Recommendation ITU-R P.1238-8, the power loss coefficients are described such that they include an implicit allowance for various loss mechanisms likely to be encountered within a single floor of a building. Therefore, power loss coefficients were derived from the measurement results at the three Tx positions that include loss mechanisms such as blockage in addition to LoS loss. The shadow fading statistics values were also derived, which are calculated by using the standard deviation of the prediction errors. The values are summarized in Table 36. These values, as well as the power loss coefficients, are important for predicting the transmission loss in indoor environments.

TABLE 35

Power loss coefficients obtained from regression results

Frequency (GHz)	Power loss coefficients, *N*			
	Tx1	**Tx2**	**Tx3**	**Mean value**
0.8	21.7	23.4	22.3	22.5
2.2	21.0	21.7	19.5	20.7
4.7	20.1	20.4	18.9	19.8
26.4	17.6	19.3	21.5	19.5
37.1	15.4	15.4	16.1	15.6

TABLE 36

Shadow fading statistics, standard deviation obtained from regression results

Frequency (GHz)	Shadow fading (dB)			
	Tx1	**Tx2**	**Tx3**	**Mean value**
0.8	3.3	3.8	3	3.4
2.2	2.5	2.2	2.3	2.3
4.7	3.4	2.7	2.1	2.7
26.4	2.6	2.9	2.8	2.8
37.1	2.6	3.2	1.5	2.4

In addition, the frequency dependency of the power loss coefficients was analysed. Figure 43 shows the frequency dependency of (a) the values in Table 35, and (b) the values described in the current Recommendation ITU-R P.1238. It should be noted that the values in Recommendation ITU-R P.1238 were derived from measurements in various environments, and so it is difficult to simply compare with the results obtained here. In this figure, the regressed result is also shown by the solid line. As can be seen in this figure, the power loss coefficients decrease as the frequency increases, meaning that they have a frequency dependency. Such frequency dependency could be used for developing the power loss coefficient model.

FIGURE 43

Frequency dependency of power loss coefficients

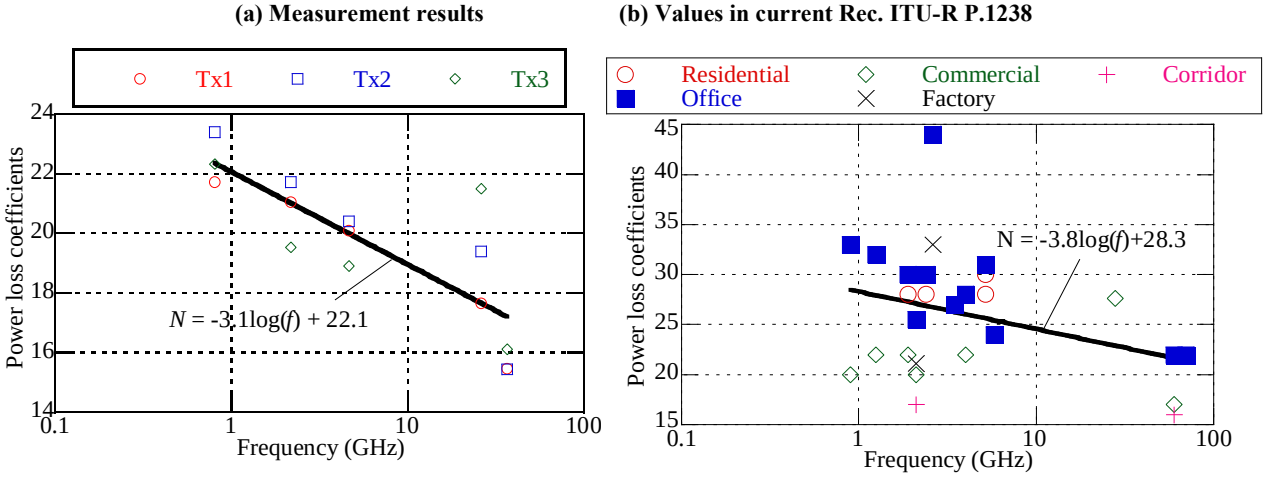

6.1.5 Conclusion

This contribution presented measurement results of five frequency bands up to 37 GHz in an office environment, as well as the power loss coefficients and the shadow fading characteristics. It was shown that the power loss coefficients have a frequency dependency, which could be used for developing the power loss coefficient model.

6.2 Study 2: Power loss coefficients and shadow fading statistics (Frequency bands: 28, 38 GHz)

6.2.1 Executive summary

This section provides additional information for the power loss coefficients and shadow fading statistics included in Recommendation ITU-R P.1238. This study focuses on the frequency bands 28 GHz and 38 GHz based on measurements made in indoor office and indoor commercial (train station and airport terminal) environments.

6.2.2 Background and proposal

Table 37 and Table 38 show the proposed power loss coefficients and shadow fading statistics, respectively.

TABLE 37

Power loss coefficients, *N*, for indoor transmission loss calculation

Frequency (GHz)	Residential	Office	Commercial	Factory	Corridor	Data Centre
28	–	18.4[2] 29.9[2]	27.6[1] 17.9[2, 3] 24.8[2, 3]	–	–	–
38	–	20.3[2] 29.6[2]	18.6[2, 3] 25.9[2, 3]	–	–	–

Notes to Table 37:

(1) Railway station (170 m × 45 m × 21 m(H)) and airport terminal (650 m × 82 m × 20 m(H)): NLoS case, 60° half-power beam width antenna for transmitter is set at the height of 8 m, and 10° beam width for receiver is set at 1.5 m on the floor. The value was obtained from the maximum path gain among various Tx and Rx antenna orientations.

(2) The upper number is for LoS cases and the lower number is for NLoS cases.

(3) The environments are same to (8) and a Tx antenna with 60˚ beamwidth is set at the height of 8 m and a Rx with an omni-directional antenna is set at the height of 1.5 m.

TABLE 38

Shadow fading statistics, standard deviation (dB), for indoor transmission loss calculation

Frequency (GHz)	Residential	Office	Commercial
28	–	3.4(2) 6.6(2)	6.7(1) 1.4(2, 3) 6.4(2, 3)
38	–	4.6(2) 6.8(2)	1.6(2, 3) 5.5(2, 3)

(1) Railway station (170 m × 45 m × 21 m(H)) and airport terminal (650 m × 82 m × 20 m(H)): NLoS case, 60° half-power beam width antenna for transmitter is set at the height of 8 m, and 10° beam width for receiver is set at 1.5 m on the floor. The value was obtained from the maximum path gain among various Tx and Rx antenna orientations.

(2) The upper number is for LoS case and the lower number is for NLoS case.

(3) The environments are same to (1) and a Tx antenna with 60˚ beamwidth is set at the height of 8 m and a Rx with an omni-directional antenna is set at the height of 1.5 m.

6.2.3 Measurement setup and procedure

The path loss measurement campaign was conducted with a 28 and 38 GHz channel sounder system, which was developed by the ETRI. Table 39 shows the specification of the channel sounder.

TABLE 39

Specification of the channel sounder

Description	Specification	
Carrier frequency	28 GHz	38 GHz
Channel bandwidth	500 MHz	
Maximum TX power	29 dBm	21 dBm
Automatic gain control range	< 60 dB	

The measurement campaign was conducted in three areas: a) an ETRI office, b) Seoul railway station, and c) Incheon airport terminal. The ETRI office is a typical indoor office environment. Seoul railway station and Incheon airport terminal are the representative indoor commercial environments in Korea.

6.2.3.1 Path loss measurements in indoor office environments

The size of the office is 72 m × 23 m × 2.6 m. There are cubicle areas, meeting rooms, corridors, pillars, etc. The locations of the TX and RX are shown in Fig. 44. The outside walls are composed of concrete and large tempered glass, whereas the inside walls and ceilings are made of reinforced concrete, steel and plaster board. The path loss measurements were collected at two TX locations and 48 RX locations. In Fig. 44, the red stars show the TX locations and the blue circles show the LoS RX locations. The red and green circles show the NLoS RX locations. The heights of the TX and the RX are 2.5 m and 1.2 m, respectively. The transmitting antenna and the receiving antenna are omni-directional antennas.

FIGURE 44

Path loss measurement campaign in an ETRI office (Site 1):
(a) Layout of the measurement scenario, (b) Installation of measurement equipment

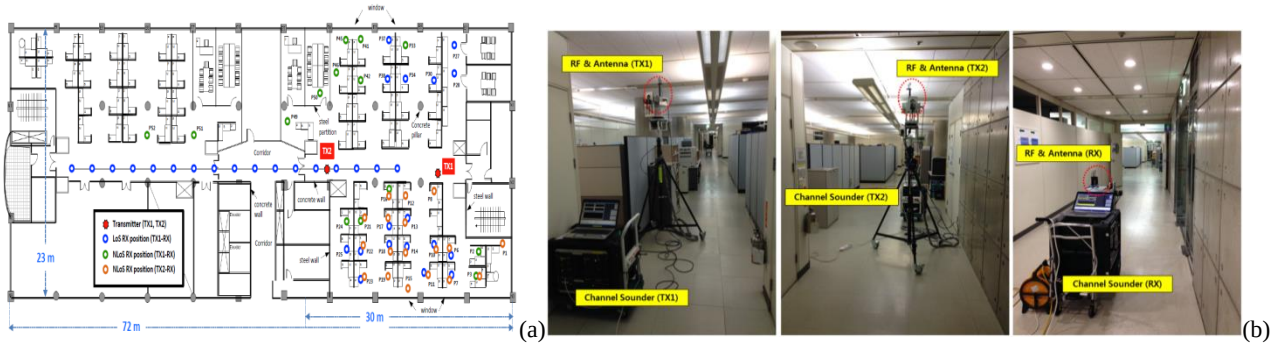

6.2.3.2 Path loss measurements in indoor commercial environments

The path loss measurements were collected in two indoor commercial environments. Horn antennas with 60 and 40 degree beamwidths were used at TX for 28 and 38 GHz measurements, respectively. The TX antenna direction was fixed to the measurement area. At RX, an omni-directional antenna was installed. For detail information about the locations of the antennas and the direction of the transmitting antennas is shown in Figs 45 and 46.

The first measurement site is Seoul railway station as shown in Fig. 45 where the antenna locations of the measurements are marked. Seoul railway station is a large hall with a dimension of 170 m × 45 m × 21 m. There are many stores, ticketing boxes, and offices. The ceiling and walls are constructed with steel frames and thick tempered glasses. In Fig. 45, the blue and green circles denote LoS locations and NLoS locations, respectively. The TX antenna was set up at 8 m high. The RX antenna moved while maintaining the antenna height at 1.5 m.

The second site is Incheon airport terminal as shown in Fig. 46. Incheon airport terminal is a very large hall with a dimension of 650 m × 82 m × 20 m. There are many reception tables, banks, stores, and many partitions. In Fig. 45, the blue and green circles denote LoS locations and NLoS locations, respectively. The TX antenna was set up at the height of 8 m. The RX antenna moved at the height of 1.5 m.

FIGURE 45

Path loss measurement campaign in Seoul railway station (Site 2):
(a) Layout of the measurement scenario, (b) Installation of the measurement equipment

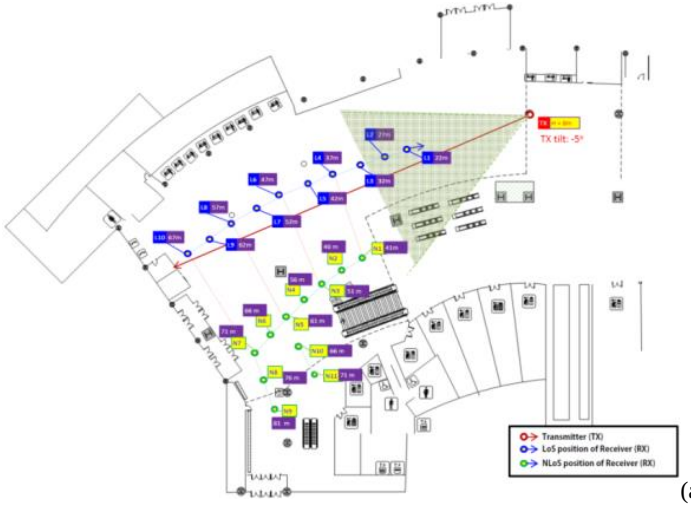

(a)

(b)

FIGURE 46

Path loss measurement campaign in Incheon airport terminal (Site 3):
(a) Layout of the measurement scenario, (b) Installation of the measurement equipment

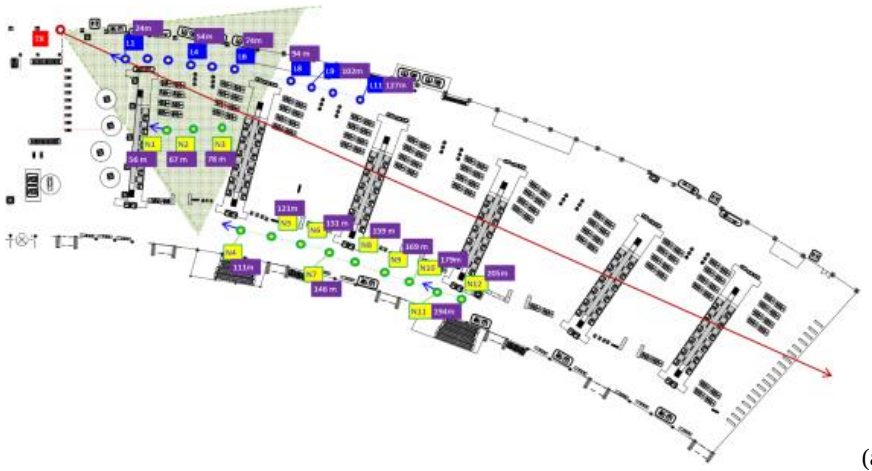

(a)

(b)

6.2.4 Validation results

We analysed the measurement result based on the path loss model in Recommendation ITU-R P.1238-8, which is given by

$$L_{total} = L(d_o) + N \log_{10}\left(\frac{d}{d_0}\right) + L_f(n) \quad (25)$$

where d is the distance from TX to RX, d_0 is the reference distance, N is the path loss exponent, and n is the number of floors between the stations (i.e. TX and RX). $L(d_0)$ is the path loss at the reference distance and $L_f(n)$ is the floor penetration loss. In this document, the reference distance is set by 1 m and the path loss at the reference distance is assumed to be free space loss. Since TX and RX are on the same floor, the floor penetration loss is zero. Figures 47 and 48 show the measurement results and the fitted curves for the indoor office and the indoor commercial environments, respectively.

FIGURE 47

Measurement results of indoor office environments: (a) 28 GHz, (b) 38 GHz

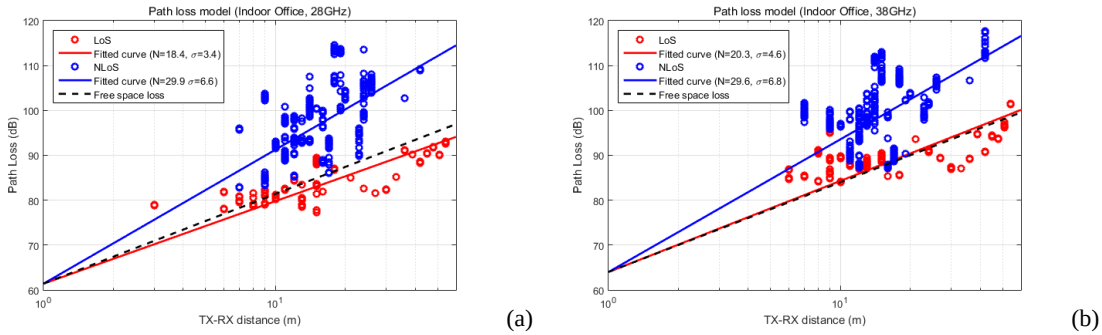

(a) (b)

FIGURE 48

Measurement results of the indoor commercial environments: (a) 28 GHz, (b) 38 GHz

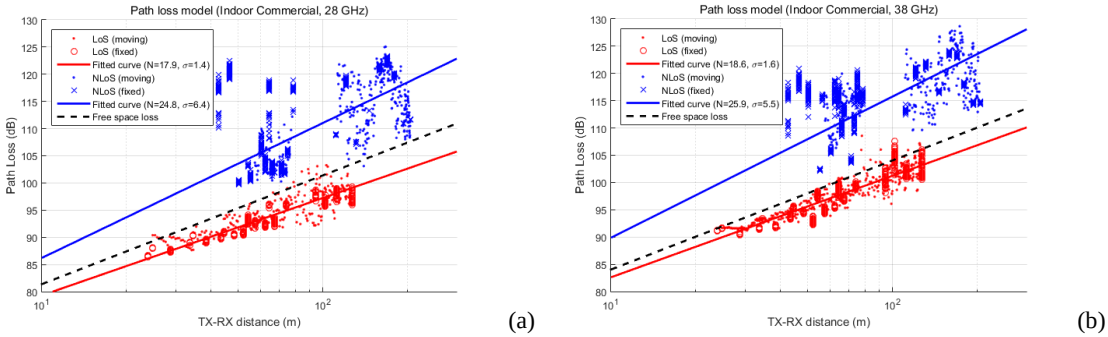

(a) (b)

Table 40 shows the optimized parameters based on the measurements. In the Table, σ is the standard deviation of the log-normal shadow fading. It can be seen that the path loss exponents and the shadow fading standard deviations of NLoS environments are larger than those of LoS environments. It can also be seen that the path loss exponents and the shadow fading standard deviations of 38 GHz are larger than those of 28 GHz.

TABLE 40

Path loss coefficients (*n*) and standard deviation (σ) of CI model at 28 GHz and 38GHz

Environments	Frequency	LoS		NLoS		The range of dist. (m)
		N	**σ (dB)**	***N***	**σ (dB)**	
Office	28GHz	18.4	3.4	29.9	6.6	< 60
	38GHz	20.3	4.6	29.6	6.8	< 60
Commercial	28GHz	17.9	1.4	24.8	6.4	< 210
	38GHz	18.6	1.6	25.9	5.5	< 210

6.2.5 Conclusion

These results and analyses were used as a basis to propose the new path loss exponents and the shadow fading standard deviations for 28 and 38 GHz.

6.3 Study 3: Power loss coefficients, shadow fading statistics, rms delay spread parameters (Frequency bands: 51-57, 67-73 GHz)

6.3.1 Executive summary

This section provides additional information for the power loss coefficients, shadow fading statistics and rms delay spread parameters included in Recommendation ITU-R P.1238. This study focuses on the frequency bands 51-57 GHz and 67-73 GHz based on measurements made in three indoor environments which include a computer cluster room, classroom and corridor.

6.3.2 Background and proposal

Tables 41, 42 and 43 show the proposed power loss coefficients, shadow fading statistics, and rms delay spread parameters, respectively.

TABLE 41

Power loss coefficients, *N*, for indoor transmission loss calculation

Note: The original values from this study were reworked so that they are consistent with the methodology used for the other values in the corresponding Table in Recommendation ITU-R P.1238. The reworked values are shown below.

Frequency (GHz)	Residential	Office	Commercial	Factory	Corridor	Data Centre
51-57	–	15[10]	–	–	13[10] 16.3[4, 10]	–
67-73	–	19[11]	–	–	16[11] 17.6[4, 11]	–

[4] Computer room where there are many computers around the room.

[10] Transmit antenna beamwidth 56.3º, synthesised 360º in azimuth at receiver with 19.7º beamwidth in elevation.

[11] Transmit antenna beamwidth 40º, synthesised 360º in azimuth at receiver with 14.4º beamwidth in elevation.

TABLE 42

Shadow fading statistics, standard deviation (dB), for indoor transmission loss calculation

Frequency (GHz)	Residential	Office	Commercial
51-57	–	2.7	–
67-73	–	2.1	–

TABLE 43

rms delay spread parameters

Freq. (GHz)	Environ-ment	Polari-zation	Time delay resolution (ns)	Tx beam width (degrees)	Rx beam width (degrees)	A (ns)	B (ns)	C (ns)	Note for A, B, C
51-57	Computer cluster	VV/HH	0.5	56.3	18.4	0.69	0.96	2.89	(1)
					18.4(3)	2.14	10.7	29.7	(1, 2)
	Office/ classroom	VV/HH	0.5	56.3	18.4	0.56	0.65	4.29	(1)
					18.4(3)	1.6	15.8	26.7	(1, 2)
	Corridor	VV/HH	0.5	56.3	18.4	0.54	0.72	1.34	(1)
					18.4(3)	0.81	8.9	44.6	(1, 2)
67-73	Computer cluster	VV/HH	0.5	40	14.4	0.36	0.57	2.4	(1)
					14.4(3)	1.1	10.9	28.1	(1, 2)
	Office/ classroom	VV/HH	0.5	40	14.4	0.33	0.5	6.39	(1)
					14.4(3)	1.59	12.6	25.9	(1, 2)
	Corridor	VV/HH	0.5	40	14.4	0.36	0.47	1.2	(1)
					14.4(3)	0.49	6.11	35.2	(1, 2)

(1) 20 dB threshold.

(2) Receiver antenna was rotated in a step of 5º around 360 degrees in measurements. The value represents a directional delay spread when the bore-sight of receiver antenna is not aligned to the direction of transmitter.

(3) The original values (320º) from this study were changed to reflect the actual beamwidth of the antenna.

6.3.3 Measurement setup and procedure

Wideband measurements in three typical indoor environments were performed which include a computer cluster room, classroom and corridor. The measurements were performed at two frequencies in the 50-75 GHz band identified by WRC-15 as possible bands for future wireless communications. The measurements were obtained with dual polarised antennas at the transmitter and at the receiver using a 2 by 2 wideband channel sounder. The measurements were performed with 6 GHz bandwidth between 51-57 GHz and 67-73 GHz and analysed with 2 GHz bandwidth.

Horn antennas were used at the receiver with a beam width (18.4º in the E plane and 19.7º in the H plane at 50 GHz and 14.4º in the E plane and 15.4º in the H plane at 67.5 GHz). At the transmitter two horn antennas were used and these have beam widths (56.3º in the E plane and 51.4º in the H plane at 50 GHz and 40º in the E plane and 38º in the H plane at 67.5 GHz). To perform dual polarisation measurements, a twist was used at one of the transmit channels and another at one of the

receive channels. To enable LoS, NLoS and the synthesis of non-directional propagation, the receiver was mounted on a turntable which was rotated in 5 degree steps to cover all azimuthal angles.

Following calibration rms delay spread for 20 dB threshold below the peak and the coefficients of the path loss model for the four polarisations were estimated using the least square fit. The data from each set of measurements were grouped for the co-polarised and cross-polarised antennas and the results for the path loss coefficients and for the rms delay spread are proposed to be added to the current Recommendation.

6.3.3.1 Summary of measurements

The multiband wideband chirp channel sounder at Durham University was used to carry out measurements in the 50-75 GHz band with 2 transmit and 2 receive antennas. The sounder was used to measure the channel response in different indoor environments including a classroom, a corridor, and a computer cluster room, shown in Fig. 49.

FIGURE 49

Measured indoor environments (a) classroom, (b) corridor, (c) computer cluster

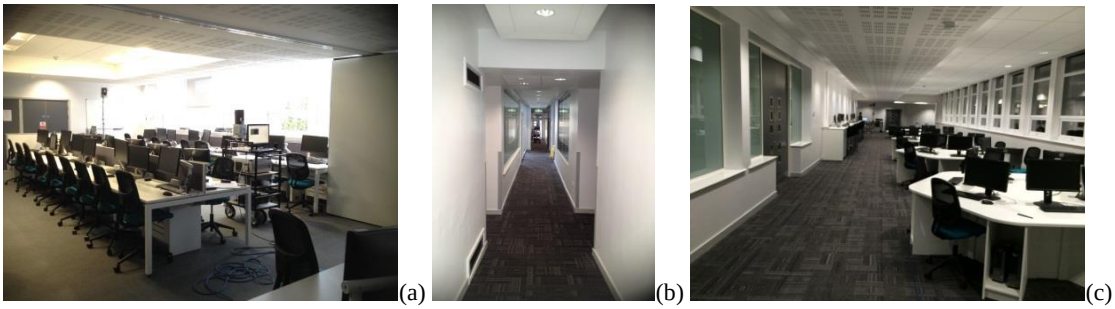

For these measurements, the transmitter and receiver were mounted on trolleys with the transmitter being held in a fixed location with the RF head unit being mounted close to the ceiling at about 2.35 m and the receiver antenna was mounted on the trolley at 1.6 m.

6.3.4 Validation results

The data were used to synthesise the received power from an omnidirectional antenna to estimate the path loss and for each angle of arrival the rms delay spread was estimated. The omni-directional power was estimated by taking the sum of the received power from the power angular profile illustrated in Fig. 50 for one of the locations in the classroom environment. The transmitter and receiver used high stability rubidium standards which also enabled the synthesis of the omni-directional power delay profiles as shown in Fig. 51 for the VV and VH polarisations in the same environment.

FIGURE 50

Power versus angle of rotation for the dual polarised antennas in the classroom environment

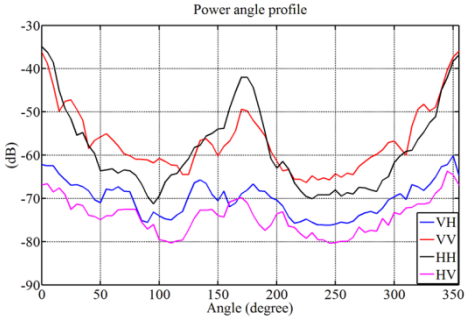

FIGURE 51

Synthesised omni-directional power delay profile (a) VV and (b) VH

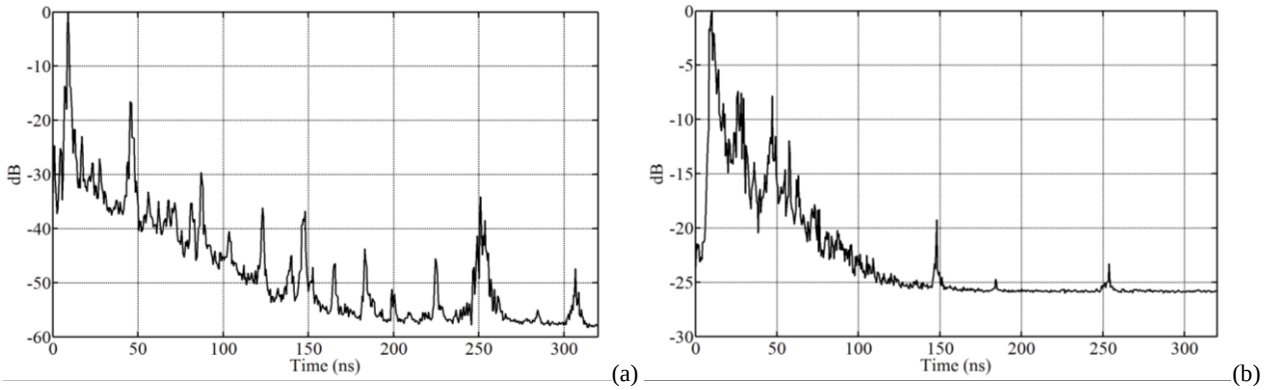

The rms data were estimated for each angle of arrival and then separated as LoS and NLoS for the back beam of the antenna. All LoS data were unobstructed. The estimated values of the rms delay spread are given in Table 44.

TABLE 44

rms delay spread in LoS and NLoS

Band	Environment	Polarisation	LoS 10%; 50%; 90%	NLoS 10%; 50%; 90%
51 – 57	Computer Cluster	VV/HH	0.69; 0.96; 2.89	2.14; 10.74; 29.71
		VH/HV	0.98; 2.33; 8.14	3.19; 11.14; 31.90
67 – 73		VV/HH	0.36; 0.57; 2.4	1.06; 10.91; 28.08
		VH/HV	0.58; 1.26; 5.39	2.27; 8.54; 26.61
51 – 57	Corridor	VV/HH	0.54; 0.72; 1.34	0.81; 8.90; 44.55
		VH/HV	0.83; 5.16; 14.34	2.72; 10.36; 43.04
67 – 73		VV/HH	0.36; 0.47; 1.20	0.49; 6.11; 35.16
		VH/HV	1.04; 7.94; 21.47	1.51; 6.40; 34.18
51 – 57	Classroom	VV/HH	0.56; 0.65; 4.29	1.60; 15.75; 26.67
		VH/HV	2.92; 7.58; 14.66	7.06; 14.37; 21.02
67 – 73		VV/HH	0.33; 0.50; 6.39	1.59; 12.55; 25.85
		VH/HV	2.80; 11.69; 22.76	5.84; 13.40; 22.72

The power delay profiles were also used to estimate the parameters $L(do)$ and N as in equation (26) in the Recommendation and the results for the three environments are given in Table 45 for the co-polarized antennas where σ gives the standard deviation of the fit.

$$L_{total} = L(d_o) + N \log_{10} \frac{d}{d_o} + L_f(n) \quad (26)$$

TABLE 45

Path loss parameters

Band	Environment	N	$L(d_o = 1m)$	σ
51 – 57	Computer room	14.5	55.1	2.7
67 – 73		18.8	54.6	2.1
51 – 57	Corridor	16.9	44.7	1.1
67 – 73		12.8	57.7	0.8
51 – 57	Classroom	26.0	39.4	0.6
67 – 73		27.3	48.1	1.4

6.3.5 Conclusion

These results and analyses were used as basis to propose the new power loss coefficients, shadow fading statistics and rms delay spread parameters.

6.4 Study 4: Power loss coefficients (Frequency band: 70 GHz)

6.4.1 Executive summary

This section provides additional information for the power loss coefficients included in Recommendation ITU-R P.1238. This study focuses on the frequency band 70 GHz based on measurements made in an indoor office environment.

6.4.2 Background and proposal

Table 46 shows the proposed power loss coefficient.

TABLE 46

Power loss coefficients, *N*, for indoor transmission loss calculation

Frequency (GHz)	Residential	Office	Commercial	Factory	Corridor	Data Centre
70	–	22(1)	–	–	–	–

(1) 60 GHz and 70 GHz values assume propagation within a single room or space, and do not include any allowance for transmission through walls. Gaseous absorption around 60 GHz is also significant for distances greater than about 100 m which may influence frequency reuse distances (see Recommendation ITU-R P.676).

6.4.3 Measurement setup and procedure

Measurements were performed in an office. The area measured was 22 × 12.5 × 3.5 m. The walls were made of metal, and metal bookshelves were set along the walls. Along the window, there were low bookshelves also made of metal. The ceiling was made of plasterboard, and fluorescent lights and air conditioning units were positioned on the ceiling. The flooring was made of metal, which was covered by a carpet. Table 47 shows the measurement parameters, and Fig. 52 shows the measurement conditions in the office.

TABLE 47

Measurement conditions (Office)

Frequency	Polarization	Tx antenna	Rx antenna	Environment	Antenna height
70 GHz	V	60°	15°, 30°, 60°	LoS 1, 2, 3, 5, 7, 10, 14 m	1 m
70 GHz	V	60°	15°, 30°, 60°	NLoS 3, 7, 10, 14 m	1 m

FIGURE 52

Measurement environment (Office)

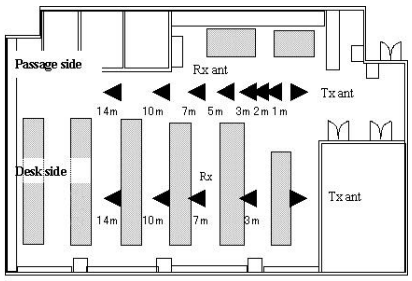

We measured the distance characteristics on the passage and desk sides of the office. The LoS was between the Tx and Rx on the passage side. Because the average height of the office fixtures on the desk side was 1.2 m, the environment between the Tx and Rx could be classified as a NLoS.

6.4.4 Validation results

Figure 53 shows the measurement results. *N* was obtained by using the least square method for each environment. Equation (1) with *N*=20 and 24 approximates the LOS and NLOS in the office results well, respectively. *N*=22 approximates the total results. The results are summarized in Table 48.

FIGURE 53

Measurement results

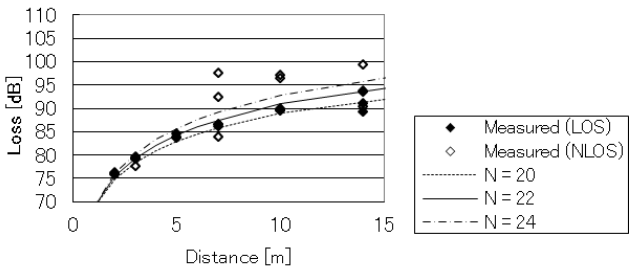

TABLE 48

Power loss coefficients *N*

Frequency	Office (LoS)	Office (NLoS)	Office (Total)
70 GHz*	20	24	22

* 70 GHz values assume propagation within a single room or space, and do not include any allowance for transmission through walls.

6.4.5 Conclusion

Based on the results and analyses above, a new power loss coefficient value is proposed for 70 GHz.

6.5 Study 5: Power loss coefficients (Frequency band: 300 GHz)

Note: Although the scope of this ITU-R Report is up to 100 GHz, this study for 300 GHz is still provided for possible future extension of frequency usage in indoor environments.

6.5.1 Executive summary

This section provides additional information for the power loss coefficients included in Recommendation ITU-R P.1238. This study focuses on the frequency band 300 GHz based on measurements made in indoor office and corridor environments.

6.5.2 Background and proposal

Table 49 shows the proposed power loss coefficients.

TABLE 49

Power loss coefficients, *N*, for indoor transmission loss calculation

Frequency (GHz)	Residential	Office	Commercial	Factory	Corridor	Data Centre
300	–	20[15]	–	–	19.5[9, 15]	20.2[15]

[9] Transmitter and receiver are on LoS corridor.

[15] Transmit and received antennas have 10° beamwidth.

6.5.3 Measurement setup and procedure

6.5.3.1 First measurement campaign – office and corridor environments

In a first measurement campaign, propagation loss was measured by using 300 GHz continuous wave in an anechoic chamber as shown in Fig. 54 to confirm the transmitter (TX) and receiver (RX). Subsequently propagation loss in office and corridor environments was measured. The maximum transmission distance was a few tens of meters in the line-of-sight situation because the output power was limited to –15 dBm by a used RF device performance. In the measurement, directional antennas were used by considering actual 300 GHz wireless applications. The aperture size of antenna is 6 mm × 8.36 mm and the antenna gain is 25 dBi as shown in Fig. 55. The antenna heights of TX and RX were 1.1 m above the floor. The measured polarization was set to vertical. For path loss measurement, the TX was fixed and RX was moved by using a platform truck. Table 50 summarizes these parameters.

FIGURE 54

Propagation measurement in anechoic chamber

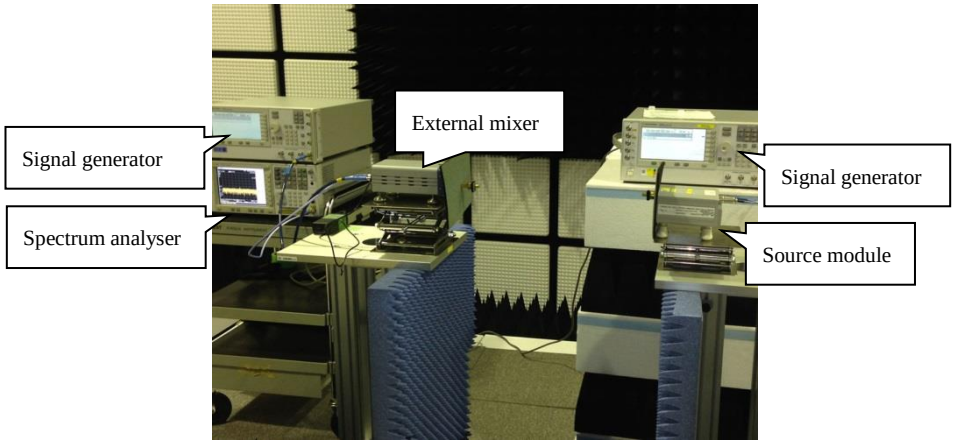

FIGURE 55

Standard gain horn antenna

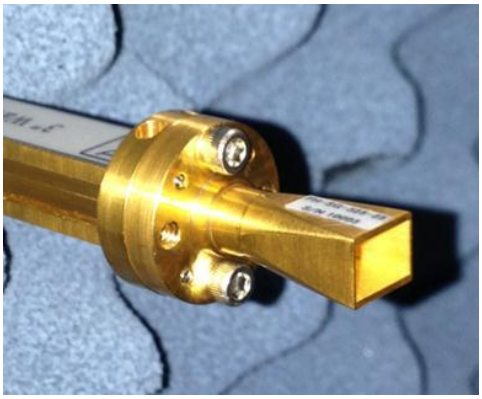

(a) Standard gain horn

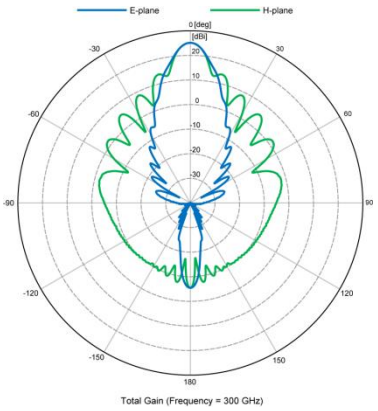

(b) Simulated antenna directivity

TABLE 50

Measurement parameters

Measured frequency	300 GHz (CW)
Output power	−15 dBm
TX and RX antennas	Standard gain horn Gain: 25 dBi (HPBW 10 degree) Height: 1.1 m above the floor

Figure 56 shows the measurement system for indoor environments. The TX and RX were put on the trucks and the RX position was changed in the measurement. There was no human in the environments during the measurement to keep the static condition. The measured distance was up to 12 m for office and 35 m for corridor environments in the line-of-sight situation.

FIGURE 56

Measurement system for indoor environment.

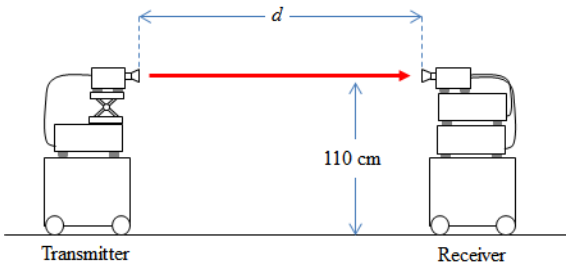

The snapshots of transmitter and receiver are shown in Fig. 57. The indoor measurement was carried out in the office and corridor environments as shown in Fig. 58.

FIGURE 57

Snapshots of transmitter and receiver: (a) Transmitter, (b) Receiver

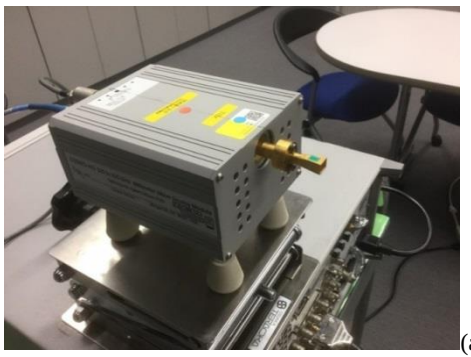
(a)

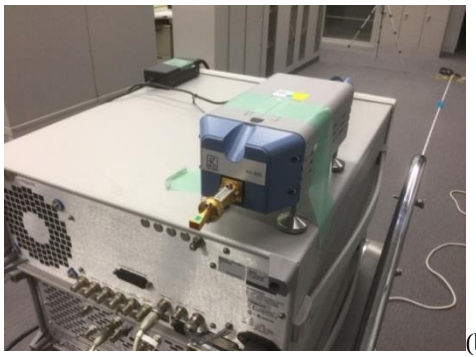
(b)

FIGURE 58

Snapshots of measurement in the office and corridor environments: (a) Office, (b) Corridor


(a)


(b)

6.5.3.2 Second measurement campaign – data centre environment

In a second measurement campaign, propagation loss was measured by using 300 GHz continuous wave in a data centre environment as shown in Fig. 59(a) and (b). The server arrangement is mixed with regular intervals and non-regular intervals. The server body is made of metal, the ceiling is plasterboard, and the floor is concrete covered by carpet. In the path loss measurement, the transmitter (TX) position is fixed and the receiver (RX) position is changed. The antenna heights of TX and RX were set as 2.15 m from the floor, and the RX antenna height is changed to examine the antenna height effects.

The snapshots of TX and RX modules are the same as in the first measurement campaign, shown in Fig. 57. TX and RX modules were put on the server rack. There was no human in the environment during the measurement to keep the static condition. The measured distance was up to 22.3 m in the line-of-sight situation. In the measurement, directional antennas were used by considering actual 300 GHz wireless applications. As in the first measurement campaign, the aperture size of the antenna is 6 mm x 8.36 mm and the antenna gain 25 dBi, as shown in Fig. 55. The measured polarization was set to vertical. The output power was limited to −15 dBm by a used RF device performance. Table 51 summarises these parameters.

FIGURE 59

(a) Data centre environment, (b) Server arrangement in the data centre

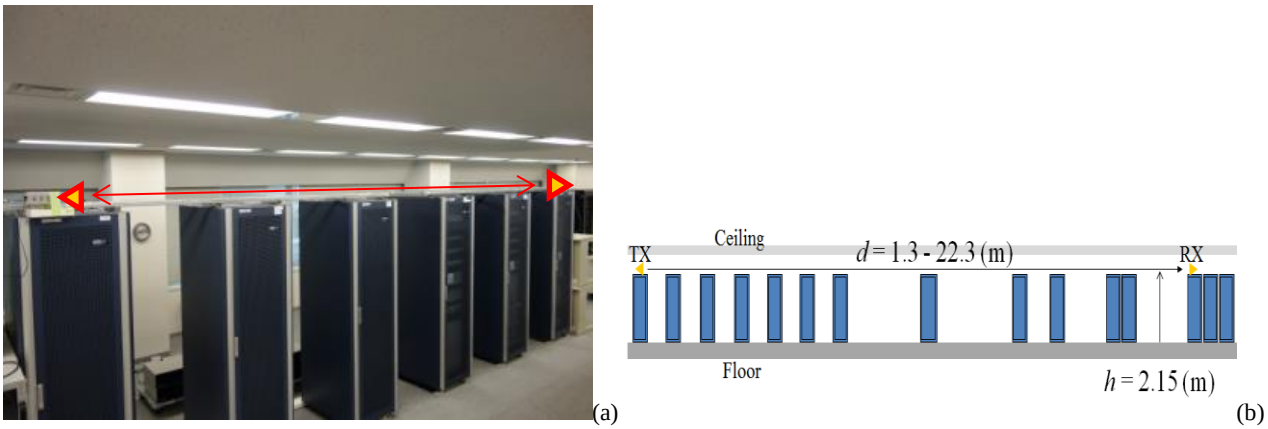

TABLE 51

Measurement parameters – second measurement campaign

Measured frequency	300 GHz (CW)
Output power	−15 dBm
TX and RX antennas	Rectangular horn Gain: 25 dBi (HPBW 10 degree)

6.5.4 Validation results

6.5.4.1 Results for the office and corridor environments

The relationship between the received power and the transmission distance in the anechoic chamber is shown in Fig. 60. In this Figure the simulation result by a moment method (MoM) including antenna structure is also plotted. It was confirmed that the pass loss coefficient is $N = 20$ identical with the free space loss in the far field.

FIGURE 60

Received power measurement in the anechoic chamber

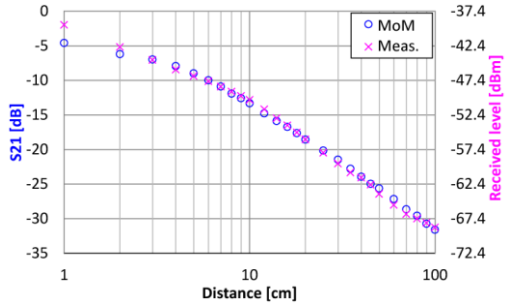

Measured path loss results in the office and corridor environments are shown in Fig. 61. By a linear approximations, path loss coefficients were extracted as N = 20 and 19.5 for each environment. The coefficient of office environment was roughly identical with the free space loss, because antenna half power beam width was narrow as 10 degrees. The coefficient of corridor environment was slightly decreased from N = 20.

FIGURE 61

Measured path loss results (a) in the office environment, (b) in the corridor environment

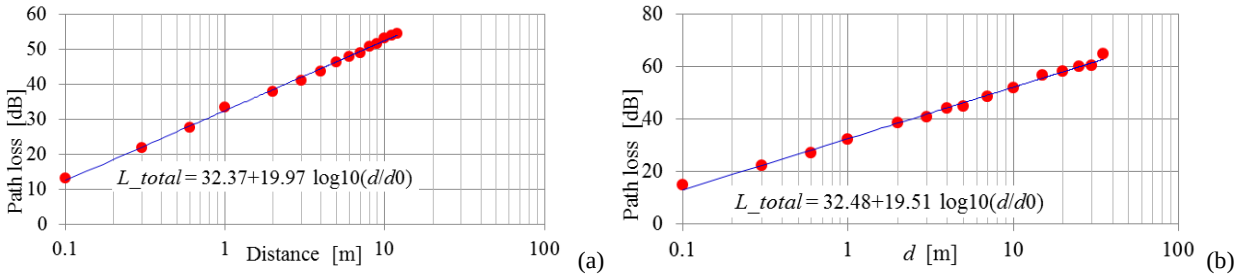

6.5.4.2 Results for the data centre environment

The relationship between the measured path loss and the transmission distance in the data centre is shown in Fig. 62. By a linear approximation, path loss coefficients were extracted as N = 20.2. The coefficient of the data centre environment was roughly identical with the free space loss, however, it had about ±5 dB deviation.

FIGURE 62

Measured path loss results in the data centre environment

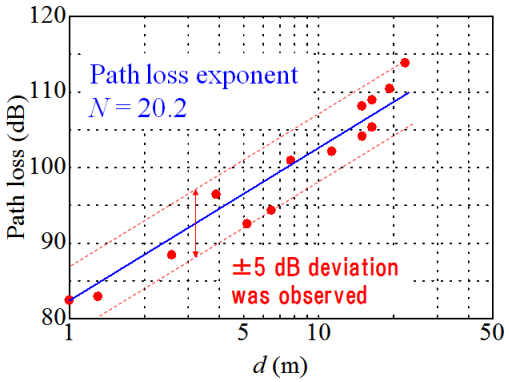

6.5.5 Conclusion

The path loss coefficients of office and corridor environments at 300 GHz have been extracted using directional antennas. The coefficient of office environment was roughly identical with the free space loss of $N = 20$, and the coefficient of corridor environment was slightly decreased to $N = 19.5$. These parameters are also close in value to the coefficient at 60 and 70 GHz of Recommendation ITU-R P.1238.

The path loss coefficients of a data centre environment at 300 GHz have been extracted using directional antennas. The path loss coefficient was $N = 20.2$ which is roughly identical with the free space loss of $N = 20$, however, it has a ±5 dB deviation by interference of direct and reflection waves.

The new power loss coefficients were proposed based on the results and analyses.

6.6 Study 6: Rms delay spread parameters (Frequency bands: 28, 38 GHz)

6.6.1 Executive summary

This study provides additional information for the rms delay spread parameters included in Recommendation ITU-R P.1238. This study focuses on the frequency bands 28 and 38 GHz based on measurements made in indoor commercial environments (Seoul railway station and Incheon international airport terminal)

6.6.2 Background and proposal

Table 52 shows the proposed rms delay spread parameters.

TABLE 52

rms delay spread parameters

Freq. (GHz)	Environ-ment	Polari-zation	Time delay resolution (ns)	Tx beam width (degrees)	Rx beam width (degrees)	A (ns)	B (ns)	C (ns)	Note for A, B, C
28	Commercial	VV	2	60	Omni	17 36	34 65	64 86	(1, 2)
38	Commercial	VV	2	40	Omni	4 42	26 69	55 82	(1, 2)

(1) Upper and lower values are LoS and NLoS cases, respectively.

(2) 20 dB threshold.

6.6.3 Measurement setup and procedure

6.6.3.1 Channel sounder

The channel sounder operates with 4 095 chips pseudo random noise (PN) mode, 500 Mcps chip rates, 2 ns measurement resolution. A channel sounder was implemented using a swept time delay cross-correlation technique. Transmitter (TX) is installed at the height (Hb) of 8.2 m. Its conducting power is 29 dBm at 28 GHz and 21 dBm at 38 GHz carrier frequency. A receiver is at the height (Hm) of 1.7 m. During the measurement, the location of a TX was fixed, and a RX on the floor was positioned at LoS or NLoS environments. A TX antenna has the directional horn type with half-power-beamwidth (HPBW) of 40^0 at 38 GHz or 60^0 at 28 GHz in order to mostly cover the measurement area (railway station or airport terminal), and a RX antenna has the beam pattern of omnidirectional type. Both the TX and RX antenna have the same vertically polarization.

6.6.3.2 Omnidirectional measurements in an indoor commercial environment

Measurements were performed in the Seoul railway station and the Incheon airport terminal in the Republic of Korea. The features of these indoor environments are given below and shown in Fig. 63.

– Site 1 (Seoul railway station): The measurement was carried out in a large hall with a dimension of 80 m (length) × 45 m (width) × 21 m (height) located on the 1st floor of terminal building. The ceiling and walls of the hall are built with steel frames and thick tempered glasses. The floors are constructed with steel-reinforced concrete. There are offices, ticketing boxes and shops in the hall. A large electric notice board informing train departure-and-arrival time is on the wall.

– Site 2 (Incheon airport terminal): The measurement has been carried out in a big hall with a dimension of 320 m (length) × 82 m (width) × 20 m (height) which is on the third floor of the airport passenger terminal building. Building materials are similar to the Seoul railway station except for parallel arranged check-in booths.

FIGURE 63

Measurement environments

(a) Seoul railway station

(b) Incheon airport terminal

Considering available measurement data including both LoS and NLoS environment, a maximum TX to RX measurement distance was determined as within either 150 m at 38 GHz or 85 m at 28 GHz. At every measurement location, 441 power delay profile (PDP) samples were obtained. The maximum floor space for the measurements was 3 600 m^2 in the railway station and 26 240 m^2 in the airport terminal.

The rms delay spread (DS) was derived for four categories (LoS at 38 GHz, LoS at 28 GHz, NLoS at 38 GHz, and NLoS at 28 GHz) from gathering the measured PDPs given by the square of the magnitude of the channel impulse response (CIR). The threshold was used for determining the multipath if PDPs have enough peak-to-spurious dynamic range to ensure the integrity of the results. For the results reported in this document, the threshold was set 20 dB below the peak of PDP. The

parameters chosen to provide the statistical description of the multipath effects are median values that occur frequently, 10%, and 90% values of the cumulative distribution on omnidirectional rms DS.

6.6.4 Validation results

Firstly, typical DS parameters estimated from average delay profiles for indoor environments are given in Table 5 in § 4.3 of Recommendation ITU-R P.1238-8. The values given in the Table represent the largest hall sizes likely to be encountered in each environment. Based on the rms DS given in Recommendation ITU-R P.1238-8, A(10%), B(50%), and C(90%) values of the CDF on rms DS at 28 GHz and 38 GHz. For an indoor commercial environment, it was found that omnidirectional rms DS depends on both frequency and LoS/NLoS environment from results in Table 52.

6.6.5 Conclusion

This study describes additional information on measurement environment and the process for deriving the proposed rms delay spread parameters. From the results, these parameters could be applied for indoor environments such as public commercial indoor area at 28 and 38 GHz.

6.7 Study 7: Rms delay spread parameters (Frequency bands: 30, 60 GHz)

6.7.1 Executive summary

This study provides additional information for the rms delay spread parameters included in Recommendation ITU-R P.1238. This study focuses on the frequency band 60 GHz based on measurements made in various indoor office environments (computer cluster, office/classroom, corridor).

6.7.2 Background and proposal

Table 53 shows the proposed rms delay spread parameters.

TABLE 53

rms delay spread parameters

Freq. (GHz)	Environ-ment	Polari-zation	Time delay resolution (ns)	Tx beam width (degrees)	Rx beam width (degrees)	A (ns)	B (ns)	C (ns)	Note for A, B, C
29.3-31.5	Computer cluster	Dual(1)	0.45	35	35	1.2	2.5	14	(2)
			0.45	35	35	1.6	17.6	34	(3)
					18.4	2.14	10.7	29.7	(2, 8)
	Office/ classroom	VV/HH	0.5	56.3	18.4	0.56	0.65	4.29	(2)
					18.4	1.6	15.8	26.7	(2, 8)
	Corridor	VV/HH	0.5	56.3	18.4	0.54	0.72	1.34	(2)
					18.4	0.81	8.9	44.6	(2, 8)

TABLE 53 (*end*)

Freq. (GHz)	Environ-ment	Polari-zation	Time delay resolution (ns)	Tx beam width (degrees)	Rx beam width (degrees)	A (ns)	B (ns)	C (ns)	Note for A, B, C
58.7-63.1	Computer cluster	VV	0.22	15.4	15.4	1.0	5.2	10.6	(4)
		VV	0.9	15.4	2.2	1.2	12	37.5	(5)
	Office(6)	VV	0.22	Omni	Omni	0.68	1.7	4	(6)
		VV	0.22	Omni	Omni	0.45	1.77	5.2	(7)

(1) Mean value of VV, VH, HV, and HH.

(2) 20 dB, and (3) 30 dB threshold.

(4) 30 dB threshold, receiver pointing towards transmitter.

(5) 20 dB threshold, receiver antenna rotated around 360 degrees.

(6) Tx and Rx are on body to on body and (7) on body to off body.

(8) Receiver antenna was rotated in a step of 5^{o} around 360 degrees in measurements. The value represents a directional delay spread when the bore-sight of receiver antenna is not aligned to the direction of transmitter.

6.7.3 Measurement setup and procedure

Under the Open Call 1 of CREW (Cognitive Radio Experimental World), measurements were performed in three of the test beds: the air cabin in EADS, the office environment at the Technical University of Berlin (TUB) and the semi-shielded environment in iMinds to estimate channel parameters including path loss. The measurements were performed with 550 MHz bandwidth with waveform repetition rate equal to ~1.1 kHz in the ISM 1 band (2.2-2.75 GHz) using the multi band radio channel sounder recently developed at Durham University [1]. Where possible the measurements were taken at the positions of the nodes in the test beds. Thus for example in the measurements at TUB, the antennas were placed in close proximity to the nodes which are all mounted on the ceiling in different rooms on the same floor. Similarly in the test bed at iMinds, the antennas were placed in the locations of the nodes which are at about 1.5 m above ground.

In addition to three frequency bands below 6 GHz, the sounder has up and down converters to two mm wave bands: 30 GHz and 60 GHz with 2 transmit and two receive channels.

In a first measurement campaign, was used in a wide corridor environment as shown in Fig. 64. For these measurements, the transmitter and receiver were mounted on trolleys with the receiver being held in a fixed location with the 60 GHz unit mounted close to the ceiling at 2.35 m as illustrated by the arrow in Fig. 64(a) and the receiver antenna was mounted on the side of the trolley at 1.46 m as in Fig. 64(b). The measured environment is shown in Fig. 64(c) where it can be seen to be a long wide corridor with workstations with computers and a light well to one side as indicated by the blue arrow on the right hand side and offices on the opposite side. The measurements were taken along a path starting from a distance of ~8.7 m to a distance of 35 m. The measurements were performed with a bandwidth of 4.4 GHz and waveform duration of 819.2 μs. To enable the 2 by 2 MIMO measurements two-way switching at the transmitter was used while receiving in parallel.

FIGURE 64

Experimental set up for the two by two measurements in the indoor environment (a) receiver location with antenna set up as close as possible to ceiling, (b) receiver trolley with antenna mounting, and (c) overview of the measured environment with the red arrow indicating the location of the receiver trolley

(a) (b) (c)

In a second measurement campaign, the sounder was used to measure the delay spread in a computer cluster environment as shown in Fig. 65. For these measurements, the transmitter and receiver were mounted on trolleys with the transmitter being held in a fixed location with the 30 GHz or 60 GHz unit being mounted close to the ceiling at about 2.35 m as illustrated by the arrow in Fig. 65(a) and the receiver antenna was mounted on the trolley at 1.5-1.6 m as in Fig. 65(b). For the 30 GHz measurements both the transmitter and receiver used dual polarised antennas. At the transmitter the transmission was switched sequentially between the two polarisations while at the receiver the two polarisations were received simultaneously. For the 60 GHz measurements a single horn antenna was used at the transmitter while at the receiver a lens antenna (with 2.2 in the E plane and 2.6 in the H plane) mounted on the receiver unit was used to estimate the channel response as a function of angle of arrival. For this the receiver unit was mounted on a turntable which was controlled to rotate at 5 degree steps to generate 73 channel responses for each location.

FIGURE 65

Experimental set up for the measurements in the indoor environment

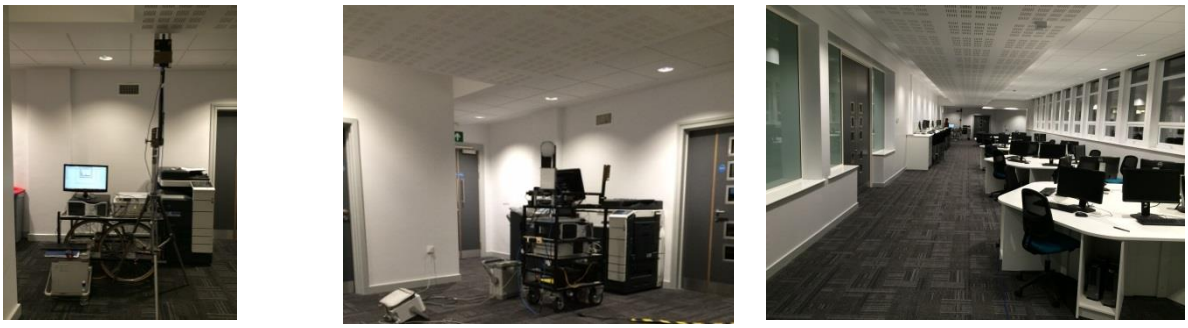

(a) transmitter location with antenna set up as close as possible to ceiling

(b) receiver trolley with lens antenna mounted on rotating table

(c) overview of the measured environment

The measured environment is shown in Fig. 65(c) where it can be seen to consist of workstations with computers, a light well on one side as indicated by the arrow on the right hand side and offices on the opposite side.

6.7.4 Validation results

6.7.4.1 First measurement campaign

Following thorough calibration of the sounder, the wideband data were processed to obtain the power delay profiles (see Fig. 66 for an example of power delay profile at 60 GHz), and the area under the profile integrated to estimate the received energy as in equation (1) of Recommendation ITU-R P.1407.

FIGURE 66

Power delay profile at 60 GHz for a single channel in one of the measured locations

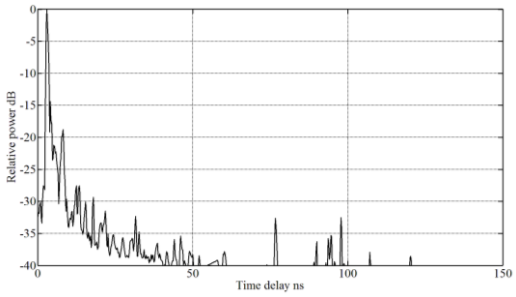

The path loss was then evaluated where in the TUB and iMinds measurements wideband omni-directional antennas were used and in the 60 GHz measurements, two horn antennas with directional beam equal to 15.4°.

The estimated path loss dependence on distance in the 2.625 GHz band in the two measured environments is shown in Fig. 67(a) and (b) where the slope of the curve, n is equal to 4.4 for the office environment in the TUB data and 3.3 for the iMinds measurements.

FIGURE 67

Estimated path loss in (a) office environment in TUB and (b) iMinds with the path loss coefficient fit

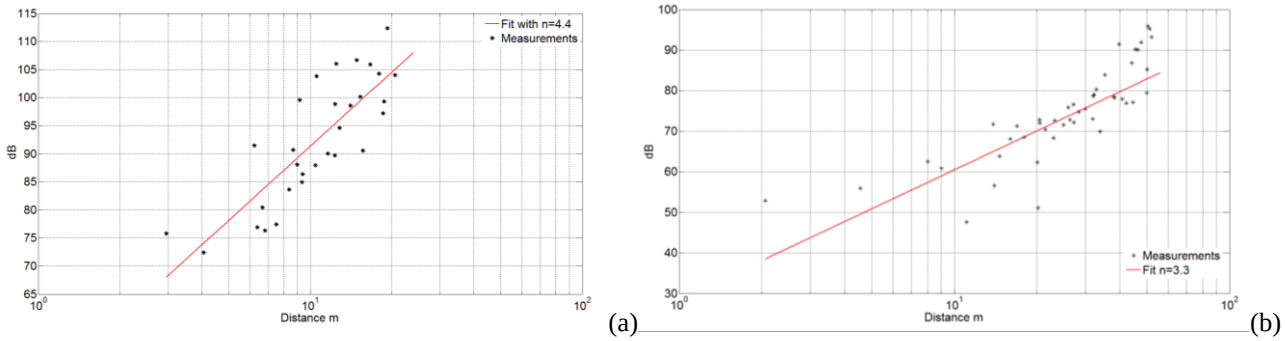

Since all the measurements displayed a dynamic range of at least 40 dB the rms delay spread was computed for 20 and 30 dB threshold levels. The resulting CDF for the thresholds is shown in Fig. 68 which also displays the rms delay spread for the 30 dB threshold for all the four MIMO channels. The Figure shows that the difference between the four MIMO channels is small. Taking the median values gives an rms delay spread of 0.42, and 5.13 ns for the 20, and 30 dB thresholds, respectively and corresponding 90% values equal to 0.69, and 10.65 ns. The 20 dB threshold is seen in the main to capture the dominant components whereas the lower threshold captures the farther away components.

FIGURE 68

(a) rms delay spread for two threshold levels for a single transmitter and receiver channel at 20 dB and for all the four channels for the 30 dB threshold , (b) rms delay spread from all the data for the two threshold levels

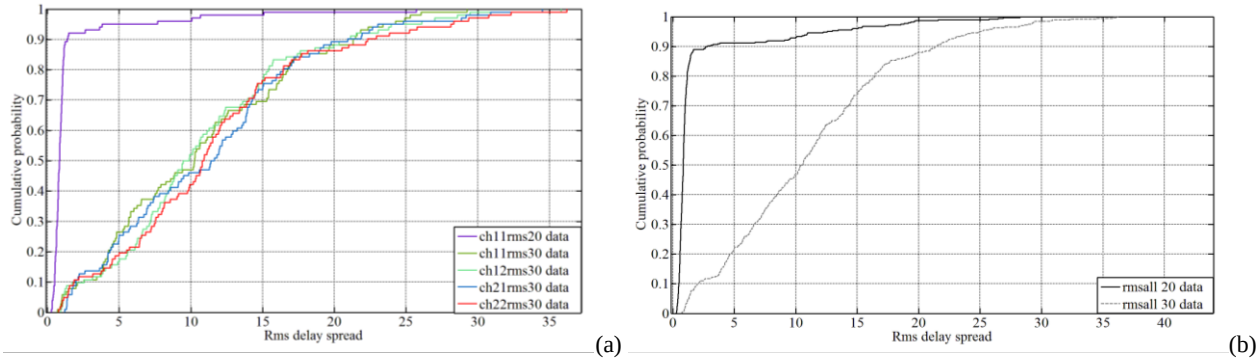

Figure 69 displays the path loss versus distance and the estimated path loss coefficient estimated using the least squares method which is lower than the free space loss.

The extent of the rms delay spread in the measured environment could be due to the glass windows surrounding the space which led to highly reflective surfaces. The lower path loss coefficient can also be attributed to the presence of these reflections which seem to enhance the received energy computed from the area under the power delay profile.

FIGURE 69

Path loss versus range and fit of path loss coefficient

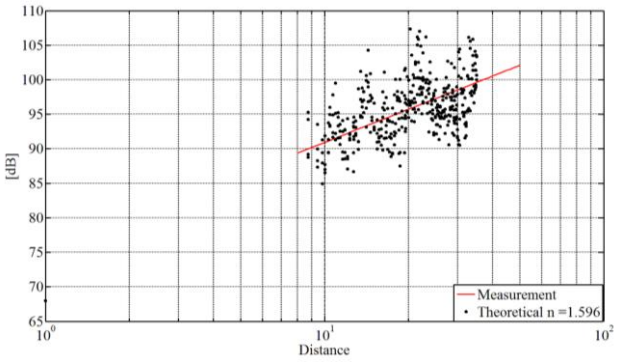

On body networks have also been measured at 60 GHz as in Fig. 70 with the transmitter and receiver antennas placed on body [2]. Measurements were performed with various movements as well as from an on body antenna to an antenna fixed on a trolley and moved away from the transmitter for distances up to 6 m. Each data file consisted of 15 second of continuous measurements. An example is illustrated in Fig. 71.

FIGURE 70

Configuration of on body measurements

FIGURE 71

Examples of power delay profile (a) on body to off body antenna, (b) on body measurements

(a) (b)

The data were analysed to estimate the delay spread as in Fig. 72.

FIGURE 72

rms delay spread of on body and on body to off body measurements

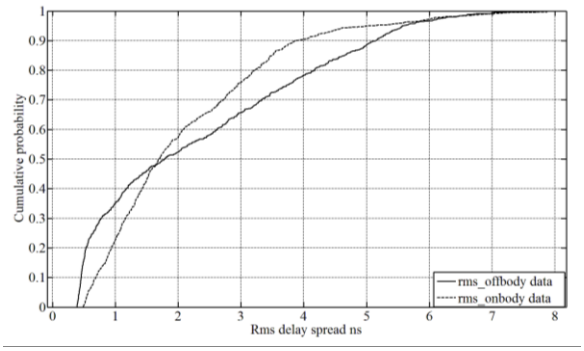

6.7.4.2 Second measurement campaign

60 GHz measurements: The measurements were taken along a path starting from a distance of ~2.2 m to a distance of 27 m with a bandwidth of 4.4 GHz and 819.2 µs waveform duration. The data were subsequently analysed with a 1.1 GHz bandwidth resolution and an example of the power delay profile as a function of angle of arrival is shown in Fig. 73 for one of the locations.

FIGURE 73

Power delay profile at a single location for different angles of arrival

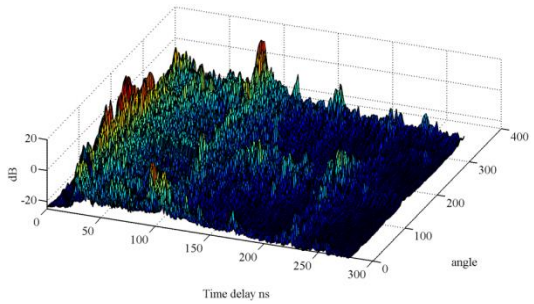

For each power delay profile, a 20 dB threshold below the peak was used to estimate the rms delay spread and all power delay profiles not meeting the threshold level were discarded from the CDF shown in Fig. 74. For the 19 measured locations a total of 1 387 delay profiles were used with 1 376 delay profiles meeting the threshold criterion. Table 54 summarises the results of the 10%, 50% and 90% values as estimated from the CDF.

FIGURE 74

Cumulative distribution function of rms delay spread for lens antenna for all angles of arrival

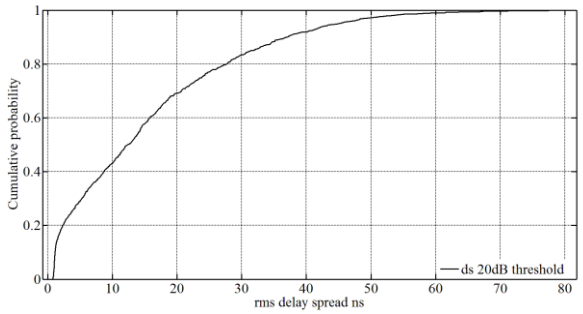

TABLE 54

Summary of rms delay spread for 20 dB threshold for different antenna orientation

Parameter	10%	50%	90%
20 dB rms delay spread	1.2 ns	12 ns	37.5 ns

30 GHz measurements: The measurements were performed with 2.2 GHz bandwidth and 819.2 μs waveform duration. A total of 21 locations were measured over distances from 3 to 31 m. The transmit antenna mounted at 2.25 m and the receiver antenna at 1.3 m above ground. Dual polarised antennas at both ends were used. Figure 75 displays the normalised power delay profile for the four channels whereas Fig. 76 displays the relative power delay profiles for the 21 locations for the V to H polarised antennas.

FIGURE 75

Power delay profiles with the dual polarised antennas (top left) V to H, (top right) V to V, (bottom left) H to H, (bottom right) H to V

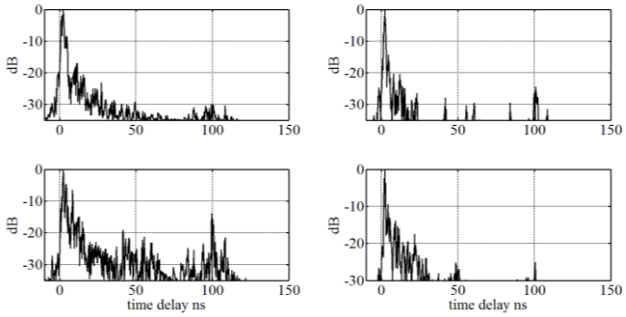

FIGURE 76

Power delay profiles for the V to H antennas for all the measured locations

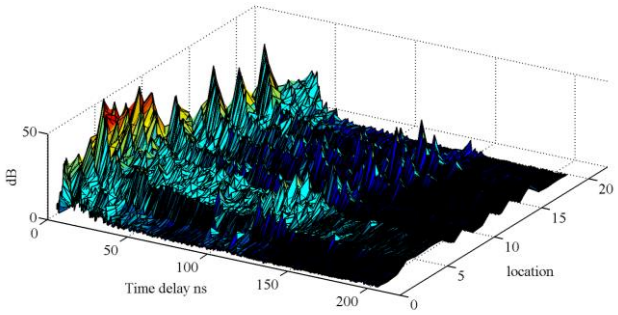

The data were analysed with the full bandwidth. Both 20 dB and 25 dB thresholds were subsequently used to estimate the rms delay spread as shown in Fig. 77(a) for the co-polarised and cross polarised antennas and Fig. 77(b) for all the data with 20 dB threshold. A summary is given in Table 55.

FIGURE 77

rms delay spread:

(a) For both dual polarised antennas for 20 and 25 dB threshold (b) For all the data for 20 dB threshold

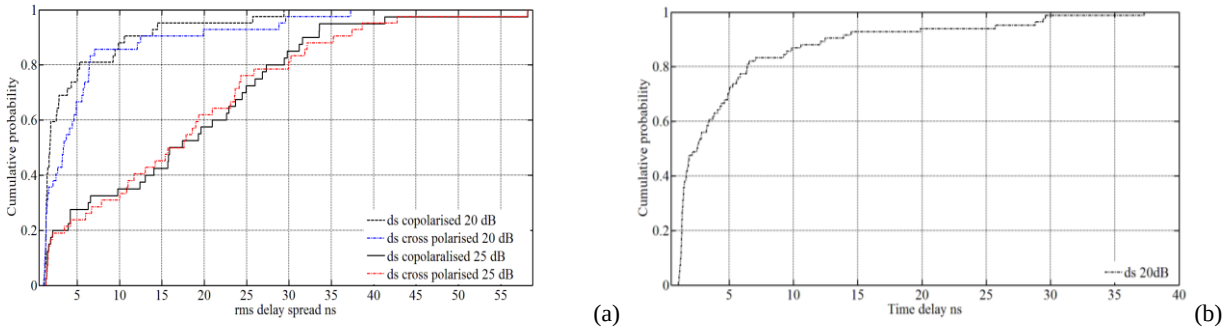

TABLE 55

Summary of rms delay spread for 20 dB threshold for different antenna polarisation

Parameter	10%	50%	90%
20 dB rms delay spread	1.2 ns	3.4 ns (cross-polarised)	7 ns (cross-polarised)
	1.2 ns	1.7 ns (co-polarised)	10.6 ns (co-polarised)
All data	~1.2 ns	2.5 ns	14 ns
25 dB	1.6 ns	17.6 ns	33.6 ns (co-polarised)
	1.6 ns	17.6 ns	37 ns (cross-polarised)
All data	1.6 ns	17.6 ns	34 ns

6.7.5 Conclusion

Based on above measurement results and observations, new rms delay spread parameters were included in Recommendation ITU-R P.1238.

6.7.6 References

[1] Sana Salous, Adnan Cheema and Xavier Raimundo, Radio channel propagation measurements and spectrum sensing using an agile chirp sounder, IC1004 TD(14)09032, Ferrara, Italy, 5-7 February, 2014.

[2] Sana Salous, Adnan Cheema and Xavier Raimundo, radio propagation measurements using a multi-band agile chirp sounder, URSI GA, GASS 2014, pp 1-4.

6.8 Study 8: Antenna directivity dependence of static rms delay spread in NLoS (Frequency band: 60 GHz)

6.8.1 Executive summary

This study provides additional information to the antenna directivity dependence of static rms delay spread in NLoS at 60 GHz, included in Recommendation ITU-R P.1238.

Corresponding to the requirement of new spectrum resources for the expansion of the existing services and incoming new services, the study of millimetre wave bands (30 to 300 GHz) has been improved [1]. At high frequency bands, above 60 GHz band have been considered for providing the highest speed services[2][3]. But the transmission rate is limited by delay spread. This is more sensitive at millimetre-wave band because of high speed and very small wavelength [4].

To study the delay spread characteristics in the millimetre-wave band, about four types of antenna beamwidth have been measured and about eight types of antenna beamwidth have been simulated in an empty office room with only a partition by ray-tracing method. To verify the validity of the ray-tracing method, propagation characteristics were measured in the office with NLoS and compared to simulated results.

In this Report, the static rms delay spread in NLoS is proposed according to the beamwidth of a receive antenna at 60 GHz and add some parameters in Recommendation ITU-R P.1238.

6.8.2 Background and proposal

Table 56 shows the proposed parameters for antenna directivity dependence of static rms delay spread in NLoS at 60 GHz

TABLE 56

Example of antenna directivity dependence of static rms delay spread

Frequency (GHz)	Tx antenna	Rx antenna beamwidth (degrees)	Static rms delay spread (90^{th} percentile) (ns)	Room size (m)	Remarks
60	Omnidirectional	Omnidirectional	22	13.0 × 8.6 Empty office room	Ray-tracing NLoS
		60	21		
		10	10		
		5	6		

6.8.3 Measurement setup and procedure

The radio propagation measurements at 60 GHz was done in an empty office, the size was 13 × 8.6 × 3 m. The transmitter was composed of a signal generator, a power amplifier, and an omnidirectional antenna which was located on the corner of the room. The receiver was composed of a low noise amplifier, a spectrum analyser, a laptop computer for data storage, and 4 antennas, they

were an omnidirectional antenna and 3 horn antennas each beamwidth 45º, 30º, 12º. The radio path was made NLoS installing a partition before the transmitter. The height of transmitter and receiver was 1.5 m equally, and the distance between them was from 1.8 m to 9.8 m. The receiver system was set on a 2 m length of rail to move mechanically very precisely, 2 mm step, smaller than a half wavelength. It was possible to see the characteristics of the short term fading in this case.

Figure 78(a) shows a top view of measurement office room that is represented by x-y coordinate with 1 m step. The centre of the room is (0,0) and the transmitter is located at (−3.2, −5.5). Figure 78(b) is one of the measurement photos, Table 57 provides the measurement specifications, and Fig. 78(c) is a partition for NLoS.

A ray tube method of a ray-tracing was used for simulation in the same conditions of Fig. 78(a). The tree of ray-tracing was considered three times reflections include a diffraction or four times reflections, and some penetration through obstacles.

FIGURE 78

(a) Top view of measurement environment, (b) Measurement photo, (c) A partition for NLoS

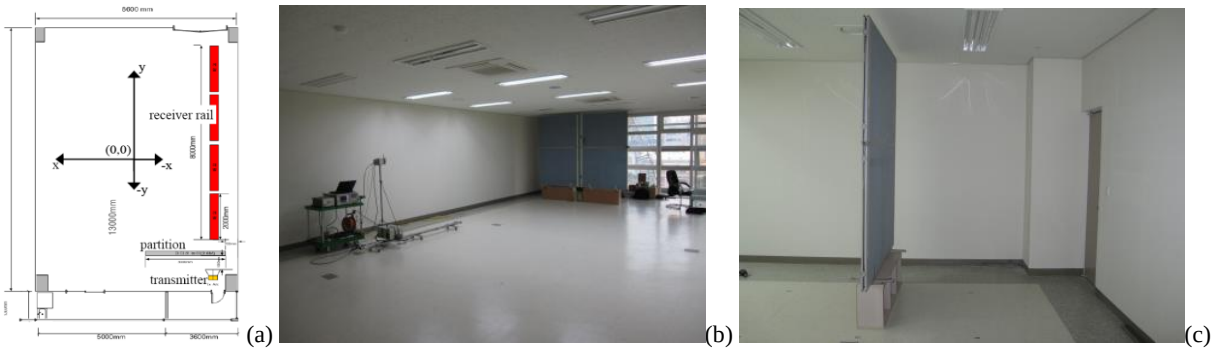

(a) (b) (c)

TABLE 57

Measurement specifications

Tx antenna	Omnidirectional antenna
Rx antennas	4 types beamwidth : omni, 45º, 30º, 12º
Distance between Tx and RX	straight line, from 1.8 m to 9.8 m (y = −3.7 ~ +4.3)
Height of Tx and Rx	1.5 m
Measurement spacing	2 mm step
Empty room size	13 × 8.6 × 3 m

6.8.4 Validation results

Figure 79(a), (b), (c), (d) with the measured and simulated results show the level of the received signals based on distance between transmitter and receiver. They almost agree with each other and the difference of them is represented by the rms error of equation (27).

$$RMSE(s,m)=\sqrt{\frac{\sum_{i=1}^{n}(s_i-m_i)^2}{n-1}} \tag{27}$$

The receive antenna of Fig. 79(a) shows a 12º beamwidth and it shows 6.8 dB of rms error. Figure 79(b) shows a 30º beamwidth of the receive antenna and 5.8 dB of rms error. Figure 79(c) shows a 45º beamwidth of the receiving antenna and 6.9 dB of rms error. The omni directional receive

antenna of Fig. 79(d) is 7.3 dB of rms error. Overall, the rms error distributes between the 5.8 ~ 7.3 dB, and they are a severe variation due to including the short term fading. If it were considered as long term fading, the rms error is expected much reduced.

FIGURE 79

Comparison of measurement and simulation results:
(a) beamwidth 12 degrees, RMSE : 6.8dB, (b) beamwidth 30 degrees, RMSE : 5.8dB
(c) beamwidth 45 degrees, RMSE : 6.9dB, (d) omnidirectional antenna, RMSE : 7.3dB

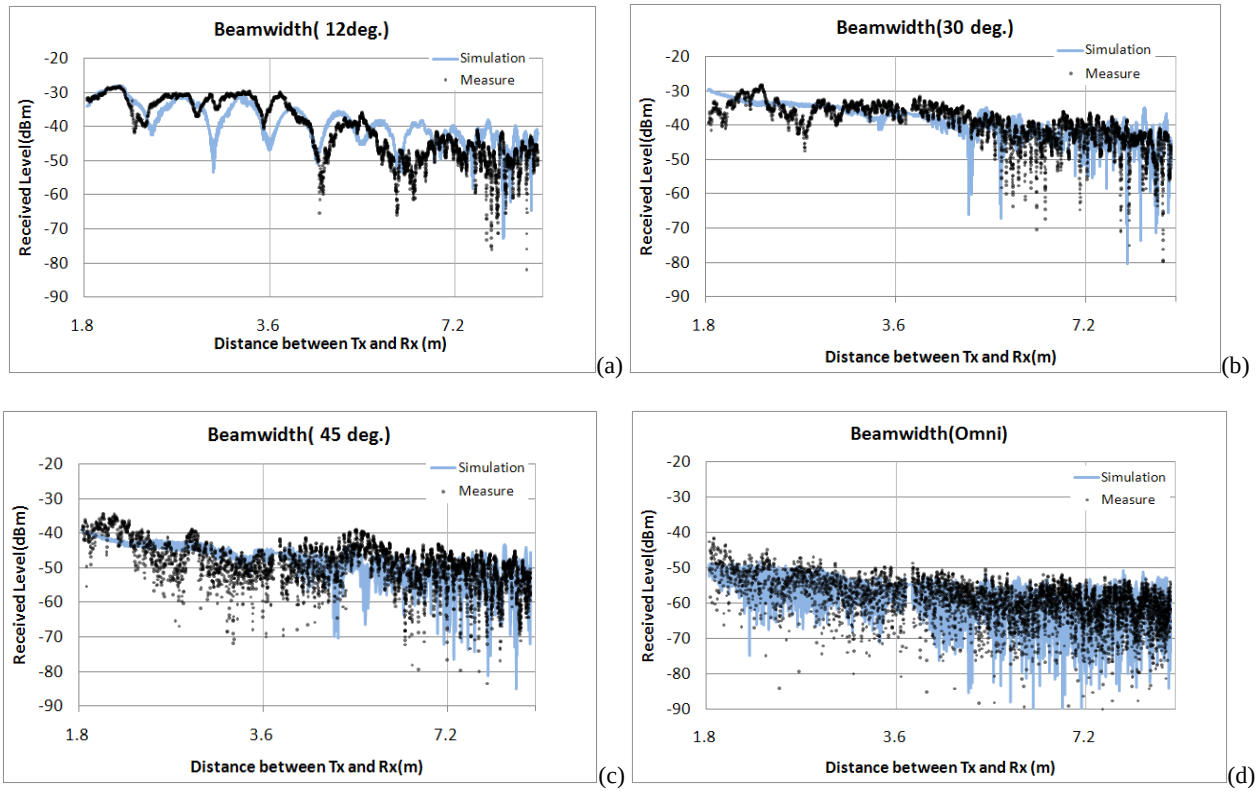

Ray-tracing as one of the analytical method can make a much more accurate prediction of radio propagation characteristics than the other statistical prediction methods [5]. The statistical propagation model in a millimetre-wave band can be obtained by analysing the measured data in various conditions and environments. However, satisfactory results cannot be obtained if the measurement is difficult. Therefore, the simulations have been conducted with various conditions instead of measuring in the real environments. After that, the propagation model can be obtained by statistical parameters extracted from simulation results. The accuracy of the prediction results are obtained from comparing them to the actual measurement results. The obtained rms errors are within about 6 ~ 7 dB in Fig. 80, these are very accurate results because the short term fading has been considered which has 20 ~ 30 dB of instantaneous fluctuation.

FIGURE 80

RMS delay spread according to beamwidth of antenna in NLoS

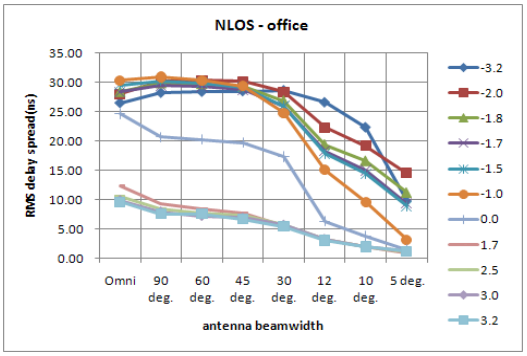

The channel impulse response $h(\tau)$ of equation (27) is obtained using a ray-tracing simulation.

$$h(\tau) = \sum_{i=0}^{I-1} p_i \exp(j\phi_i)\delta(\tau - \tau_i) \tag{28}$$

And the rms delay spread is

$$\tau_{rms} = \sqrt{\frac{\sum_{i=0}^{I-1} \tau_i^2 \cdot p_i^2}{\sum_{i=0}^{I-1} p_i^2} - \tau_n^2} \tag{29}$$

where

$$\tau_n = \frac{\sum_{i=0}^{I-1} \tau_i \cdot p_i^2}{\sum_{i=0}^{I-1} p_i^2} \tag{30}$$

Figure 81 shows simulation results of the rms delay spread according to the variation of antenna beamwidth by a ray-tracing method with Fig. 78(a)'s conditions. Figure 81 shows the comparison of measured and simulated rms delay spread according to the beamwidth of antennas in NLoS. They are very similar to each other. It shows that the narrower the beamwidth of the antenna used indoor, the smaller the delay spread, because an antenna with narrow beamwidth cannot receive many multipath reflection waves.

FIGURE 81

Comparison of measured and simulated RMS delay spread according to beamwidth of antenna in NLoS

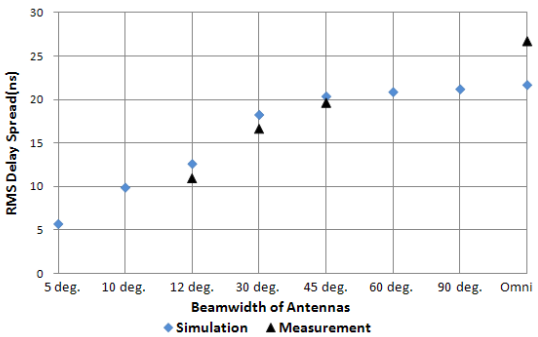

6.8.5 Conclusion

The measurements and simulations have been used to study the delay spread characteristics in a millimetre-wave band. Propagation characteristics were measured according to antenna beamwidth in an empty office room with only a partition for NLoS and obtained the accuracy of the simulation from a ray-tracing method compared to the measurement results. Static rms delay spread was analysed in an empty office room.

Based on the results and analyses, new values for the antenna directivity dependence of static rms delay spread were included in Recommendation ITU-R P.1238.

6.8.6 References

[1] S.K.Yong, C.Chong and S.S. Lee, "Generalization and parameterization for 802.15.3c channel model," IEEE P802.15 Working Group for Wireless Personal Area Networks (WPANs), IEEE 15-05-0261-00-003c, SAIT, 2005.

[2] N. Moriatis and P. Constantinou, "Indoor channel measurements and characterization at 60 GHz for wireless local area network applications," IEEE Trans. Antennas Propagat., vol. 52, no. 12, pp. 3180-3189, Dec. 2004.

[3] H. Xu, "Terrestrial Radio Wave Propagation at Millimeter-wave Frequencies", Ph. D. Dissertation, Virginia Polytechnic Institute and State University, Mat 2000.

[4] T. Manabe, Y. Miura, and T. Ihara, "Effect of Antenna Directivity on Indoor Multipath Propagation Characteristics at 60GHz", IEEE Journal on Select. Areas in Comm., vol. 14, no. 3, Apr. 1996.

[5] D. Dardari, L. Minelli, V. Tralli, and O. Andrisano, "Fast Ray-tracing Characterization of Indoor Propagation Channels at 60GHz", VTC'97, pp. 989-993, 1997.

6.9 Study 9: Effects of antenna beamwidth to multipath delay and angular spread (Frequency bands: 28, 38 GHz)

6.9.1 Executive summary

This study observes the effect of antenna beamwidth for multipath propagation characterization in various indoor office environments to derive coefficients of delay spread and angular spread as a function of antenna beamwidth. Measurements were conducted at 28 GHz and 38 GHz.

6.9.2 Background and proposal

The rms delay spread *DS* depends on half-power beamwidth of antenna θ (degree):

$$DS(\theta) = \alpha \times \log_{10}\theta \quad \text{ns} \tag{31}$$

where α is a coefficient of rms delay spread and the range of θ is defined as $10^{o} \leq \theta \leq 120^{o}$. Table 58 lists the typical values of the coefficients and a standard deviation σ based on each measurement condition. The coefficients of delay spread represent cases when the boresights of antennas were aligned to have a maximum receiving power in LoS and NLoS situations, respectively.

TABLE 58

Typical coefficients for rms delay spread

Measurement conditions								Coefficients of rms delay spread	
f **(GHz)**	**Environment**	**Scenario**	h_1 **(m)**	h_2 **(m)**	**Range (m)**	**Tx beamwidth (degree)**	**Rx beamwidth (degree)**	**α**	**σ (ns)**
28	Railway Station	LoS	8	1.5	8-80	60	10	8.25	16.11
		NLoS						37.54	27.22
	Airport Terminal	LoS			8-200			7.53	15.98
		NLoS						63.9	96.57
38	Railway Station	LoS	8	1.5	8-80	40	10	4.18	4.33
		NLoS						24.85	28.48
	Airport Terminal	LoS			8-200			4.46	14.13
		NLoS						54.54	80.72
	Office	LoS	2.5	1.2	7-24	omni	10	1.16	12
		NLoS						15.13	21.8

The rms angular spread *AS* depends on half-power beamwidth of antenna θ (degree):

$$AS(\theta) = \alpha \times \theta^{\beta} \quad \text{degree} \tag{32}$$

where α and β are coefficients of rms angular spread and the range of θ is defined as $10^{o} \le \theta \le 120^{o}$. Table 59 lists the typical values of the coefficients and standard deviation σ based on each measurement condition. The coefficients of angular spread represent cases when the boresights of antennas are aligned to have a maximum receiving power in LoS and NLoS situations, respectively.

TABLE 59

Typical coefficients for rms angular spread

Measurement conditions								Coefficients of rms angular spread		
f **(GHz)**	**Environment**	**Scenario**	h_1 **(m)**	h_2 **(m)**	**Range (m)**	**Tx beam-width (degree)**	**Rx beam-width (degree)**	**α**	**β**	**σ (degree)**
28	Railway Station	LoS	8	1.5	8-80	60	10	0.5	0.77	2.3
		NLoS						0.25	1.0	2.32
	Airport Terminal	LoS			8-200			1.2	0.49	2.18
		NLoS						0.3	0.96	3.12

TABLE 59 (*end*)

Measurement conditions								Coefficients of rms angular spread		
f **(GHz)**	**Environment**	**Scenario**	h_1 **(m)**	h_2 **(m)**	**Range (m)**	**Tx beam-width (degree)**	**Rx beam-width (degree)**	**α**	**β**	**σ (degree)**
38	Railway Station	LoS	8	1.5	8-80	40	10	1.14	0.54	3.36
		NLoS						0.16	1.1	3.24
	Airport Terminal	LoS			8-200			2.0	0.34	1.36
		NLoS						0.34	0.93	2.99
	Office	LoS	2.5	1.2	7-24	omni	10	0.07	1.22	5.58
		NLoS						0.17	1.07	4.81

6.9.3 Measurement setup and procedure

6.9.3.1 Measurement equipment

Table 60 lists a detailed specification of the ETRI's channel sounder measuring the spatial and temporal characteristics of a 500 MHz wideband channel at the centre frequencies of 28 and 38 GHz [4]. As shown in Fig. 82, the positioner can mount a directional horn antenna and can rotate the orientation of the horn antenna both horizontally and vertically with 1° accuracy to control the bore-sight of transmitting/receiving beams during measurements.

TABLE 60

Specifications of ETRI's channel sounder

System parameters		Specifications
Centre frequency		28 / 38 GHz
Channel Bandwidth		500 MHz
PN code length of probing signal		4095 chips
Maximum TX power (w/o antenna)	28 GHz	29 dBm
	38 GHz	21 dBm
Multipath resolution		2 ns
HPBW of pyramidal horn antenna and gain	28 GHz	10^o(24.4 dBi), 60^o (9.9 dBi)
	38 GHz	10^o(24.6 dBi), 40^o (12.6 dBi)

FIGURE 82

ETRI's mmWave channel sounder

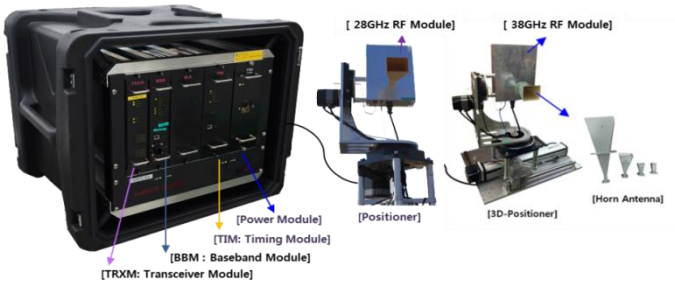

6.9.3.2 Measurement scenarios

A first indoor measurement campaign has been carried out in Seoul railway station and Incheon international airport terminal. Detailed features of each measurement place are summarized as below.

– Seoul railway station, Korea (ST): A large hall with a dimension of 170 m × 45 m × 21 m (height) located on the 1st floor of passenger terminal building. The ceiling and walls of the hall are built with steel frames and thick tempered glasses. The floors are constructed with steel-reinforced concrete. There are offices, ticketing boxes and shops in the hall. A large electric notice board informing train departure-and-arrival time is on the wall.

– Incheon airport terminal, Korea (AP): A big hall with a dimension of 650 m × 82 m × 20 m (height) located on the third floor of a passenger terminal building. Building materials are similar to those of the Seoul railway station except for the parallel-arranged check-in booths.

Figure 83 shows the layouts of measurement sites on which locations of a transmitter (TX) and a receiver (RX) are marked. To emulate typical hot-spot scenarios, the TX antenna (a 60° HPBW horn antenna for 28 GHz and a 40° antenna for 38 GHz measurement) was installed at a height of 8 m from the floor and the RX antenna (a 10° HPBW horn antenna for both 28 and 38 GHz) at 1.5 m (pedestrian level). During measurement, the location of TX was fixed, and the RXs were placed at LoS and NLoS positions. The bore-sight direction of the TX antenna was directed to cover the entire range of interest. On the other hand, the bore-sight of the RX antenna was rotated with a step size of 10° in the azimuth from 0° to 350° and in the co-elevation from −10° to 10°.

FIGURE 83

Layout of measurement scenario in (a) Seoul Railway station (ST), (b) Incheon Airport terminal (AP)

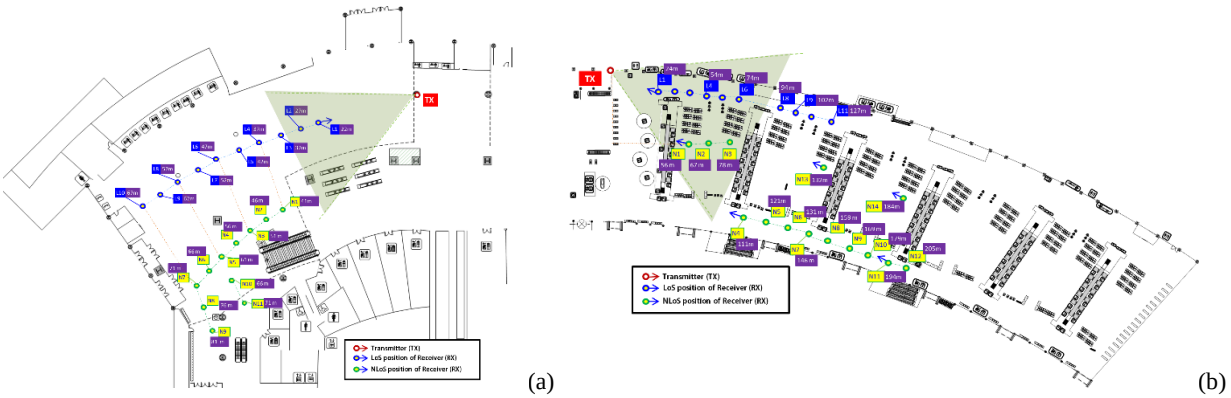

A second measurement campaign has been conducted in a typical office environment at 38 GHz. It is noted that the channel sounder can measure the multipath distribution characteristics using a 500 MHz wideband probing signal with a temporal resolution of 2 ns and an angular domain of 1 degree. Figure 84 shows the office map on which the locations of transmitter (TX) and receiver

(RX) are marked. The office has a dimension of 33 m (L) × 23 m (W) × 2.6 m (H), in which cubicle areas, meeting rooms, pillars, etc. are laid out.

The outside walls of the building are composed of concrete and large tempered glass, whereas the inside walls and ceilings are made of reinforced concrete, steel and plaster board. As shown in the Figure, measurement data are collected at the links between two TX (red points) and 20 RX locations (blue, green and purple points distributed evenly in the office) for LoS and NLoS situations. The separation distance of TX to RX ranges from 7 m to 24 m.

FIGURE 84

Layout of measurement scenario in a typical office environment

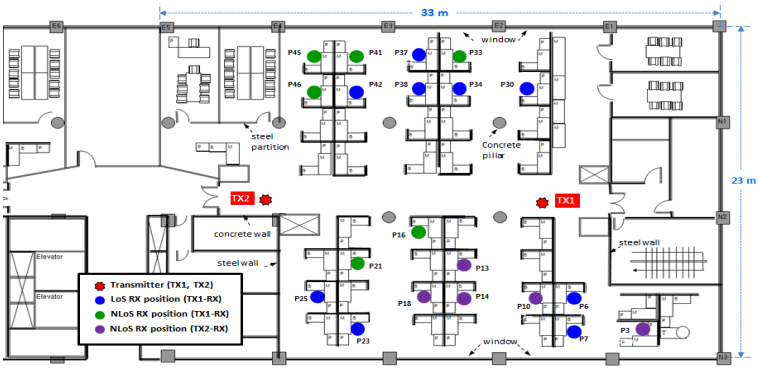

Figure 85 shows the photographs of channel sounders including the TX and RX antennas at the height of 2.5 m and 1.2 m, respectively. All the setting parameters of the channel sounder were same as the previous measurement campaign except that an omnidirectional antenna at the TX and a 10° HPBW horn antenna at the RX side were used, respectively. During measurements as shown in Fig. 85, the horn antenna mounted on the positioner was rotated in the step size of 10° in the azimuth from 0° to 350° and in the co-elevation from −15° to 45°. The measured data are used to derive the delay and angular spread characteristics of multipath arrivals.

FIGURE 85

Measurement campaign in the office (picture)

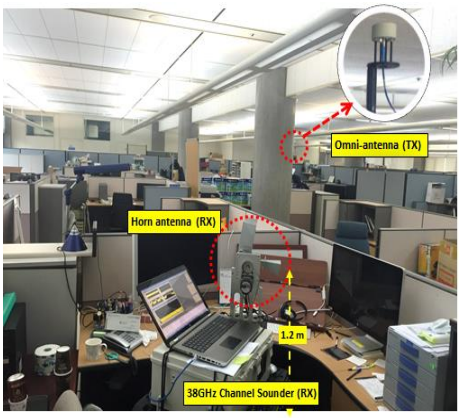

For the calculation of a directional rms DS with respect to the beamwidth of receiving antenna, CIRs collected through a 360° antenna steering are used. All the procedures were followed as described above, which included steps of combining CIRs to calculate the PADS, searching a certain angular range using a PAW, obtaining the PDP by summing in angular domain within the observed window, and deriving the DS in the PDP. It should be noted that the delay spread was calculated within an

angular range in which the highest received power is detected. The threshold was set to 20 dB to determine the delay spread.

6.9.4 Validation results

6.9.4.1 Rms delay spread vs. antenna beamwidth

For the first measurement campaign, the RX antenna is rotated by a certain number of steps (N = 36) in azimuth directions. Therefore, each CIR is collected at a different bore-sight direction respectively. From measured CIRs, it is possible to derive a directional rms delay spread (DS) as the following steps [1]-[3].

- The PADS is calculated by using the Bartlett beamforming technique [5] for decoupling the influence of antenna radiation pattern from measured CIRs.
- Define a PAW depending on the antenna's beamwidth to search.
- Search an angular range having the highest power using the PAW in the three-dimentional PADS i.e. power, delay and angle of arrival domain.
- The PDP is obtained by summation in angular domain within the observed angular range in the PADS.
- Calculate a DS from multipath components which are only within a given threshold level in the PDP.

The threshold was set to 20 dB to determine received multipath components since the power delay profiles have enough peak-to-spurious dynamic range to ensure the integrity of the results. The range of PAW was given from 10^o to 120^o. The directional rms delay spread values of each LoS and NLoS case were derived separately. It is noted that a delay spread is calculated within the observed angular range in which the highest received power is obtained. That is, it can be understood that the beam alignment between TX and RX is well established.

Figure 86 shows the DS curves obtained from measurement data at 28 GHz and 38 GHz for LoS and NLoS case, respectively. To obtain the best fitting curve, means of rms DS for each beamwidth are used.

FIGURE 86

Measurement results of directional rms delay spread: (a) LoS, (b) NLoS

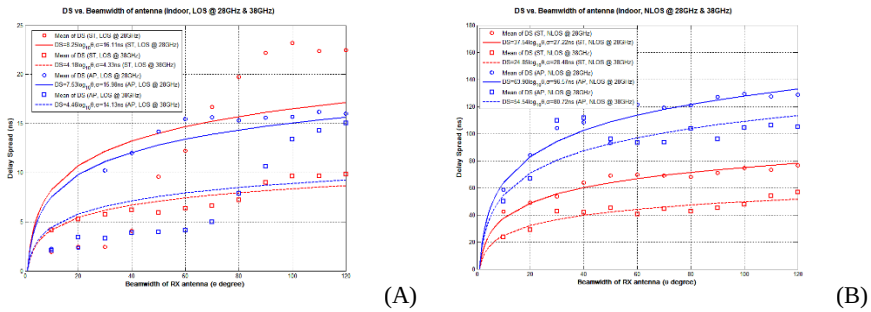

(A) (B)

Based on the measurement results, the following observations are made.

- The DS has a strong dependency on the antenna beamwidth. The difference of DS between a narrow beamwidth antenna and a wider one looks considerably large.
- The DSs of a NLoS case is larger than the values of a LoS case
- The DS curves of 28 GHz are higher than the lines of 38 GHz at both LoS and NLoS cases.
- For a LoS case, the DS curve of ST is close to the one of AP in the same frequency band.

- For a NLoS case, the DS curves of AP are seen as higher than ST. It means that multipath components in AP are more widespread in the delay domain than the circumstance of ST. It is noted that the hall size of AP is bigger than the ST.

The rms delay spread DS with respect to θ which follows a normal distribution with the standard deviation σ is given by;

$$DS(\theta) = \alpha \times \log_{10}\theta \quad \text{ns} \tag{33}$$

where the range of θ is defined as $0^o \leq \theta \leq 120^o$.

Table 61 summarizes the typical coefficients of DS model and standard deviation σ for each measurement scenario and frequency band.

TABLE 61

Directional rms delay spread parameters

Indoor environments			**rms delay spread (ns)**	
			α	**σ (ns)**
Railway Station (ST)	28GHz	LoS	8.25	16.11
		NLoS	37.54	27.22
	38GHz	LoS	4.18	4.33
		NLoS	24.85	28.48
Airport Terminal (AP)	28GHz	LoS	7.53	15.98
		NLoS	63.9	96.57
	38GHz	LoS	4.46	14.13
		NLoS	54.54	80.72

For the second measurement campaign, for the calculation of a directional rms DS with respect to the beamwidth of receiving antenna, CIRs collected through a 360^o antenna steering are used. All the procedures of the first campaign were followed, which include steps of combining CIRs to calculate the PADS, searching a certain angular range using a PAW, obtaining the PDP by summing in angular domain within the observed window, and deriving the DS in the PDP. It should be noted that the delay spread was calculated within an angular range in which the highest received power is detected. The threshold was set to 20 dB to determine the delay spread. Figure 87 shows the DS curves for LoS and NLoS cases.

FIGURE 87

Measurement results of rms delay spread for LoS and NLoS (office at 38 GHz)

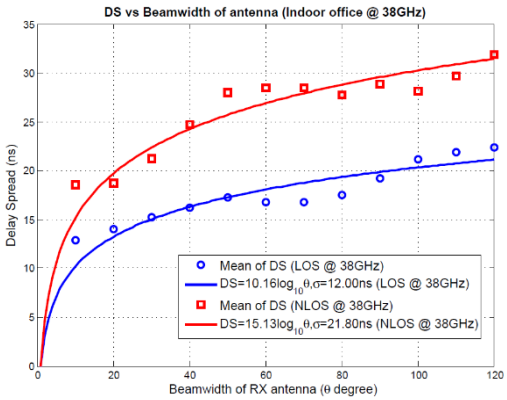

Based on the measurement results in a typical office environment at 38 GHz, the following observations are made.

– The DS has a strong dependency on the antenna beamwidth. The wider beamwidth has the larger DS.

– The DSs at NLoS case is larger than those of LoS case.

– These properties are very similar to the measurement results in commercial environments at 28 and 38 GHz

Table 62 summarizes the typical coefficients of DS model and a standard deviation σ for LoS and NLoS situations, respectively, in a typical indoor office environment.

TABLE 62

rms delay spread parameters

Indoor environments			**rms delay spread (ns)**	
			α	**σ (ns)**
Office	38 GHz	LoS	10.16	12
		NLoS	15.13	21.8

6.9.4.2 Rms angular spread vs. antenna beamwidth

For the first measurement campaign, the rms AS can be easily derived from the PAS. The PAS is calculated from the PADS by summation in delay domain [1]-[3]. To calculate the directional rms AS, the threshold level was set to 20 dB. Figure 88(a) and (b) show the AS curves which were obtained from measurement data at 28 and 38 GHz for LoS and NLoS cases, respectively. To derive the best fitting curve, mean values of AS for each beamwidth are used.

FIGURE 88

Measurement results of directional rms angular spread: (a) LoS, (b) NLoS

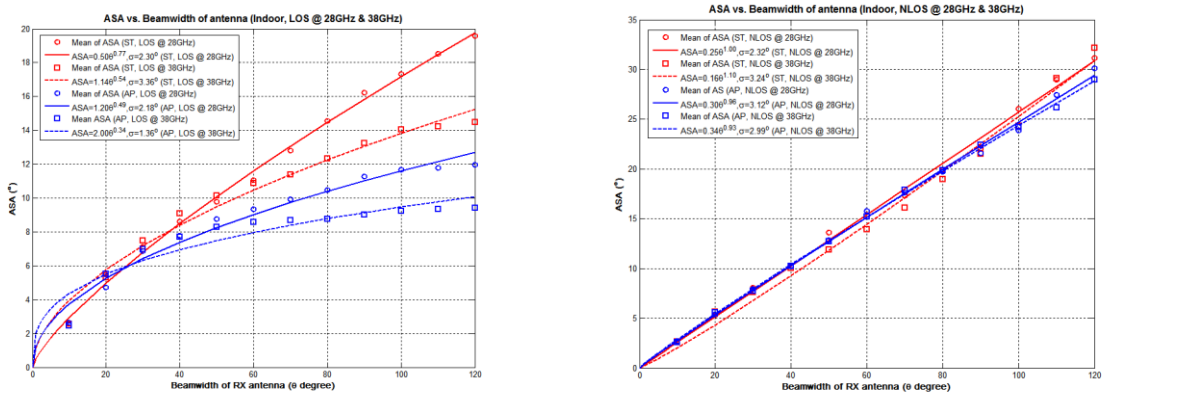

(a) (b)

From measurement results, the following can be observed:

– The AS shows a strong dependency on the antenna beamwidth as similar to the DS. The wider beamwidth of the antenna is the larger angular spread.

– For the LoS case, the AS of 28 GHz is higher than the curve of 38 GHz. However, the frequency dependency is not seen in case of NLoS.

– For the NLoS case, the angular spread continuously increase from narrow to wider beamwidths.

– For the LoS case, the AS values of ST are larger than the AP environment. On the other hand, the values of ST and AP are similar in case of NLoS. The multipath components in AP are more spread in the delay domain but the spread in angular domain is similar to the circumstance of ST.

The rms angular spread AS with respect to θ which follows a normal distribution with the standard deviation α is given by;

$$AS(\theta) = \alpha \times \theta^{\beta} \quad \text{degree} \tag{34}$$

where the range of θ is defined as $0^{o} \leq \theta \leq 120^{o}$.

The typical coefficients of angular spread model AS and standard deviation σ for each measurement scenario and frequency band are summarized in Table 63.

TABLE 63

Directional rms angular spread parameters

Indoor environments			rms angular spread (degree)		
			α	β	σ (°)
Railway Station (ST)	28 GHz	LoS	0.5	0.77	2.3
		NLoS	0.25	1.0	2.32
	38 GHz	LoS	1.14	0.54	3.36
		NLoS	0.16	1.1	3.24
Airport Terminal (AP)	28 GHz	LoS	1.2	0.49	2.18
		NLoS	0.3	0.96	3.12
	38 GHz	LoS	2.0	0.34	1.36
		NLoS	0.34	0.93	2.99

For the second measurement campaign, the rms AS depending on the antenna's beamwidth is derived using the same methods as in the first campaign. To calculate the directional rms AS, the threshold level was set to 20 dB. Figure 89 shows the AS curves which are obtained from measurement data at 38 GHz for LoS and NLoS situations, respectively.

FIGURE 89

Measurement results of rms angular spread for LoS and NLoS (office at 38 GHz)

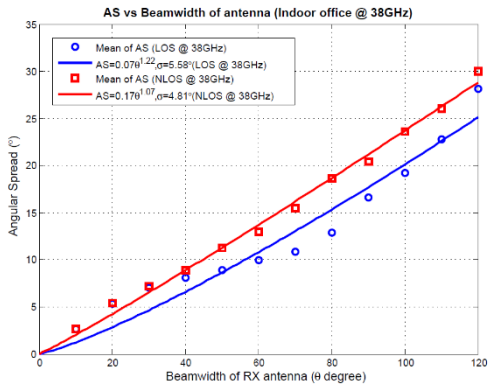

From measurement results, it can be observed the following properties.

– The AS shows a strong dependency on the antenna beamwidth as similar to the DS. When the beamwidth of RX antenna is wider, the larger angular spread is observed.

– For the NLoS case, the angular spread monotonically increases as beamwidth increases

– These properties are very similar to the measurement results in commercial environments at 28 and 38 GHz

Table 64 summarizes the typical coefficients of AS model and a standard deviation σ for LoS and NLoS situations, respectively, in a typical indoor office environment.

TABLE 64

rms angular spread parameters

Indoor environments			rms angular spread (degree)		
			α	β	σ (°)
Office	38GHz	LoS	0.07	1.22	5.58
		NLoS	0.17	1.07	4.81

6.9.5 Conclusion

Based on above measurement results and observations, new prediction models for delay spread and angular spread associated with antenna beamwidth were included in Recommendation ITU-R P.1238.

6.9.6 References

[1] M.-D. Kim et al., "Directional Delay Spread Characteristics based on Indoor Channel Measurements at 28 GHz," PIMRC 2015, pp. 505–509, Aug. 2015.

[2] M.-D. Kim et al., "Directional Multipath Propagation Characteristics based on 28GHz Outdoor Channel Measurements," in Proc. The European Conference on Antennas and Propagation (EuCAP), April, 2016.

[3] M.-D. Kim et al., "Investigating the Effect of Antenna Beamwidth on Millimeter-wave Channel Charaterization," accepted in 2016 The URSI Asia-Pacific Radio Science Conference (AP-RASC), August, 2016.

[4] H.-K. Kwon et al., "Implementation and Performance Evaluation of mmWave Channel Sounding System", in Proc. IEEE AP-S 2015, July 2015.

[5] M. Bartlett, "Smoothing Periodograms from Time-Series with Continuous Spectra," Nature, vol. 161, 1948.

6.10 Study 10: Effect of movement of objects in the room (Frequency band: 70 GHz)

6.10.1 Executive summary

The movement of persons within the room cause temporal variations of the indoor propagation characteristics. Therefore the measurements had been executed in an exhibition hall using a frequency band of 70 GHz and antenna height of about 1-2 m propagation paths.

In this study, a statistical procedure is proposed to estimate mean fade duration in an hour over short range propagation path.

6.10.2 Background and proposal

Measurements at 70 GHz have shown that the mean fade duration due to body shadowing were 0.52 s, 0.25 s and 0.09 s for the fade depth of 10 dB, 20 dB and 30 dB, respectively, in which the mean walking speed of persons was estimated at 0.74 m/s with random directions and human body thickness was assumed to be 0.3 m.

Measurements indicate that the mean number occurrence of body shadowing in an hour caused by human movement in an office environment is given by:

$$\overline{N} = 260 \times D_p \tag{35}$$

where D_p ($0.05 \leq D_p \leq 0.08$) is the number of persons per square metre in the room. The total fade duration per hour is then given by:

$$T = \overline{T_s} \times \overline{N} \tag{36}$$

where $\overline{T_s}$ is mean fade duration.

6.10.3 Measurement setup and procedure

The measurement of propagation characteristics was carried out in an exhibition hall, and investigated the characteristic of the shadowing loss due to human movement. Figure 90 shows a measurement layout in an exhibition hall. Table 65 shows measurement conditions. The width of this hall was 22 m times 13 m with wooden inner walls [1]. A vector network analyser (VNA) was used in order to measure propagation loss. Propagation path was set in front of exhibition booths. The transmitting frequency was set at 70.0 GHz, and a carrier wave (CW) was transmitted. The instantaneous variation of the received level was measured for several transmitting antenna heights and propagation distances.

FIGURE 90

A measurement layout in an exhibition hall

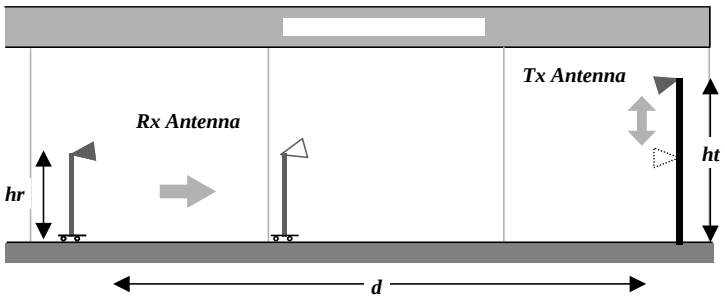

TABLE 65

Measurement conditions

Frequency	70.0 GHz (CW)	
Polarization	Vertical	
Antenna (3 dB beam width)	Wave Guide Horn (15 degrees)	
Antenna height	Tx	1.05 m, 2.05 m
	Rx	1.05 m
Propagation Distance	3.3 m, 7.3 m, 10.8 m	

6.10.4 Validation results

6.10.4.1 Characteristics of cumulative probability distributions of attenuation level

Figure 91(a) shows cumulative probability distributions of attenuation level measured for several propagation distances when a person crossed the path at a speed of about 1 m/s.

Figure 91(b) shows cumulative probability distributions of attenuation level measured for several transmitting antenna heights.

FIGURE 91

Cumulative probability distributions of attenuation level measured for:
(a) several propagation distances, (b) several transmitting antenna heights

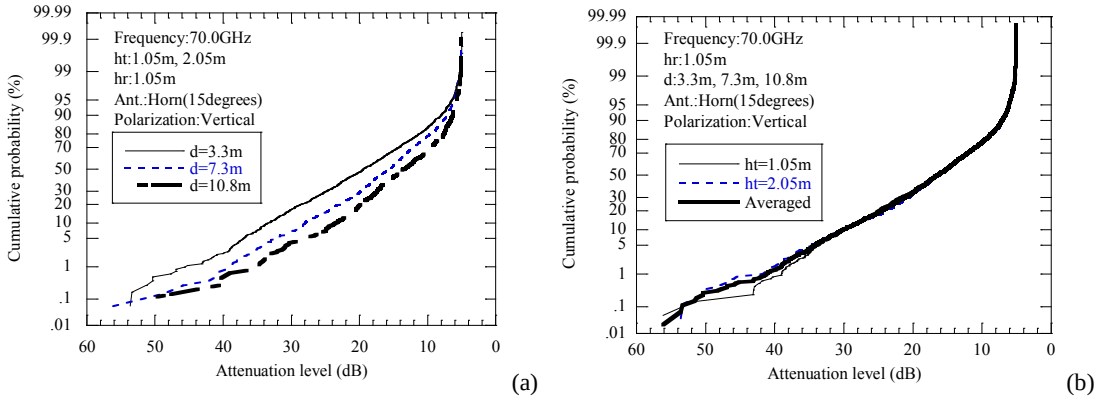

6.10.4.2 Investigation of mean fade duration

Variations of mean fade durations versus attenuation level are shown in Fig. 92(a). This Figure shows measured results when the transmitting antenna height was fixed at 2.05 m. According to Fig. 92(a), the fade duration becomes longer in 3.3 m path in comparison with other paths. This is because the attenuation had occurred in the limited area near the receiving antenna.

Variations of mean fade durations versus attenuation level when each transmitting antenna height was fixed at 1.05 m and 2.05 m are shown in Fig. 92(b). The mean fade duration decreased gradually in proportion with the attenuation level. Furthermore variations of mean fade duration became small in the range of more than 25 dB. For example, when the attenuation level is 16.4 dB, the mean fade duration was estimated about 0.35 s from Fig. 92(b). The mean fade duration at 70.0 GHz when the attenuation level was 10 dB, 20 dB, and 30 dB then the fade duration was 0.52 s, 0.25s, and 0.09 s, respectively. According to the measurement results at 37 GHz in an indoor office environment reported in Recommendation ITU-R P.1238, at a fade depth of 10 dB, the mean fade duration was 0.11 s and at a fade depth of 15 dB, the mean duration was 0.05 s.

FIGURE 92

Variation of mean fade durations: (a) ht=2.05 m, (b) ht=1.05 m, 2.05 m

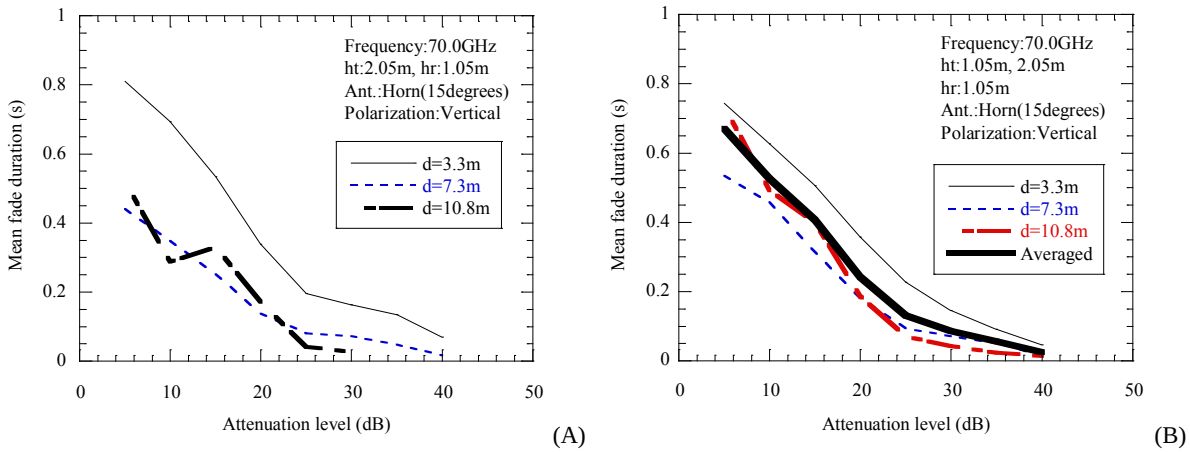

6.10.4.3 Characteristics of human movement

In order to presume the total amount of fade duration per hour, it is necessary to describe not only the mean fade duration but also the characteristics of human movement in the actual environment.

6.10.4.3.1 Measurement procedure

The investigation was carried out in two different sized offices. A sample of propagation path layout in the office is shown in Fig. 93. The 2 or 3 LoS paths were set in each office, and the number of each path interruption occurrence was investigated. The measurement was carried out from 8:30 to 17:00.

FIGURE 93

A sample of propagation path layout in the office

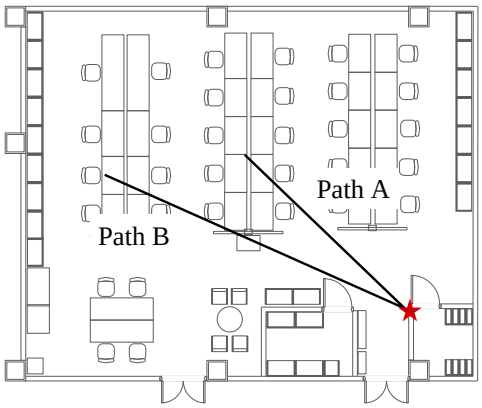

6.10.4.3.2 Measurement results of human movement

The number of path interruption occurrence (N) when people cross the propagation path in an hour is shown in Fig. 94. A horizontal axis indicates a density of population per one square meter. In this Figure, *N* of 57 was measured at lunchtime. Although there was variation by measurement time zone, the N increased gradually in proportion with density of population per one square meter (*Dp)*.

In Fig. 94, a regression curve is shown and it is expressed as follows.

$$N = 260 \times Dp \tag{37}$$

Here, $0.05 \leq Dp \leq 0.08$.

FIGURE 94

Characteristics of the number interruption occurrence per hour

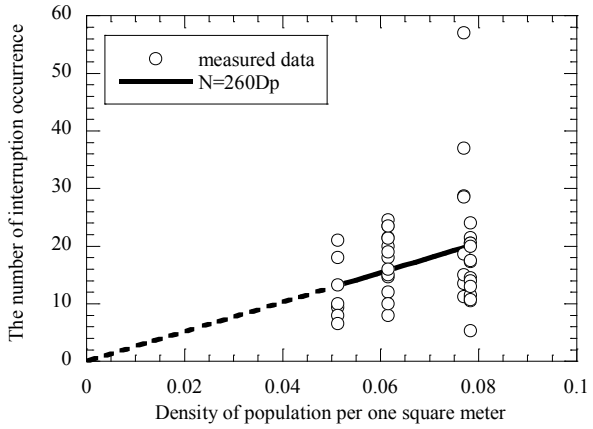

6.10.4.4 Estimated total amount of fade duration per hour

It was proposed that a total amount of fade duration per hour (*T*) was estimated by using density of population and the number of fade occurrence. The *T* was expressed as follows.

$$T = Ts\_ave \times N \tag{38}$$

Where, *T* is a total amount of fade duration per hour in seconds, *Ts_ave* is the mean fade duration in second, and *N* is the number of fade occurrence per hour.

6.10.5 Conclusion

Propagation measurements were carried out in actual circumstances where humans randomly moved, in order to design a millimetre-wave ad-hoc wireless access system. In addition to characteristics of shadowing loss, characteristics of fade duration were analysed. Furthermore, human movement was observed in offices, the relations between the number of path interruption occurrences and the density of population per one square meter was derived. As a result, it was possible to estimate the total amount of fade duration per hour by using the statistical function of attenuation level and density of population per one square meter.

6.10.6 References

[1] F. Ohkubo, et al., "Millimeter-Wave Ad-Hoc Wireless Access System II- (5) Statistical Characteristics of Shadowing Loss due to Human Movement-", TSMMW2003, Mar. 2003.

7 Studies for outdoor-to-indoor environments

Compilation of measurement data related to outdoor-to-indoor environments (building entry loss) can be found in Report ITU-R P.2346 [1].

7.1 References

[1] Report ITU-R P.2346 – Compilation of measurement data relating to building entry loss.